Abstracts

The 26th Hiroshima International Symposium on Synchrotron Radiation

Materials Science using VUV-SX Synchrotron Radiation

March 10- 11, 2022

Faculty Club, Hiroshima University and Online

Hiroshima Synchrotron Radiation Center, Hiroshima University

Supported by

Higashihiroshima City

The Japanese Society for Synchrotron Radiation Research

Program

Oral Session

DAY 1 ・Thursday, 10 March, 2022

Opening (Chairperson: T. Okuda)

09:30 – 09:40 Greeting
Manabu ABE (*Vice President, Hiroshima University, Japan*)

09:40 – 10:10 Overview of HiSOR Activities
Kenya SHIMADA (*Director, Synchrotron Radiation Center, Hiroshima University, Japan*)

10:10 – 10:20 Break

Oral Session 1 (Chairperson: S. Ideta)

10:20 – 10:55 **Ilya BELOPOLSKI** (*RIKEN, Japan*)
"Observation of linked loops in a quantum ferromagnet: a new paradigm for topology in physics"

10:55 – 11:30 **Chaoyu CHEN** (*Southern University of Science and Technology, China*)
"Electronic Structure Study on the Intrinsic Magnetic Topological Insulator Mn-Bi-Te family"

11:30 – 12:05 **Jayita NAYAK** (*Indian Institute of Technology Kanpur, India*)
"Experimental evidence of six-fold degenerate Fermions in $PdSb_2$"

12:05 – 13:15 Lunch

Poster Session (Chairperson: H. Sato)

13:15 – 14:00	Student Short Oral Session (1~2 min/each)
14:00 – 16:00	Poster Session

Oral Session 2 (Chairperson: M. Sawada)

16:10 – 16:45	**Goro SHIBATA** (*Tokyo University of Science, Japan*) "Angle-dependent XMCD as a Probe of Anisotropic Spin-density Distribution"
16:45 – 17:20	**Yuichi YAMASAKI** (*National Institute for Materials Science, Japan*) "X-ray Magnetic Circular Dichroism in a Chiral Antiferromagnet"

DAY 2 ・Friday, 11 March, 2022

Oral Session 3 (Chairperson: H. Sato)

09:30 – 10:05	**Kazuki SUMIDA** (*Japan Atomic Energy Agency, Japan*) "Spin-Resolved Photoemission of Heusler-Type Weyl Ferromagnet Films"
10:05 – 10:40	**Yoshihiko TOGAWA** (*Osaka Prefecture University, Japan*) "Chirality-Induced Spin Polarization in Chiral Crystals"
10:40 – 11:00	Break

Oral Session 4 (Chairperson: H. Namatame)

11:00 – 11:35	**Yoshifumi TAKASHIMA** (*Nagoya University, Japan*) "Construction and Operation of Superconducting Bending Magnets in Aichi-SR"
11:35 – 12:10	**Masahiro KATOH** (*Hiroshima University, Japan*) "Recent Results from Design Study on HiSOR-2"
12:10 – 13:30	Lunch

Oral Session 5 (Chairperson: K. Matsuo)	
13:30 – 14:05	**Toru ASAHI** （*Waseda University, Japan*） ″Applications of the Generalized High Accuracy Universal Polarimeter (G-HAUP) to Solid State Sciences″
14:05 – 14:40	**Akinari YOKOYA** （*National Institutes for Quantum Science and Technology, Japan*） ″Exploring active structures of DNA repair protein XRCC4 using CD and SAXS″

Closing Session (Chairperson: T. Okuda)	
14:40 – 14:55	Student Award Ceremony
14:55 – 15:00	Closing Remarks

Oral Session

-Oral Session-

O01 Observation of Linked Loops in a Quantum Ferromagnet

Ilya Belopolski [a,b]

a RIKEN Center for Emergent Matter Science (CEMS), Japan
b Laboratory for Topological Quantum Matter and Spectroscopy (B7), Department of Physics, Princeton University, USA

O02 Electronic Structure Study on the Intrinsic Magnetic Topological Insulator Mn-Bi-Te family

Chaoyu Chen

Southern University of Science and Technology, China

O03 Experimental Evidence of Six-Fold Degenerate Fermions in $PdSb_2$

Jayita Nayak et al.

Max Planck Institute for Chemical Physics of Solids, Germany

O04 Angle-dependent XMCD as a Probe of Anisotropic Spin-density Distribution

Goro Shibata

Department of Applied Physics, Tokyo University of Science, Japan

O05 X-ray Magnetic Circular Dichroism in a Chiral Antiferromagnet

Yuichi Yamasaki

National Institute for Materials Science, Japan

O06 Spin-Resolved Photoemission of Heusler-Type Weyl Ferromagnet Films

Kazuki Sumida

Materials Sciences Research Center, Japan Atomic Energy Agency, Japan

O07 Chirality-Induced Spin Polarization in Chiral Crystals

Yoshihiko Togawa

Department of Physics and Electronics, Osaka Prefecture University, Japan

O08 Construction and Operation of Superconducting Bending Magnets in Aichi-SR

Yoshifumi Takashima[a,b]

a Synchrotron Radiation Research Center, Nagoya University, Japan
b Aichi Synchrotron Radiation Center, Japan

O09 Recent Results from Design Study on HiSOR-2

Masahiro Katoh[a,b]

a Hiroshima Synchrotron Radiation Center, Hiroshima University, Japan
b Institute for Molecular Science, National Institutes of Natural Sciences, Japan

O10 Applications of the Generalized-High Accuracy Universal Polarimeter (G-HAUP) to Solid State Sciences

Toru Asahi[a,b] and Kenta Nakagawa[c]

a Faculty of Science and Engineering, Waseda University, Japan
b Research Organization for Nano & Life Innovation, Waseda University, Japan
c Kanagawa Institute of Industrial Science and Technology (KISTEC), Japan

O11 Exploring active structures of DNA repair protein XRCC4 using CD and SAXS

Akinari Yokoya[a,b], Kai Nishikubo[b,a], Maho Hasegaw[b,a]

a National Institutes for Quantum Science and Technology, Institute for Quantum Life Science, Japan
b Graduate School of Science and Engineering, Ibaraki University, Japan

Observation of Linked Loops in a Quantum Ferromagnet

Ilya Belopolski [a,b]

[a] RIKEN Center for Emergent Matter Science (CEMS), Wako, Saitama 351-0198, Japan
[b] Laboratory for Topological Quantum Matter and Spectroscopy (B7), Department of Physics, Princeton University, Princeton, New Jersey 08544, USA

Keywords: Linking number, Weyl loop, topological quantum matter, mathematical knot theory, angle-resolved photoemission spectroscopy (ARPES), Seifert bulk-boundary correspondence

Quantum phases can be classified by topological invariants, which take on discrete values capturing global information about the quantum state. Over the past decades, these invariants have come to play a central role in describing matter, providing the foundation for understanding superfluids, magnets, the quantum Hall effect, topological insulators and Weyl semimetals. In this talk, I will introduce a remarkable linking number (knot theory) invariant associated with loops of electronic band crossings in the mirror-symmetric ferromagnet Co_2MnGa [1-4]. We disentangle this system's rich topological structure through bulk-sensitive soft X-ray and surface-sensitive vacuum ultraviolet angle-resolved photoemission spectroscopy. We directly observe three intertwined degeneracy loops in the bulk Brillouin zone three-torus, T^3, such that each loop links each other loop twice. Through systematic spectroscopic investigation of this linked loop quantum state, we explicitly draw its link diagram and conclude, in analogy with knot theory, that it exhibits linking number (2,2,2), providing a direct experimental determination of the topological invariant. On the sample surface, we further predict and observe Seifert boundary states protected by the bulk linked loops, suggestive of a Seifert bulk-boundary correspondence. Our observation of a quantum loop link motivates the application of knot theory to the exploration of quantum matter.

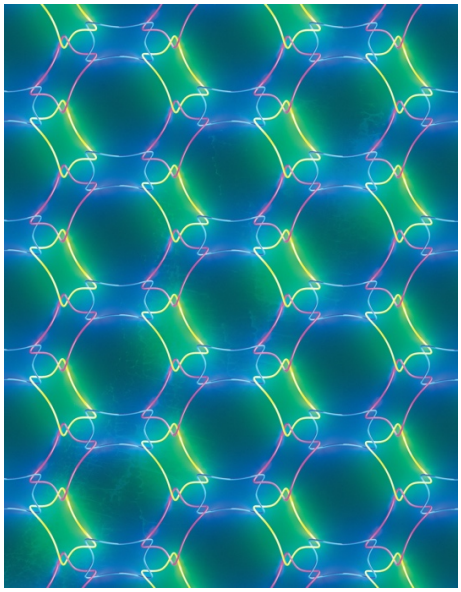

FIGURE 1. Mathematical link diagram in three-dimensional momentum space, characterizing the linking number of the linked Weyl loops (nodal lines) in the quantum ferromagnet Co_2MnGa, as characterized by ARPES.

REFERENCES

1. I. Belopolski *et al.* Observation of a linked loop quantum state. arXiv:2112.14722 and *Nature*, in press (2022).
2. I. Belopolski *et al*. Signatures of magnetic Weyl fermion annihilation in a correlated kagome magnet. *Phys. Rev. Lett.* 127, 256403 (2021).
3. I. Belopolski *et al.* Discovery of topological Weyl fermion lines and drumhead surface states in a room temperature magnet. *Science* 365, 6459 (2019).
4. M. Z. Hasan, G. Chang, I. Belopolski *et al.* Weyl, Dirac and high-fold chiral fermions in topological quantum matter. *Nat. Rev. Mat.* 6, 784 (2021).

19AG014, 19AG004, 19AU002, 19AU007, 19BG006, 19BG044, 19BU002, 19BU005 and 19BU012 BL-1 and Laser-ARPES

Electronic Structure Study on the Intrinsic Magnetic Topological Insulator Mn-Bi-Te family

Chaoyu Chen[a]

[a]*Southern University of Science and Technology*
Shenzhen 518055, China

Keywords: ARPES, Intrinsic magnetic topological insulator, topological surface state, gap.

The layered $MnBi_{2n}Te_{3n+1}$ family represents the first intrinsic magnetic topological insulator ever discovered, providing an ideal platform to explore novel areas of physics such as the quantum anomalous Hall effect at elevated temperature and axion electrodynamics. In this talk I will present our recent studies on the electronic structure, especially the topological surface state Dirac cone of $MnBi_{2n}Te_{3n+1}$ family, including:

1. Discovery of gapless surface states in antiferromagnetic topological insulator $MnBi_2Te_4$ [1]
2. The origin of gapless surface state in Mn-Bi-Te family: surface-bulk band hybridization [2]
3. Discovery of "half-magnetic topological insulator" with magnetic gap opening of surface state [3]
4. Realization of tunable surface gap in doped $MnBi_2Te_4$ [4]

These works have established a solid electronic platform for realizing quantum anomalous hall effect at elevated temperature.

REFERENCES

1. Yu-Jie Hao, Pengfei Liu, Yue Feng, Xiao-Ming Ma, Eike F. Schwier, Masashi Arita, Shiv Kumar, Chaowei Hu, Rui'e Lu, Meng Zeng, Yuan Wang, Zhanyang Hao, Hong-Yi Sun, Ke Zhang, Jiawei Mei, Ni Ni, Liusuo Wu, Kenya Shimada, Chaoyu Chen, Qihang Liu & Chang Liu. Gapless Surface Dirac Cone in Antiferromagnetic Topological Insulator MnBi2Te4. Physical Review X 9, 041038, doi:10.1103/PhysRevX.9.041038 (2019).
2. Xiao-Ming Ma, Zhongjia Chen, Eike F. Schwier, Yang Zhang, Yu-Jie Hao, Shiv Kumar, Ruie Lu, Jifeng Shao, Yuanjun Jin, Meng Zeng, Xiang-Rui Liu, Zhanyang Hao, Ke Zhang, Wumiti Mansuer, Chunyao Song, Yuan Wang, Boyan Zhao, Cai Liu, Ke Deng, Jiawei Mei, Kenya Shimada, Yue Zhao, Xingjiang Zhou, Bing Shen, Wen Huang, Chang Liu, Hu Xu & Chaoyu Chen. Hybridization-induced gapped and gapless states on the surface of magnetic topological insulators. Physical Review B 102, 245136, doi:10.1103/PhysRevB.102.245136 (2020).
3. Ruie Lu, Hongyi Sun, Shiv Kumar, Yuan Wang, Mingqiang Gu, Meng Zeng, Yu-Jie Hao, Jiayu Li, Jifeng Shao, Xiao-Ming Ma, Zhanyang Hao, Ke Zhang, Wumiti Mansuer, Jiawei Mei, Yue Zhao, Cai Liu, Ke Deng, Wen Huang, Bing Shen, Kenya Shimada, Eike F Schwier, Chang Liu, Qihang Liu & Chaoyu Chen. Half-Magnetic Topological Insulator with Magnetization-Induced Dirac Gap at a Selected Surface. Physical Review X 11, 011039, doi:10.1103/PhysRevX.11.011039 (2021).
4. Xiao-Ming Ma, Yufei Zhao, Ke Zhang, Shiv Kumar, Ruie Lu, Jiayu Li, Qiushi Yao, Jifeng Shao, Fuchen Hou, Xuefeng Wu, Meng Zeng, Yu-Jie Hao, Zhanyang Hao, Yuan Wang, Xiang-Rui Liu, Huiwen Shen, Hongyi Sun, Jiawei Mei, Koji Miyamoto, Taichi Okuda, Masashi Arita, Eike F. Schwier, Kenya Shimada, Ke Deng, Cai Liu, Junhao Lin, Yue Zhao, Chaoyu Chen, Qihang Liu & Chang Liu. Realization of a tunable surface Dirac gap in Sb-doped MnBi2Te4. Physical Review B 103, L121112, doi:10.1103/PhysRevB.103.L121112 (2021).

Experimental Evidence of Six-Fold Degenerate Fermions in $PdSb_2$

Jayita Nayak *et al.*

Max Planck Institute for Chemical Physics of Solids, Nöthnitzer Str. 40, 01187 Dresden, Germany

Keywords: Electronic structure, Multifold degenerate Fermions, Sextuple point

Condensed matter systems can exhibit quasiparticle excitations which mimic the wavefunctions of exotic fermions predicted in high energy physics. For example, Dirac and Weyl fermions exist as low energy electronic excitations of several semimetals near the Dirac points and Weyl points. Most interestingly, condensed matter systems can also realize novel fermions which have no counterpart in high energy physics because the former do not need to follow certain symmetries which are mandatory for the latter. Bradlyn *et al.* discovered that one can find threefold, sixfold, or eightfold degenerate symmetry protected points in many compounds [1]. While the threefold points can be realized in both nonsymmorphic [1,2] and symmorphic crystal structures [2], nonsymmorphic operations are essential for stabilizing sixfold and eightfold degenerate points. **The present study shows that the nonsymmorphic compound $PdSb_2$ hosts six-component fermions or sextuplets.** The sextuple points have been recently observed experimentally in the chiral compound CoSi, RhSi, and AlPt in the space group $P2_13$ (198) [3–5]. However, the latter study was mainly focused on establishing the existence of surface Fermi arcs, which are a consequence of the large Chern number associated with the sixfold crossings in this space group. By contrast, here we show for the first time the existence of sextuple points that have a vanishing Chern number and are therefore expected to show no surface Fermi arcs [6].

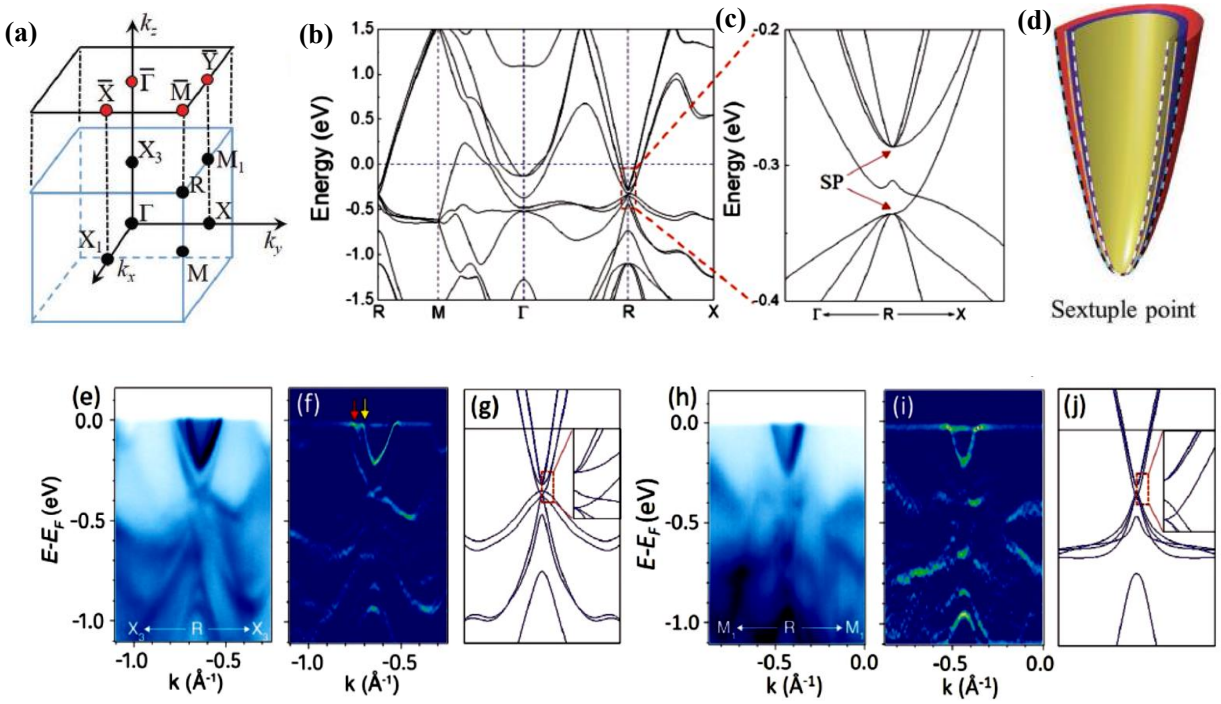

FIGURE 1. a) 3D bulk Brillouin zone (BZ) and (001) surface BZ with the high symmetry points highlighted. b) Calculated band structure along *R*–*M*–Γ–*R*–*X*. Two sextuple points (SPs) are observed at the *R* point at −0.286 & −0.334 eV below the Fermi level, indicated by red arrows in the magnified image on the right (c). Schematic representation of sextuple points (d). e) Measured band dispersion along the X_3−*R*−X_3 direction, at the photon energy 65 eV. f) The corresponding curvature intensity plot. g) Calculated band structure along X_3−*R*−X_3. Inset shows the magnified view near the sextuple point. h–j) ARPES intensity plot, the corresponding curvature intensity plot, and the calculated band structure along M_1−*R*−M_1.

REFERENCES

1. B. Bradlyn, J. Cano, Z. Wang, M. G. Vergniory, C. Felser, R. J. Cava, B. A. Bernevig, *Science* **2016**, *353*, aaf5037.
2. Z. Zhu, G. W. Winkler, Q. Wu, J. Li, A. A. Soluyanov, *Phys. Rev. X* ***6,*** 031003 (2016).
3. D. S. Sanchez, I. Belopolski, T. A. Cochran, X. Xu, J.-X. Yin, G. Chang, W. Xie, K. Manna, V. Süß, C.-Y. Huang, N. Alidoust, D. Multer, S. S. Zhang, N. Shumiya, X. Wang, G.-Q. Wang, T.-R. Chang, C. Felser, S.-Y. Xu, S. Jia, H. Lin, M. Z. Hasan, *Nature* ***567***, 500 (2019).
4. Z. Rao, H. Li, T. Zhang, S. Tian, C. Li, B. Fu, C. Tang, L. Wang, Z. Li, W. Fan, J. Li, Y. Huang, Z. Liu, Y. Long, C. Fang, H. Weng, Y. Shi, H. Lei, Y. Sun, T. Qian, H. Ding, *Nature* ***567***, 496 (2019).
5. N. B. M. Schröter, D. Pei, M. G. Vergniory, Y. Sun, K. Manna, F. de Juan, J. A. Krieger, V. Süss, M. Schmidt, P. Dudin, B. Bradlyn, T. K. Kim, T. Schmitt, C. Cacho, C. Felser, V. N. Strocov, Y. Chen, *Nat. Phys.* ***15***, 759 (2019).
6. Nitesh Kumar, Mengyu Yao, Jayita Nayak, Maia G. Vergniory, Jörn Bannies, Zhijun Wang, Niels B. M. Schröter, Vladimir N. Strocov, Lukas Müchler, Wujun Shi, Emile D. L. Rienks, J. L. Mañes, Chandra Shekhar, Stuart S. P. Parkin, Jörg Fink, Gerhard H. Fecher, Yan Sun, B. Andrei Bernevig, and Claudia Felser, *Adv. Mater.* **1906046,** pp 1-6 (2020).

Angle-dependent XMCD as a Probe of Anisotropic Spin-density Distribution

Goro Shibata[a]

[a]*Department of Applied Physics, Tokyo University of Science, 6-3-1 Niijuku, Katsushika-ku, Tokyo 125-8585, Japan*

Keywords: X-ray magnetic circular dichroism, Magnetic anisotropy, Thin films, Anisotropic charge distribution, Orbital degree of freedom, Magnetic dipole moment

Magnetic thin films often exhibit magnetic anisotropy due to epitaxial strain, surface and interfacial effects, lowered dimensionality, and so on. In general, magnetic anisotropy arises from the combined effects of anisotropic electronic structure and spin-orbit interaction (SOI). Understanding the detailed mechanism of the magnetic anisotropy in ferromagnetic thin films and controlling it have been one of the major research issues both from scientific and technological points of view. Since the electronic structure of magnetic thin films can be highly anisotropic, soft x-ray spectroscopy, including, x-ray absorption spectroscopy (XAS) and x-ray magnetic circular/linear dichroism (XMCD/XMLD), with varying incident angles and magnetic-field angles will give new insights into the magnetic anisotropy of thin films.

We have developed the 'vector-magnet' apparatus for XMCD and XMLD measurements, in which the direction of the magnetic field can be varied two-dimensionally [1]. It has been theoretically predicted that the "magnetic dipole moment" M_{T} or "electric quadrupole moment" Q_{zz}, which represent the anisotropy of spin/charge density distribution (i.e. elongation or shrinkage of electron orbitals of magnetic ions), can be deduced through such angle-dependent XMCD and XMCD measurements [2,3]. In this talk, I will introduce our recent studies on the magnetic anisotropy of $La_{1-x}Sr_xMnO_3$ (LSMO) thin films via the angle-dependent XMCD and XMLD measurements [4,5]. LSMO is a material which shows ferromagnetic metallicity in the widest ranges of hole concentration x and has highest Curie temperature above the room temperature among colossal-magnetoresistive perovskite manganites. From the angle-dependent XMCD experiments [4], it has been demonstrated that the anisotropy of the spin-density distribution of Mn 3*d* electrons changes depending on the epitaxial strain and that it is correlated with the change of strain-induced magnetic anisotropy [6]. From the XMLD experiments [5], changes in the charge-density anisotropy of Mn 3*d* electrons induced by the spin polarization has been observed, which can be understood as the inverse process of the strain-induced magnetic anisotropy. These angle-dependent XMCD and XMLD measurements will pave a new way for elucidating the origin of magnetic anisotropy in various transition-metal thin films by directly probing the anisotropic electronic structure.

REFERENCES

1. M. Furuse *et al.*, *IEEE Trans. Appl. Supercond.* **23**, 4100704-1--4 (2013).
2. J. Stöhr and H. König, Phys. Rev. Lett. **75**, 3748--3751 (1995).
3. H. A. Dürr and G. van der Laan, Phys. Rev. B **54**, R760--R763 (1996).
4. G. Shibata *et al.*, *npj Quantum Mater.* **3**, 3-1--6 (2018).
5. G. Shibata *et al.*, *J. Phys. Soc. Jpn.* **87**, 114713-1--5 (2018).
6. G. van der Laan, *J. Phys. Condens. Matter* **10**, 3239--3253 (1998).

X-ray Magnetic Circular Dichroism in a Chiral Antiferromagnet

Yuichi Yamasaki

[a] *National Institute for Materials Science*

Keywords: X-ray magnetic circular dichroism, antiferromagnet

X-ray magnetic circular dichroism (XMCD) has become a versatile technique to ferro- and ferrimagnetic magnetic materials. The technique enables us to extract the expectation values of the element-specific spin and orbital moments. In contrast, it has been generally believed that XMCD does not occur in antiferromagnets which do not have net magnetization.

A chiral magnet Mn_3Sn exhibits a coplanar 120° antiferromagnetic (AFM) order on breathing Kagomé-type Mn network, which breaks the time reversal symmetry and allows the anomalous Hall effect [1] and the magneto-optical Kerr effect (MOKE) [2] even though the magnetic moments almost cancel each other. We have theoretically investigated a possibility of x-ray magnetic circular dichroism (XMCD) in the AFM state of Mn_3Sn [3]. The spin operator term in XMCD, the so-called S_z term, should be negligibly small as well as the net magnetization. However, it is clarified that the anisotropic magnetic dipole (AMD) operator term, the so-called T_z term, remains uncancelled in the AFM order and is linked to the augmented (cluster) magnetic octupole (see Figure). Based on this prediction, XMCD experiments were performed on bulk crystals of Mn_3Sn. As a result, we succeeded in observing XMCD at Mn-L absorption edge and demonstrated that the XMCD signal is purely coming from the T_z tern by its magnetic field and incident angle dependence and comparing with theoretical calculations of the spectrum [4].

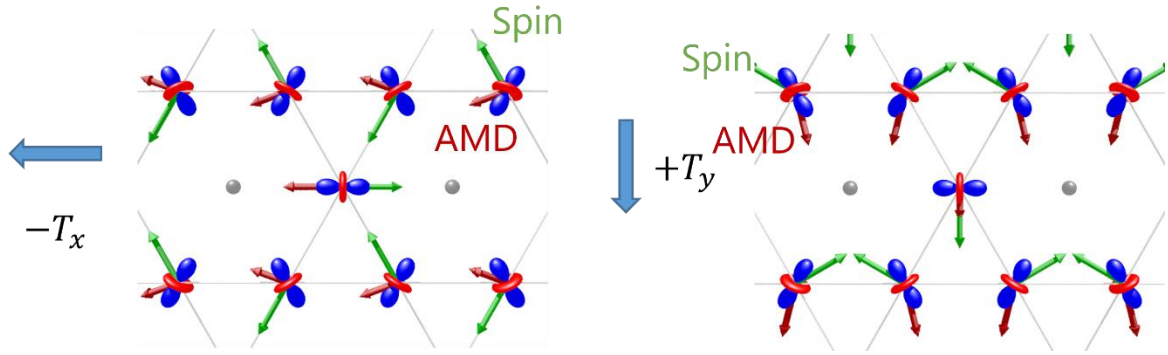

REFERENCES

1. S. Nakatsuji, N. Kiyohara, and T. Higo, Nature 527, 212 (2015).
2. T. Higo, et al., Nat. Photonics 12, 73 (2018).
3. Y. Yamasaki, H. Nakao, T. Arima, J. Phys. Soc. Jpn. 89, 083703 (2020)
4. M. Kimata, Y. Yamasaki, Tetsuya Nakamura, *et al*., Nat. Commun. 12, 5582 (2021)

Spin-Resolved Photoemission of Heusler-Type Weyl Ferromagnet Films

Kazuki Sumida[a]

[a]*Materials Sciences Research Center, Japan Atomic Energy Agency, Hyogo 679-5148, Japan*

Keywords: Spin-resolved ARPES, Heusler alloy, Weyl ferromagnet, Anomalous Nernst effect, Berry curvature.

When electric and thermal currents flow through a ferromagnet, an electric field emerges orthogonally to the current path [Fig. 1(a)]. The two effects are, respectively, called the anomalous Hall (AHE) and Nernst (ANE) effects and are exploited as operating mechanisms in various novel applications. The associated transverse voltage of the electric field is empirically proportional to its spontaneous magnetization. In contrast to the general belief, recent discoveries of both large AHE and ANE, which do not scale with magnetization, have elicited great surprise. In particular, the observed ANE thermopower and AHE conductivity of single crystalline bulk Co_2MnGa and Co_2MnAl are an order of magnitude larger than those of other ferromagnets with similar magnetizations [1,2,3]. These transverse properties are postulated to arise from a Berry curvature emerging within band structures near the Fermi energy (E_F).

Topologically non-trivial Weyl semimetals possessing massless fermions characterized by zero-gap and linear band dispersions are promising candidates featuring a large Berry curvature. Weyl fermions in solids can be realized in materials that break inversion symmetry or time-reversal symmetry. With the breaking of such symmetries, Weyl nodes appear as pairs in momentum space and act as magnetic monopoles with positive and negative chiralities. To date, Weyl fermions have been verified in experiments in non-centrosymmetric (e.g., TaAs-family) and magnetic materials (e.g., Mn_3Sn) through angle-resolved photoelectron spectroscopy (ARPES) and magneto-transport measurements [4,5].

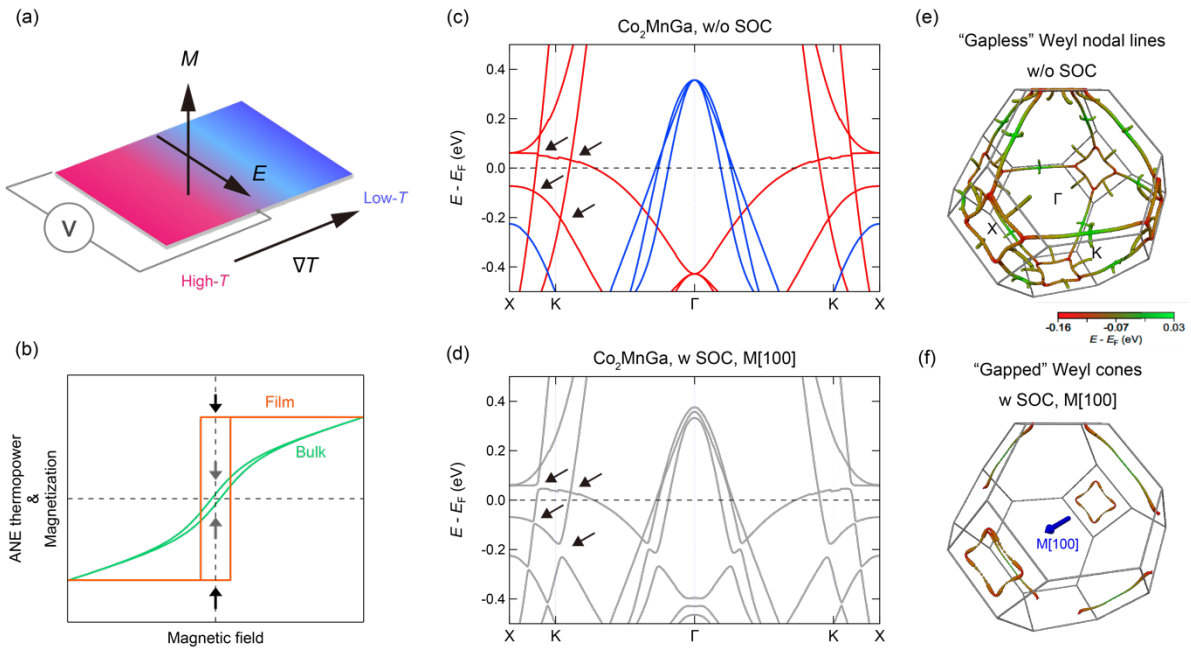

FIGURE 1. Schematic illustrations of (a) the ANE and (b) the ANE thermopower and magnetization of Heusler alloy in bulk and film forms. Black and gray arrows indicate the remanence magnetization. (c,d) Calculated band structures of Co_2MnGa Heusler alloy without and with spin-orbit coupling (SOC). Red and blue colors correspond to the majority and minority spin. (e,f) Three-dimensional view of the Weyl nodal lines of Co_2MnGa without and with SOC. Color corresponds to the location of the Weyl node. The blue arrow in (f) indicates the direction of magnetization.

Recently, Co_2MnGa and Co_2MnAl Heusler alloys have also been theoretically predicted to be a ferromagnetic Weyl semimetal [6] and has been experimentally demonstrated in the bulk form to exhibit large anomalous transport properties under an external magnetic field [1,2,3]. The nature of this highly symmetric crystal creates mirror-symmetry-protected Weyl nodal lines in the band structure as encountered by theory [Figs. 1(c) and 1(e)] and experiments [7]. However, the nodal lines lead to vanishing Berry curvature when integrated over the whole Brillouin zone and cannot explain the observed phenomena. One way to obtain a large Berry curvature is to gap out their nodal lines using remanent magnetization or an external magnetic field (specifically, to break the mirror symmetry) [Figs. 1(d) and 1(f)]. Yet, the experimental evidence for broken mirror symmetry was not provided by the recent ARPES measurement on bulk Co_2MnGa crystal because the remanent magnetization was negligible [Fig. 1(b)] as applying external magnetic fields is not permitted in this measurement. For practical applications in which zero-field operation and gigantic outputs are a requirement, it is thus indispensable to truly understand the band structure responsible for the anomalous transport properties in films with full remanent magnetization.

In this talk, I show the spin-polarized band structure and anomalous transport properties of ferromagnetic Co_2MnGa thin films [8]. Growth of high-quality thin films possessing full remanent magnetization and in situ spin-resolved ARPES (SARPES) measurements permit access to their non-trivial band structures modified by the broken mirror symmetry. We observed spin-polarized Weyl cones located mostly at a Lifshitz quantum critical point and a flat band of surface states [Fig. 2]. Furthermore, when the energy associated with the "massive" Weyl cone approaches E_F, the AHE and ANE conductivities systematically increase as the electron number rises. In particular, the ANE reaches thermopower of ~6.2 μV/K at room temperature, which is the highest amongst magnetic films to the best of our knowledge. In addition, I also present the spin-polarized band structure of the quaternary $Co_2Mn(Al,Si)$ Heusler film. We succeeded in doping electrons about 350 meV in the Weyl ferromagnet Co_2MnAl by Si substitution and revealed that the spin-polarized multiple Weyl cones and half-metallic gap coexist in the bulk electronic structure [9].

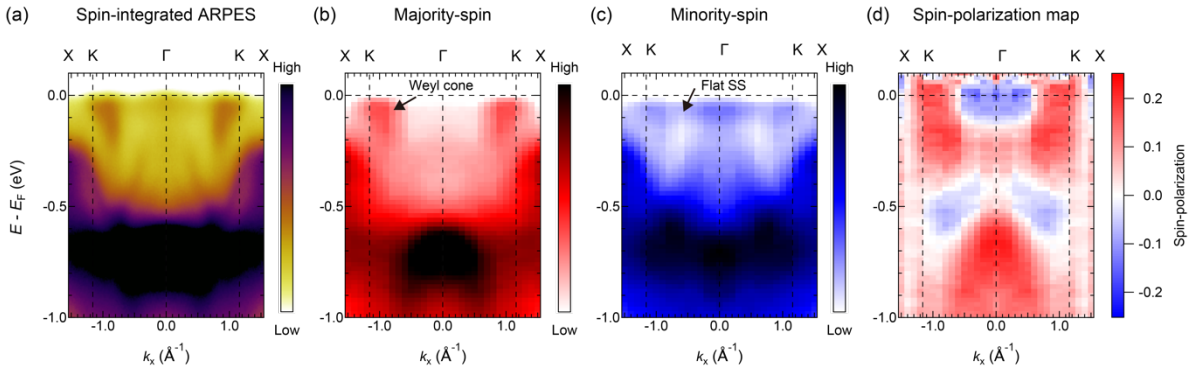

FIGURE 2. (a) Spin-integrated ARPES image of Co-rich Co_2MnGa film along Γ-K-X line recorded at 80 eV with *p*-polarized light. (b,c) SARPES images of the majority and minority spin states. (d) Spin-polarization map. ARPES and SARPES images are symmetrized with respect to the Γ point.

REFERENCES

1. A. Sakai *et al*., *Giant anomalous Nernst effect and quantum-critical scaling in a ferromagnetic semimetal*, Nat. Phys. **14**, 1119 (2018).
2. S. N. Guin *et al*., *Anomalous Nernst effect beyond the magnetization scaling relation in the ferromagnetic Heusler compound Co_2MnGa*, NPG Asia Materials **11**, 16 (2019).
3. P. Li *et al*., *Giant room temperature anomalous Hall effect and tunable topology in a ferromagnetic topological semimetal Co_2MnAl*, Nat. Phys. **11**, 3476 (2020).
4. S.-Y. Xu *et al*., *Discovery of a Weyl fermion semimetal and topological Fermi arcs*, Science **349**, 613 (2015).
5. K. Kuroda *et al*., *Evidence for magnetic Weyl fermions in a correlated metal*, Nat. Mater. **16**, 1090 (2017).
6. J. Kuebler and C. Felser, *Weyl points in the ferromagnetic Heusler compound Co_2MnAl*, EPL **114**, 47005 (2016).
7. I. Belopolski *et al*., *Discovery of topological Weyl fermion lines and drumhead surface states in a room temperature magnet*, Science **365**, 1278 (2019).
8. K. Sumida *et al*., *Spin-polarized Weyl cones and giant anomalous Nernst effect in ferromagnetic Heusler films*, Commun. Mater. **1**, 89 (2020).
9. K. Sumida *et al*., *in preparation.*

Chirality-Induced Spin Polarization in Chiral Crystals

Yoshihiko Togawa

Department of Physics and Electronics, Osaka Prefecture University, Sakai, Osaka 599-8531 Japan

Keywords: Chirality, Spin polarization, Macroscopic spin response

A role of chirality in materials is discussed in terms of an emergence of macroscopic spin response, being inspired by recent works on chiral magnetism and chirality-induced spin polarization. These viewpoints may bring us to a new frontier of chiral material science. In this connection, we will focus the experimental findings that chiral materials exhibit a spin-polarized state when the charge current is injected into them [1-4]. A spin-polarized transport occurs in a linear regime of the current-voltage characteristics. Importantly, a robust protection of the spin polarization enables a nonlocal spin transport over micrometers or longer. A comprehensive understanding of these nontrivial spin response remains an important issue and may clarify the interplay between structural and dynamical chirality. This work was done in collaboration with the laboratory members in OPU. I sincerely appreciate their great efforts on performing experiments.

REFERENCES

1. A. Inui, R. Aoki, Y. Nishiue, K. Shiota, Y. Kousaka, H. Shishido, D. Hirobe, M. Suda, J. Ohe, J. Kishine, H. M. Yamamoto, Y. Togawa, *Physical Review Letters* **124**, 166602 (2020).
2. Y. Nabei, D. Hirobe, Y. Shimamoto, K. Shiota, A. Inui, Y. Kousaka, Y. Togawa, and H. M. Yamamoto, *Applied Physics Letters* **117**, 052408 (2020).
3. K. Shiota, A. Inui, Y. Hosaka, R. Amano, Y. Onuki, M. Hedo, T. Nakama, D. Hirobe, J. Ohe, J. Kishine, H. M. Yamamoto, H. Shishido, and Y. Togawa, *Physical Review Letters* **127**, 126602 (2021).
4. H. Shishido, R. Sakai, Y. Hosaka, and Y. Togawa, *Applied Physics Letters* **119**, 182403 (2021).

Construction and Operation of Superconducting Bending Magnets in Aichi-SR

Yoshifumi Takashima[a,b]

[a] *Synchrotron Radiation Research Center, Nagoya University, Furo-cho, Chikusa-ku, Nagoya City, Aichi, 464-8601, Japan*
[b] *Aichi Synchrotron Radiation Center, Minamiyamaguchi-cho 250-3, Seto City, Aichi, 489-0965, Japan*

Keywords: Superconducting magnet, Storage ring.

Aichi Synchrotron Radiation Center (Aichi-SR) started public use of synchrotron radiation in March 2013 [1]. The facility is operated mainly by Aichi Science & Technology Foundation and is supported by universities, Aichi Prefecture, and industry. At present, 11 beamlines are in operation, including one each from industry and university, and a new beamline for the industry is under construction.

Accelerators of the Aichi-SR consist of a 50 MeV linear accelerator, a 1.2 GeV booster synchrotron, and a 1.2 GeV electron storage ring of a 72 m circumference [2-5]. A notable feature of the Aichi-SR accelerator is that it uses superconducting bending magnets (superbends) to supply synchrotron radiation to multiple beamlines with energies exceeding 10 keV, despite the relatively low electron energy of 1.2 GeV [6]. The magnetic lattice configuration is the four-fold symmetry of triple-bend cell. In the unit cell of the three bending magnets, the two at both ends are normal-conducting magnets with a magnetic field of 1.4 T and a bending angle of 39°, and the one in the center is a superconducting magnet with a peak magnetic field of 5 T and a bending angle of 12°. Figure 1 and Figure 2 show the layout of the accelerators, and the flux of synchrotron radiation from the superbend and the normal-conducting bending magnet at Aichi-SR.

For the cooling of the superbends, a small 4K-GM type refrigerator is placed one by one in each superbend, and the superconducting coils are cooled directly. The direct cooling method, which does not use liquid helium, is advantageous not only in terms of cost but also in terms of ease of maintenance, such as handling in case of quenching. Figure 3 shows a photo of the suberbends.

The refrigerators of the superbends need to be maintained after 10,000 hours of operation. Immediately after the refrigerator was replaced, the temperature rose to about 60 K, but it reached below 3.6 K in about 24 hours. The maintenance of the refrigerators is done once a year, and in all cases since the construction of Aichi-SR, the coil temperature returns to below 3.6 K after the maintenance.

The superbends of the Aichi-SR have had some trouble with the refrigerators, but no problem with the magnets themselves and are now operating smoothly.

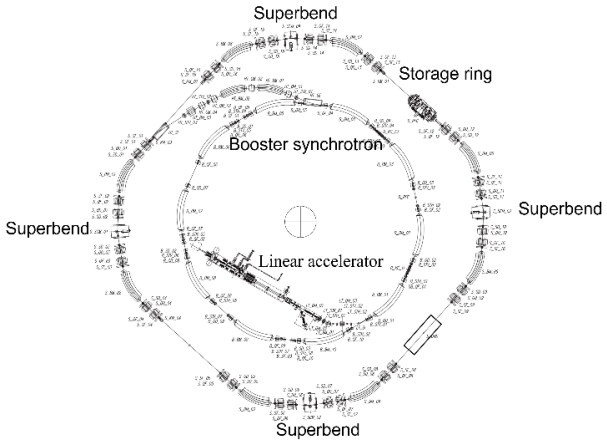

FIGURE 1. Layout of Aichi-SR accelerators.

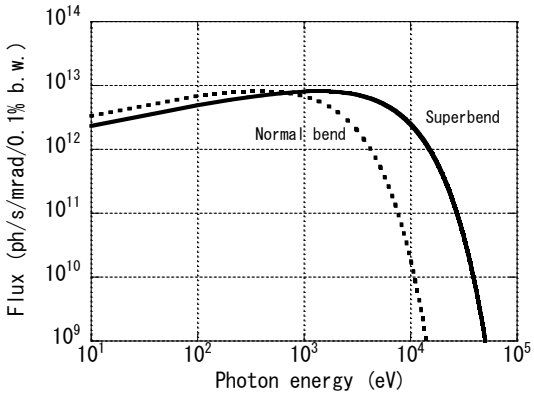

FIGURE 2. Flux of synchrotron radiation from the superconducting bending magnet (Superbend) and the normal-conducting bending magnet (normal bend).

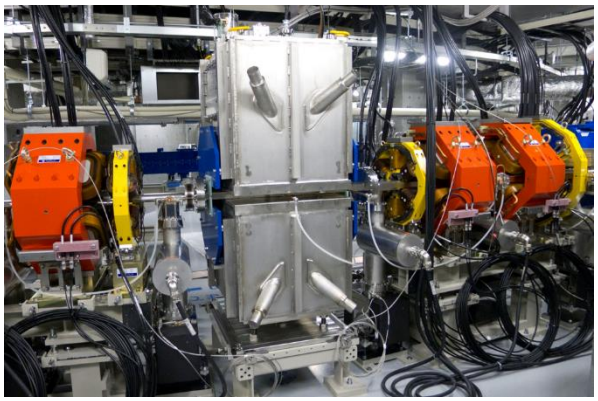

FIGURE 3. Superconducting bending magnet of Aichi-SR.

ACKNOWLEDGMENT

I want to great thank Prof. M. Katoh of HiSOR, Prof. M. Hosaka of USTC, and Associate Prof. N. Yamamoto of KEK for their tremendous support in the basic design, commissioning, and machine study of the Aichi-SR accelerators. In the daily operation of the Aichi-SR accelerators, I am very grateful for the contribution of the Aichi-SR accelerator division staff. Furthermore, I greatly appreciate Toshiba Corporation for their significant contribution to constructing the accelerators, including the superbends. I am also very grateful to Dr. M. Torikoshi of NIRS for allowing us to borrow their superconducting wiggler test machine.

REFERENCES

1. https://www.aichisr.jp/index.html
2. A. Mochihashi et al., "PRESENT STATUS OF ACCELERATORS IN AICHI SYNCHROTRON RADIATION CENTER", Proceedings of IPAC2017, Copenhagen, Denmark, 2017, pp. 2691-2693.
3. Y. Takashima et al., "PRESENT STATUS OF ACCELERATORS IN AICHI SYNCHROTRON RADIATION CENTER", Proceedings of IPAC2016, Busan, Korea,2016, pp. 2877-2879.
4. N. Yamamoto et al., “ACCELERATORS OF THE CENTRAL JAPAN SYNCHROTRON RADIATION FACILITY PROJECT (II)”, Proceedings of IPAC2011, San Sebastián, Spain, 2011, pp. 2987-2989.
5. N. Yamamoto et al., “ACCELERATORS OF THE CENTRAL JAPAN SYNCHROTRON RADIATION FACILITY PROJECT”, Proceedings of IPAC2010, Kyoto, Japan, 2010, pp. 2567-2569.
6. M. Hosaka et al., "PRESENT STATUS OF SUPER-CONDUCTIVE BENDING MAGNETS AT AICHI SR", Proceedings of the 10th Annual Meeting of Particle Accelerator Society of Japan, Nagoya, Japan, 2013, pp. 461-464.

Recent Results from Design Study on HiSOR-2

Masahiro Katoh[a,b]

[a]*Hiroshima University,1-3-1 Kagamiyama, Higashi-Hiroshima 739-8526, Japan*
[b]*Institute for Molecular Science, National Institutes of Natural Sciences, 38 Nishigo-Naka, Myodaiji, Okazaki, 444-8585, Japan*

Keywords: Synchrotron light source, electron storage ring.

HiSOR, a low energy and compact synchrotron light source in Hiroshima University, has two straight sections and is capable of producing high-brightness light in the vacuum ultraviolet range from two undulators. It has two normal conducting bending magnets, which have high field strength of 2.7 T and are capable of producing synchrotron radiation in a wide range including tender X-rays even with the low electron energy, 700MeV. Since no major upgrade has been made on the accelerator since its construction in 90's, the operation of HiSOR is well established and stable in these years. On the other hand, after 25 years from its construction, the hardware has been being aged and its competitiveness in terms of light source performance are being lowered among the newly constructed light sources over the world. Some of the light sources in Japan, such as Photon Factory [1] or UVSOR [2], have been upgraded with some major modifications of the hardware. SPring-8 also has an upgrade plan [3]. In case of HiSOR, it was designed and manufactured by a single company. It has a rational design without redundancy. Therefore, it is difficult to make a major modification to improve the performance or introduce new technologies to the present machine. Therefore, we have been designing a completely new ring for the future plan of the facility [4].

The latest version of the design [4] is as follows; the circumference is about 50 m and the electron energy is 500 MeV. The emittance, which is the most important parameter to achieve high brightness, is around 10nm, which is smaller by two orders of magnitudes than the present value, 400nm. It has six straight sections and four of them can be used for installing undulators. It would have a full energy injector for the top-up operation, which consists of a linear accelerator and a booster synchrotron. We believe such a new facility is ideal for further developing the research activities which have been carried out at HiSOR for over twenty years. On the other hand, this plan requires a significant budget, which may not be easy to be approved. In addition, the feasibility of this plan also depends largely on the trends of the future plans of other synchrotron light sources in Japan. Therefore, as leaving this plan as one candidate, we have started designing alternative plan, which might be realized with less budget.

To reduce the construction cost as keeping the high performance as possible, we have designed a compact storage ring as shown in Fig. 1. The circumference is about 30 m and the electron energy is 500 MeV. The emittance is 17 nm. The ring has six 2.2 m straight sections, four of which can be used for undulators. The diameter of the ring is almost same as the major axis of the present HiSOR ring. This compactness may reduce the construction cost of the accelerator. One interesting possibility is to install this ring in the present experimental hall. If this is the case, the total construction cost would be reduced significantly.

The magnetic lattice of the new design is very simple, which may be realized with combined-function magnets. The bending magnets should produce quadrupole and sextupole fields and the quadrupole magnets sextupole fields as well as dipole fields for beam steering. It was proved that, after compensating the linear chromaticity with two families of sextupoles, the dynamic aperture is sufficiently large. The beam injection may be realized with a pulsed multipole magnet [5].

In adding to making the storage ring compact, one interesting possibility to further reduce the construction cost is utilizing the present HiSOR storage ring as an injector. We can find several examples of such utilization of older storage rings as injectors for new rings, even though they were not capable of rapid cycling of acceleration [6, 7]. In our case, the electron beam from the existing 150 MeV microtron is injected to the present HiSOR ring and is accelerated up to 500 MeV, then is extracted and transferred to the new ring. Since it is expected that the construction cost of a full energy injector is almost as high as that of the new storage ring, the recycling of old accelerator is effective to reduce the cost. An interesting possibility

for further reduction of the cost is moving the present HiSOR to the injector room and constructing new storage ring in the present storage ring room.

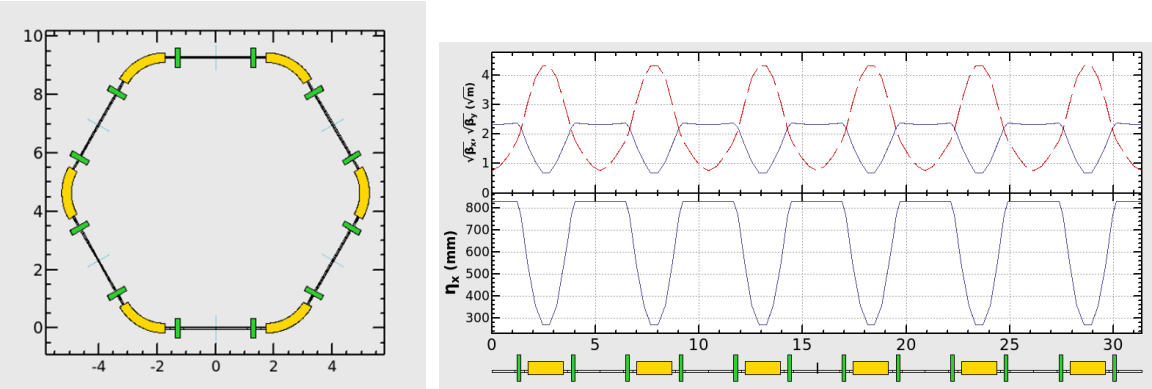

FIGURE 1. Magnetic lattice (left) and optical functions (right) of the new lattice design for HiSOR-2.

The typical synchrotron radiation spectra are shown in Fig. 2. For comparison with the present ring, we calculated the spectra for the undulators which are currently operational in the present HiSOR. The brightness is improved by more than one order of magnitudes. Since the electron energy of HiSOR-2 is lower than the present value, the spectral ranges shift to the lower photon energy. Shorter period undulators may be installed to cover the higher energy range.

In the present HiSOR, the photon energy range up to the tender X-rays is covered with the bending radiation from the high field normal conducting bending magnets. In HiSOR-2, the bending magnets will be normal conducting and have ordinary field strengths such as around 1 T. In addition, the electron energy is lower. Therefore, the bending radiation cannot cover the X-ray range. If there are strong demands for the X-rays, one idea is to replace two or three bending magnets with superconducting ones of 5 T. In this case, even with the lower electron energy, the ring can cover almost same photon energy range. The electron beam optics should be designed carefully not enlarging the emittance so much.

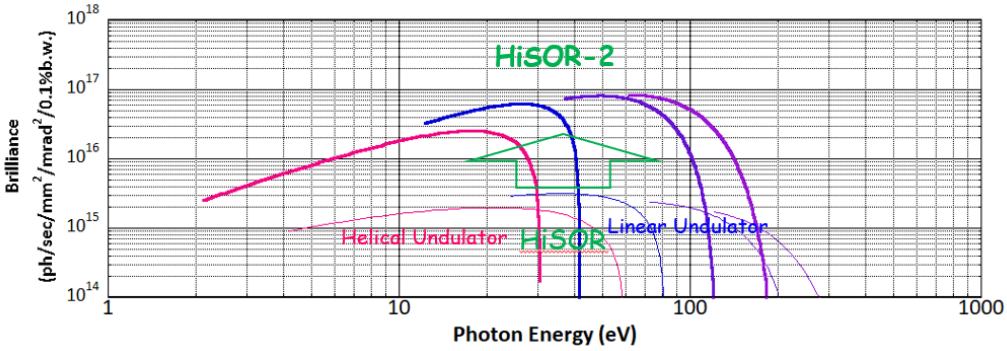

FIGURE 1. Synchrotron radiation spectra on the alternative design of HiSOR-2. The undulator parameters are same as the present HiSOR.

REFERENCES

1. M. Katoh *et al*., *J. SYNCHROTRON RAD.* 5(3) 366 - 368 (1998).
2. M. Katoh *et al*., *Nucl. Instr. Meth. A*. 467, 68 - 71 (2001).
3. http://rsc.riken.jp/pdf/SPring-8-II.pdf.
4. S. Matsuba *et al., J. Phys. Conf. Ser*. 1350 012015-1~5 (2019).
5. K. Hirata *et al*., HiSOR Activity Report 2019, 12 (2020), .
6. G. LeBlanc *et al*., Proc. EPAC'96, 345 (1996).
7. S.P. Møller *et al*., Proc. iPAC2013, 64 (2013).
6. K. Hiramatsu *et al*., HiSOR Activity Report 2020, 11 (2021).

Applications of the Generalized-High Accuracy Universal Polarimeter (G-HAUP) to Solid State Sciences

Toru Asahi[a,b] and Kenta Nakagawa[c]

[a] *Faculty of Science and Engineering, Waseda University, 2-2 Wakamatsu-cho, Shinjuku-ku, Tokyo, 162-8480, Japan.*
[b] *Research Organization for Nano & Life Innovation, Waseda University, 513 Wasedatsurumaki-cho, Shinjuku-ku, Tokyo, 162-0041, Japan.*
[c] *Kanagawa Institute of Industrial Science and Technology (KISTEC), 705-1 Shimo-imaizumi, Ebina, Kanagawa, 243-0435, Japan*

Keywords: Magneto-optics, Faraday rotation, CeF_3 single-crystal, G-HAUP.

The optical study on condensed matters is a powerful tool for investigating spatial symmetry breaking and/or time-reversal symmetry breaking. Optical activity (OA) and circular dichroism (CD) are related to spatial and time-reversal symmetry. Natural OA and CD, which are reciprocal signals, were observed when the spatial symmetry was broken. On the other hand, Faraday rotation and magnetic circular dichroism, which are non-reciprocal signals, were observed when the time-reversal symmetry was broken. [1] Here, we emphasize the consideration of linear birefringence (LB) and linear dichroism (LD) in the measurement of OA and CD in anisotropic crystals. LB and LD are optical anisotropies that denote the difference in refractive indices and absorptions, respectively, between two orthogonally polarized lights in an anisotropic crystal. Schellman *et al.* [2] reported that LB and LD signals are usually 10^3–10^5 times larger in magnitude than OA and CD signals. Therefore, the accurate separation of OA and CD from LB and LD is a challenge. Furthermore, Shindo *et al.* [3] pointed out that optical elements, devices, and detectors installed in polarization modulation spectroscopy cause serious systematic errors and non-negligible artifacts. This critical issue has been widely recognized in the field of chiral science. Many research groups have developed optical measurement theories and polarimeters to overcome this issue. Eventually, OA and CD in the anisotropic condensed matter were successfully measured. In particular, we developed a novel optical apparatus called the generalized-high accuracy universal polarimeter (G-HAUP), which simultaneously measures the wavelength dependences of the OR, CD, LB, and LD in an anisotropic medium. [4–10] Regardless, some researches in the field of magneto-optics neglected optical anisotropies, systematic errors, and artifacts in OA and CD measurements.

This study investigates the wavelength dependences of linear birefringence, linear dichroism, Faraday rotation and magnetic-circular dichroism in a single crystal rare-earth fluoride, namely CeF_3. The subject material selected Faraday rotator in the present study CeF_3 single crystal, is characterized by its wide transparency range (300 nm to 2500 nm) and an outstanding Verdet constant, besides of being uniaxial. Cerium is usually found as a trivalent ion Ce^{3+} in condensed matter. The electronic configuration of Ce^{3+} is $1s^2 2s^2 2p^6$ … $4d^{10} 4f^1 5s^2 5p^6$. Electronic transitions from 4*f* to 5*d* confer the magneto-optical properties observable in the UV-Vis-IR region1. In a previous report, the refractive indices of the ordinary and extraordinary light rays in single crystal CeF_3 at 633 nm were determined as 1.616 and 1.609, respectively. Therefore the LB is 0.007, comparable to that of the α-quartz crystal along its *a* axis. Even at this low order of LB magnitude (10^{-3}), the OR of the crystal cannot be accurately measured by conventional optical apparatuses [16]. Previously, When a sample is subjected to a magnetic field applied parallel/anti-parallel to the light propagation direction, the G-HAUP can measure its FR and Magnetic-CD (MCD). In this study, we measured the wavelength dependences of the FR, MCD and optical anisotropy in CeF_3 single crystal along the optic axis (*c* axis) and perpendicular to the optic axis (*a* axis) with the G-HAUP. [9] A magnetic field parallel/anti-parallel to the light propagation was generated by Nd-Fe-B (NIB) magnets introduced for that purpose.

We prepared a 307-μm thick (001) plate of single-crystal CeF_3 by polishing. In structure, the CeF_3 crystal belongs to the uniaxial and optically inactive crystal point group D_{3d}. Therefore, when the magnetic field is applied parallel to the light propagation direction, FR occurs only along the *c* axis. To apply the magnetic

field parallel or anti-parallel to the light propagation direction, we mounted the sample on a pinhole plate, and sandwiched it between two ring NIB permanent magnets. The wavelength dependences of the Verdet constant along the *c* axis at 25 °C are plotted as black rhombuses in Fig. 1(c). The Verdet constants along the *c* axis were positive over the observed wavelength region, indicating that the right-handed circularly-polarized light propagates faster than its left-handed counterpart.

We then prepared a 58.0-μm thick (100) plate sample of single-crystal CeF_3 by polishing. Before measuring the magneto-optical properties, we determined the wavelength dependences of the LB, LD, OR and CD along the *a* axis in the absence of the magnetic field at 25 °C (blue rhombuses in Fig. 1). The LB along this axis was of the same order of magnitude as the LB of α-quartz crystal (Fig. 1(a)). However, the LDs were almost zero over the wavelength region (Fig. 1(b)). This result is consistent with the UV-Vis spectrum, which exhibits no significant absorption above 282 nm.

Then, the wavelength dependences of the LB, LD, FR, and MCD along the *a* axis under a magnetic field parallel to the light propagation direction at 25 °C were measured (red rhombuses in Fig. 1). In general, reversing the magnetic field direction inverted the signs of FR and MCD. Therefore, in order to obtain accurate spectra, we applied the magnetic field anti-parallel to the light propagation direction, re-measured the wavelength dependences, and averaged the absolute magnitudes of both sets of measurements. The values of LB and LD hardly changed with and without the magnetic field (Fig. 1(a,b)). The Verdet constants along the *a* axis were positive throughout the wavelength region (Fig. 1(c)).

In conclusion, the wavelength dependences of LB, LD, FR and MCD were investigated along the *a* and *c* axes of single crystal CeF_3 under an applied magnetic field. These measurements were successfully collected by the G-HAUP equipped with NIB magnets. The Verdet constants along the *c* and *a* axes were positive and nearly equal in magnitude in the measured wavelength region.

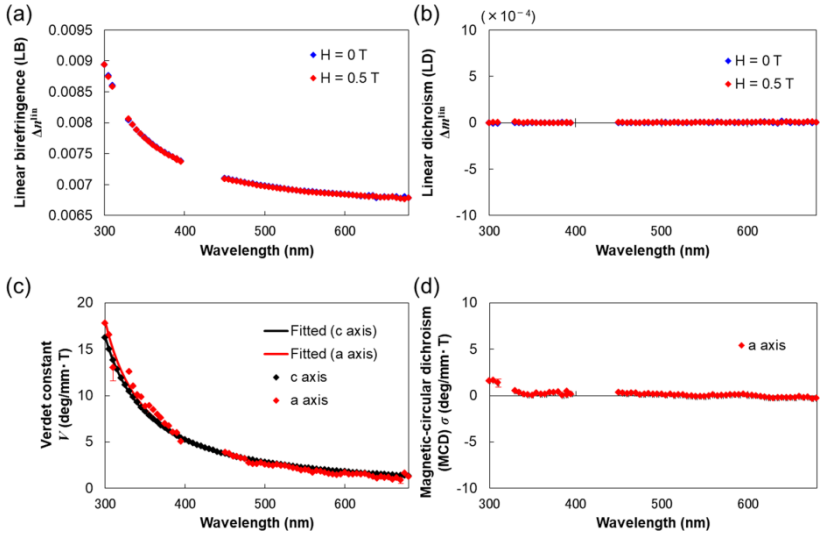

Figure 1. Wavelength dependences of the LB (a), LD (b), Verdet constant (c) and MCD (d) in single-crystal CeF_3 at 25 °C. Reproduced from Ref. [9] with permission from Springer Nature.

REFERENCES

1. L. D. Barron, Molecular Light Scattering and Optical Activity (Cambridge University Press, New York, (2004) 2nd *ed*.
2. J. A. Schellman and H. P. *Jensen, Chem. Rev.* **87**, 1359 (1987).
3. Y. Shindo, M. Nishiro, and S. Maeda, *Biopolymers* **30**, 405 (1990).
4. M. Tanaka, N. Nakamura, H. Koshima, and T. Asahi, *J. Phys. D* **45**, 175303 (2012).
5. K. Nakagawa, H. H. Lovelady, Y. Tanaka, M. Tanaka, M. Yamato, and T. Asahi, *Chem. Commun.* **50**, 15086 (2014).
6. A. Takanabe, M. Tanaka, K. Johmoto, H. Uekusa, T. Mori, H. Koshima, and T. Asahi, *J. Am. Chem. Soc.* **138**, 15066 (2016).
7. K. Ishikawa, Y. Terasawa, M. Tanaka, and T. Asahi, *J. Phys. Chem. Solids* **104**, 257 (2017).
8. K. Nakagawa, A. T. Martin, S. M. Nichols, V. L. Murphy, B. Kahr, and T. Asahi, *J. Phys. Chem. C* **121**, 25494 (2017).
9. K. Nakagawa and T. Asahi, *Sci. Rep.* **9**, 18453 (2019).
10. Kun Zhang, M. Matsumoto, K. Nakagawa, A. Matsuda, G. Shino, S. Sato, T. Ikeda, and T. Asahi, *J. Phys. Soc. Jpn.* **90**, 113702 (2021)

Exploring active structures of DNA repair protein XRCC4 using CD and SAXS

Akinari Yokoya[a,b], Kai Nishikubo[b,a] and Maho Hasegawa[b,a]

[a]*National Institutes for Quantum Science and Technology, Institute for Quantum Life Science, 2-4 Shirakata, Tokai, Ibaraki 319-1106, Japan*
[b]*Graduate School of Science and Engineering, Ibaraki University, 2-1-1, Bunkyo, Mito 310-8512, Japan*

Keywords: DNA double strand breaks, DNA repair, XRCC4, CD, SAXS, Intrinsically disordered protein.

INTRODUCTION

Ionizing radiation often produces DNA double strand breaks (DSBs). To prevent serious genetic effects from the genome damage, living cells promptly repair DSBs through several pathways. Non-homologous end joining (NHEJ) repair, which is one of the major processes, involves various proteins to rejoin separated DNA ends. XRCC4, a key player of NHEJ, constitutes a polymeric platform of the repair. Normal homodimer formation is thought to change to multimerization by post transcriptional modifications, such as phosphorylation of serine residues, by the certain kinases. So far, protein crystallography was applied to a single crystal of C-terminal deficient XRCC4. The C-terminal tail possesses five phosphorylation sites but is an intrinsically disordered region preventing it from crystallization. Our goal is to elucidate the structural character of dimer and multimer of the full length XRCC4. Two synchrotron analysis methods, namely VUC-circular dichroism (CD) and small-angle X-ray scattering (SAXS) were applied.

EXPERIMENTALS

Purification of XRCC4

To express full-length human XRCC4 (336 amino acids) linked with 6 histidine residues (HisTag), XRCC4 cDNA was obtained from human leukemia cells and inserted into the pET21d plasmid vector. The plasmid was introduced into *E. coli* cells (BL21DE3 Gold) and XRCC4 expression was induced by adding isopropyl β-D-1-thiogalactopyranoside (IPTG) to the culture medium. Using a HisTrap column, XRCC4 was extracted from harvested bacterial cells after homogenizing. The protein was eluted from the column with a buffer containing imidazole (200 mM). XRCC4 dimers were separated from its multimers by gel filtration chromatography. The agarose gel electrophoresis analysis suggested that the multimers inevitably contained a minimal DNA. We used the multimers for CD and SAXS without further purifications.

To mimic phosphorylation, we produced mutated XRCC4 proteins in which the serine residues, S260, S320, S327 or S328, were substituted with a negatively charged aspartic acid, hereinafter denoted as $XRCC4^{S260D}$, $XRCC4^{S320D}$, $XRCC4^{S327D}$ or $XRCC4^{S328D}$, respectively. The mutations were introduced in the XRCC4 coding region using a commercial kit. The results of the pseud-phosphorylated proteins were compared with wild type XRCC4 ($XRCC4^{WT}$).

CD measurements at HiSOR

CD spectroscopy was carried out at BL-12 at the Hiroshima Synchrotron Radiation Center (HiSOR). Protein sample of $XRCC4^{WT}$, $XRCC4^{S260D}$ or $XRCC4^{S327D}$ was dissolved in the sodium phosphate buffer. The sample was encapsulated in a CaF2 cell (path length, 50 μm). CD spectra were measured between 175 and 260 nm at 25°C.

SAXS measurements at the Photon Factory

SAXS was performed at BL-6A at the Photon Factory (PF) in KEK. Each XRCC4 protein sample was dissolved in HEPES buffer at 25°C. The wavelength of X-rays was 1.5 Å (8.3 keV) and the PILATUS-detector (Pixel Apparatus for the SLS) was set at 2500 mm from the sample to detect diffracted X-rays. Volume of the sample cell with a thin polyimide film window was 40 μl and the path length was 1mm.

RESULTS

Secondary structures of XRCC4 determined by CD

The obtained CD spectra of dimer and multimer of the wild type and mutated XRCC4 are shown in Fig. 1. All peak intensities at 190, 210 and 220 nm of the multimer were notably smaller than those of dimer. For

mutated proteins, we also obtained similar CD spectra of their dimer and multimer samples. The secondary structure contents of each sample were calculated using an analysis program SELCON3 and the obtained values are shown in Table 1. Comparing with a previous crystallographic study [1], α-helices and turns were significant in the intrinsically disordered C-tail. The β-strand contents were more explicit for the mutated samples. Interestingly the fraction of the β-strands was noticeably larger in multimers than in dimer.

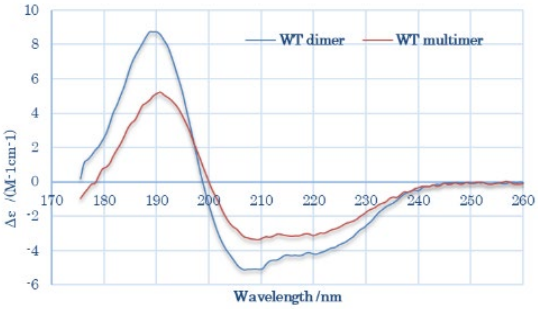

FIGURE 1. CD spectra of the dimer and multimer of wild type XRCC4.

TABLE 1. Secondary structure contents of dimer and multimer of the wild type and mutated XRCC4.

Structure content (%)			α-Helix	β-Strand	Turn	Unordered
Crystallography [1] *			38	26	8	28
CD	Wild type	dimer	50.8±0.9	5.8±0.8	20.1±2.2	23.2±2.1
		multimer	36.4±1.0	15.7±0.8	22.5±1.4	25.4±0.6
	S260D	dimer	50.2±1.9	7.1±3.6	19.7±2.7	23.0±1.2
		multimer	34.2±0.5	17.3±0.9	23.1±0.3	25.5±1.1
	S327D	dimer	47.4±2.1	11.5±4.5	18.4±4.1	22.8±1.3
		multimer	32.0±1.7	19.6±0.8	22.7±0.2	25.7±1.2

* The length of amino-acid sequence is 1th–203rd residues.

SAXS profiles of dimer and multimer of XRCC4

The scattering curve strongly depended on the state of polymerization of XRCC4 (Fig. 2). However, the pseud-phosphorylation did not noticeably affect the scattering pattern. In the low-q region for dimmers, we were able to perform Guinier plot using SAngler 2.1.3 assuming the proteins were a globular shape. For multimer, we found a q-region in which Cross-sectional Guinie plot (inset in the right panel of Fig.2) was applicable by assuming the multimers were rod shape. We obtained radii of inertia (Rg) of the dimers and cross-sectional radii of inertia (Rc) of the multimers. Rg values were about 50Å for the wild type as well as mutated ones. Rc values were slightly larger (roughly 60-70 Å) than Rg for each sample. Thus, the multimers were presumed to be filament like shape.

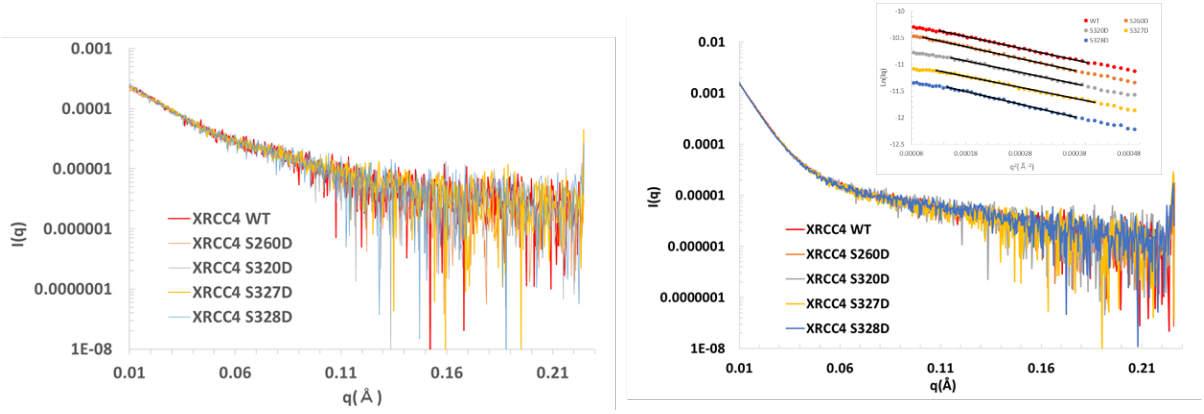

FIGURE 2. SAXS curves of dimers (left) and multimers (right) of wild type and mutated XRCC4. Inset indicates Cross-sectional Guinie plot for the scattering curves of the multimers.

DISCUSSION

The two analyses for the full-length XRCC4 in solution strongly suggest that the intrinsically disordered C-terminal tail plays an important role to induce a conformational change from inactivated homodimer to activated multimer by boosting β-strand formation as indicated by CD measurements. The phosphorylation at the C-terminal may facilitate the multimerization. Multimers formed in this way are filament-like and, presumably, include DNA molecule as a component of the super-molecular-complex of a DSB repair platform (Fig. 3).

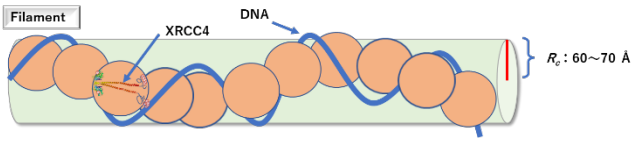

FIGURE 3. A filament model of XRCC4 multimers with DNA.

REFERENCES

1. M. S. Junop, M. Modesti, A. Guarné, R. Ghirlando, M. Gellert, and W. Yang, *EMBO J.* **19**, 5962-59 (2000).

Poster Session

The order of flash poster session

Thursday, 10 March, 2022　13:15 – 14:00

The flash talk is about 1~2 min/person.

P01S	Re-examination of the Phase Diagram of $Bi_2Sr_2CaCu_2O_{8+\delta}$ Studied by ARPES Presenter: Y. Tsubota (Hiroshima University)
P06S	lectronic structure of Half-metallic ferromagnet CrO_2 studied by VUV-ARPES Presenter: T. Setoguchi (Okayama University)
P09S	Hard X-ray absorption spectroscopy of a gold complex included by cyclodextrin Presenter: K. Baba (Hiroshima University)
P10S	Investigation of the photo-induced doping mechanism of TlBiSe2 Presenter: R. Itaya (Osaka University)
P14S	Desiccation-Induced Conformational Change of Group 3 LEA Protein in the presence of Membrane Characterized by Vacuum-Ultraviolet Circular Dichroism Spectroscopy Presenter: S. Sawada (Hiroshima University)
P15S	Orientation Analysis of Antimicrobial Peptide Magainin 2 Bound to Phospholipid Membrane by Synchrotron-Radiation Linear Dichroism Spectroscopy Presenter: M. Kumashiro (Hiroshima University)
P16S	Analysis of structural change of XRCC4 by pseudo-phosphorylation using VUV-CD and SAXS Presenter: K. Nishikubo (Ibaraki University)
P17S	NEXAFS Study of Fullerene Adsorbed on Aminothiophenol Self-Assembled Monolayer Presenter: K. Kono (Hiroshima University)
P19S	Soft X-ray Polarization Measurements of Phospholipid Multilayers Supported on Hydrophilic Si Surfaces Presenter: M. Tabuse (Hiroshima University)
P20S	Interface structure of Co ultrathin films evaporated on h-BN/Ni(111) studied by LEED analysis Presenter: W. Nishizawa (Hiroshima University)
P21S	Evolution of c-f hybridization in valence transition compound $YbInCu_4$ observed by ARPES Presenter: R. Kamimori (Hiroshima University)

P22S	Evaluation of Self-Energy in Overdoped Bi2201 by Angle-Resolved Photoemission Spectroscopy Presenter: Y. Miyai (Hiroshima University)
P23S	Direct Observation of the Three-dimensional Electronic Structure of RMnSi (R=La, Ce) with Noncentrosymmetic Antiferromagnetic Order Presenter: K. Shiraishi (Hiroshima University)
P24S	Membrane-Bound Conformations of Magainin 2 depending on the Inherent Characteristics of Membrane Revealed by Synchrotron-Radiation Circular-Dichroism Spectroscopy Presenter: R. Tsuji (Hiroshima University)
P25S	Spatial inhomogeneity in $Bi_2Sr_2CaCu_2O_{8+\delta}$ investigated by micro photoemission spectroscopy Presenter: T. Sugiyama (Hiroshima University)
P26S	Minority-spin Dominated Band Structure Near the Fermi Energy of Fe4N Film Revealed by Spin- And Angle-Resolved Photoemission Spectroscopy Presenter: K. Nakanishi (Hiroshima University)
P27S	Many-body Interactions on the Surface of the Topological Insulators Presenter: A. Kumar (Hiroshima University)
P29S	Development of Time-Resolved Vacuum-Ultraviolet Circular Dichroism Spectroscopy and its Application to the Interaction Analysis between β-Lactoglobulin and Lipid Membrane Presenter: S. Hashimoto (Hiroshima University)
P30S	Direct observation of Dirac nodal-line fermions in P-square net superconductor, $ZrP_{1.24}Se_{0.57}$ Presenter: S. Ishizaka (Hiroshima University)
P33S	Observation of fast Dirac nodal-line fermions in a nonsymmorphic superconductor, $HfP_{1.55}Se_{0.45}$ Presenter: M. Nishioka (Hiroshima University)

-Poster Session-

The poster number with "S" is eligible for the Best Student Poster Award nomination.

P01S Re-examination of the Phase Diagram of $Bi_2Sr_2CaCu_2O_{8+\delta}$ Studied by ARPES

Y. Tsubota[a], S. Kumar[b], Y. Miyai[b], K. Tanaka[c], S. Ishida[d], H. Eisaki[d], S. Nakagawa[e], T. Kashiwagi[e], M. Arita[b], H. Namatame[b], K. Shimada[b], S. Ideta[b]

a Department of Physics, School of Science, Hiroshima University, Japan
b Hiroshima Synchrotron Radiation Center, Hiroshima University, Japan
c UVSOR, Institute for Molecular Science, Japan
d National Institute of Advanced Industrial Science and Technology, Japan
e Division of Materials Science, Tsukuba University, Japan

P03 Roles of Surface and Bulk States in Magneto-transport Properties in Antiferromagnetically Ordered $Bi_{1.9}Dy_{0.1}Te_3$ Topological Insulator

Vinod K. Gangwar[a], Shiv Kumar[b], Mahima Singh[a], Zhang Yufeng[c], Chaoyu Chen[d], Eike F. Schwier[b], Kenya Shimada[b], Prashant Shahi[e], Yoshiya Uwatoko[c], Swapnil Patil[a], Anup K. Ghosh[f], Sandip Chatterjee[a]

a Department of Physics, Indian Institute of Technology (BHU), India
b Hiroshima Synchrotron Radiation Center, Hiroshima University, Japan
c Institute for Solid State Physics, University of Tokyo, Japan
d Southern University of Science and Technology, China
e Department of Physics, D.D.U. Gorakhpur University, India
f Department of Physics, Banaras Hindu University, India

P04 Hybridization of the Electronic Structure in Triple-layer High-T_c Cuprate Bi2223 Observed by ARPES

S. Ideta[a,b], S. Johnston[c], T. Yoshida[d], K. Tanaka[b], M. Mori[e], H. Anzai[f], A. Ino[a,g], M. Arita[a], H. Namatame[a], M. Taniguchi[a], S. Ishida[h], K. Takashima[l], K. M. Kojima[k], T. P. Devereaux[i], S. Uchida[h,l], A. Fujimoril[,m]

a *Hiroshima Synchrotron Radiation Center, Hiroshima University, Japan*
b Institute for Molecular Science, UVSOR-III Synchrotron, Japan
c Department of Physics and Astronomy, The University of Tennessee, USA
d Department of Human and Environmental studies, Kyoto University, Japan
e Advanced Science Research Center, Japan Atomic Energy Agency, Japan
f Graduate School of Engineering, Osaka Prefecture University, Japan
g Department of Education and Creation Engineering, Kurume Institute of Technology, Japan
h National Institute of Advanced Industrial Science and Technology, Japan
i Geballe Laboratory for Advanced Materials, Stanford University, USA
j National Institute of Advanced Industrial Science and Technology, Japan
k Centre for Molecular and Materials Science, TRIUMF, Canada
l Department of Physics, University of Tokyo, Japan
m Department of Applied Physics, Waseda University, Japan

P05 XPS study on DCL films with various film thickness

Yuji Muraoka[a], Takanori Wakita[a], Takayoshi Yokoya[a]

a Research Institute for Interdisciplinary Science, Okayama University, Japan

-Poster Session-

The poster number with "S" is eligible for the Best Student Poster Award nomination.

P06S Electronic structure of half-metallic ferromagnet CrO_2 studied by VUV-ARPES

T. Setoguchi[a], N. Kataoka[a], S. Kumar[b], S. Ideta[b], K. Shimada[b], T. Wakita[c], Y. Muraoka[a, c], T. Yokoya[a, c]

a Graduate School of Natural Science and Technology, Okayama University, Japan
b Hiroshima Synchrotron Radiation Center, Hiroshima University, Japan
c Research Institute for Interdisciplinary Science, Okayama University, Japan

P07 Soft X-ray absorption spectroscopy of cyclodextrin compounds including a noble metal atom

Kiminori Baba[a], Hiroaki Yoshida[a,b]

a Graduate School of Advanced Science and Engineering, Hiroshima University, Japan
b Hiroshima Synchrotron Radiation Center, Hiroshima University, Japan

P08 Soft x-ray photoelectron spectroscopy of the metal complex included in cyclodextrin

Kiminori Baba[a], Hitoshi Sato[b], Hiroaki Yoshida[a,b]

a Graduate School of Advanced Science and Engineering, Hiroshima University, Japan
b Hiroshima Synchrotron Radiation Center, Hiroshima University, Japan

P09S Hard X-ray absorption spectroscopy of a gold complex included by cyclodextrin

Kiminori Baba[a], Shinjiro Hayakawa[b], Hiroaki Yoshida[a,c]

a Graduate School of Advanced Science and Engineering, Hiroshima University, Japan
b Applied Chemistry program, Graduate School of Advanced Science and Engineering, Hiroshima University, Japan
c Hiroshima Synchrotron Radiation Center, Hiroshima University, Japan

P10S Investigation of the Origin of Photo-Induced Doping on $TlBiSe_2$

R. Itaya[a], Y. Toichi[a], R. Nakanishi[a], Y. Nakata[b], K. Kasai[b], K. Kuroda[c], M. Arita[d], I. Yamamoto[e], K. Fukutani[f], K. Sakamoto[a]

a Graduate School of Engineering, Osaka University, Japan
b Graduate School of Science and Engineering, Chiba University, Japan
c Graduate School of Advanced Science and Engineering, Hiroshima University, Japan
d Hiroshima Synchrotron Radiation Center, Hiroshima University, Japan
e Synchrotron Light Application Center, Saga University, Japan
f Institute for Molecular Science, National Institutes of Natural Sciences, Japan

P11 Structure of a Novel Amorphous Organic-Inorganic Hybrid Tin Cluster Exhibiting Nonlinear Optical Effects by Low-Energy XAFS Measurements

Jens R. Stellhorn[a], Shinjiro Hayakawa[a], Benedict Paulus[b], Benjamin D. Klee[b], Wolf-Christian Pilgrim[b], Stefanie Dehnen[b]

a Department of Applied Chemistry, Graduate School of Advanced Science and Engineering, Hiroshima University, Japan
b Department of Chemistry, Philipps University of Marburg, Germany

P12 Development Of A New Device For Angular Dependent Conversion Electron Yield XAFS Measurements

Shinjiro Hayakawa[a], Haruka Yoshimoto[a], Jens R. Stellhorn[a], Kenji Komaguchi[a]

a Applied Chemistry program, Graduate School of Applied Science and Engineering,, Hiroshima University, Japan

-Poster Session-

The poster number with "S" is eligible for the Best Student Poster Award nomination.

P13 C K-edge XAFS measurements for detection of unsaturated bonds in organically bridged silica materials

Shinjiro Hayakawa[a], Joji Oshita[a,b], Kei Oshima[a,b], Shogo Tendo[c], Toshinori Tsuru[d], Shinichi Wada[c]

a Applied Chemistry program, Graduate School of Applied Science and Engineering, Hiroshima University, Japan
b Smart Innovation program, Graduate School of Applied Science and Engineering, Hiroshima University, Japan
c Physics program, Graduate School of Applied Science and Engineering,, Hiroshima University, Japan
d Chemical Engineering program, Graduate School of Applied Science and Engineering, Hiroshima University, Japan

P14S Desiccation-Induced Conformational Change of Group 3 LEA Protein in the presence of Membrane Characterized by Vacuum-Ultraviolet Circular Dichroism Spectroscopy

Shun Sawada[a], Munehiro Kumashiro[b], Ryota Imaura[b], Koichi Matsuo[c]

a Faculty of Science, Hiroshima University, Japan
b Graduate School of Science, Hiroshima University, Japan
c Hiroshima Synchrotron Radiation Center, Hiroshima University, Japan

P15S Orientation Analysis of Antimicrobial Peptide Magainin 2 Bound to Phospholipid Membrane by Synchrotron-Radiation Linear Dichroism Spectroscopy

Munehiro Kumashiro[a], Ryoga Tsuji[b], Shoma Suenaga[a], Koichi Matsuo[c]

a Department of Physical Science, Graduate School of Science, Hiroshima University, Japan
b Physics Program, Graduate School of Advanced Science and Engineering, Hiroshima University, Japan
c Hiroshima Synchrotron Radiation Center, Hiroshima University, Japan

P16S Analysis of structural change of XRCC4 by pseudo-phosphorylation using VUV-CD and SAXS

Kai Nishikubo[a,b], Maho Hasegawa[a,b], Yudai Izumi[b], Kentaro Fujii[b], Koichi Matsuo[c], Yoshihisa Matsumoto[d], Akinari Yokoya[b,a]

a Graduate School of Science and Engineering, Ibaraki University, Japan
b Institute for Quantum Life Science, Quantum Life and Medical Science Directorate, National Institutes of Quantum Sciences and Technology (QST), Japan
c Hiroshima Synchrotron Radiation Center, Hiroshima University, Japan
d Tokyo Institute of Technology, Japan

P17S NEXAFS Study of Fullerene Adsorbed on Aminothiophenol Self-Assembled Monolayer

K. Kono[a], S. Wada[b,c], T. Sekitani[b,c]

a Faculty of Science, Hiroshima University Japan
b Graduate School of Advanced Science and Engineering, Hiroshima University, Japan
c Hiroshima Synchrotron Radiation Center, Hiroshima University, Japan

-Poster Session-

The poster number with "S" is eligible for the Best Student Poster Award nomination.

P18 Characterization of self-assembled monolayers of methyl-ester terminated naphthalenethiol

A. Niozu[a], H. Sunohara[b], S. Tendo[a], M. Tabuse[a], Shin-ichi Wada[a,c]
a Graduate school of advanced science and engineering, Hiroshima University Japan
b Faculty of science, Hiroshima University, Japan
c Hiroshima Synchrotron Radiation Center, Hiroshima University, Japan

P19S Soft X-ray Polarization Measurements of Phospholipid Multilayers Supported on Hydrophilic Si Surfaces

Masataka Tabuse[a], Akinobu Niozu[a], Shin-ichi Wada[a,b]
a Graduate School of Advanced Science and Engineering, Hiroshima University, Japan
b Hiroshima Synchrotron Radiation Center, Hiroshima University, Japan

P20S Interface structure of Co ultrathin films evaporated on h-BN/Ni(111) studied by LEED Intensity Analysis

Wataru Nishizawa[a], Masahiro Sawada[b]
a Graduate School of Science, Hiroshima University, Japan
b Hiroshima Synchrotron Radiation Center, Hiroshima University, Japan

P21S Evolution of c-f hybridization in valence transition compound $YbInCu_4$ observed by ARPES

R. Kamimori[a], Y. Tanimoto[b], H. Sato[c], M. Arita[c], S. Kumar[c], K. Shimada[c], K. T. Matsumoto[d], K. Hiraoka[d]
a Graduate School of Advanced Science and Engineering, Hiroshima University, Japan
b Faculty of Science, Hiroshima University, Japan
c Hiroshima Synchrotron Radiation Center, Hiroshima University, Japan
d Graduate School of Science and Engineering, Ehime University, Japan

P22S Evaluation of Self-Energy in Overdoped Bi2201 by Angle-Resolved Photoemission Spectroscopy

Y. Miyai[a], Shiv Kumar[b], T. Kurosawa[c], M. Oda[d], S. Ideta[b], K. Shimada[b]
a Graduate School of Science, Hiroshima University, Japan
b Hiroshima Synchrotron Radiation Center, Hiroshima University, Japan
c Fuculty of Science and Engineearing, Muroran Institute of Technology, Japan
d Department of Physics, Hokkaido University, Japan

P23S Direct Observation of the Three-dimensional Electronic Structure of RMnSi (R=La, Ce) with Noncentrosymmetic Antiferromagnetic Order

Kaito Shiraishi[a], Takuma Iwata[b], Kenta Kuroda[a], Munisa Nurmamat[a], Karen Nakanishi[b], Shiv Kumar[c], Kenya Shimada[c], Masashi Arita[c], Yoshinori Kotani[d], Keisuke Mitsumoto[e], Hiroshi Tanida[e], Akio Kimura[a]
a Graduate School of Advanced Science and Engneering, Hiroshima University, Japan
b Faculty of Science, Hiroshima University, Japan
c Hiroshima Synchrotron Radiation Center, Hiroshima University, Japan
d Japan Synchrotron Radiation Reseach Institute, Japan
e Liberal Arts and Sciences, Toyama Prefectural University, Japan

-Poster Session-

The poster number with "S" is eligible for the Best Student Poster Award nomination.

P24S Membrane-Bound Conformations of Magainin 2 Depending on the Inherent Characteristics of Membrane Revealed by Synchrotron-Radiation Circular-Dichroism Spectroscopy

Ryoga Tsuji[a], Munehiro Kumashiro[b], Koichi Matsuo[c]

a Physics Program, Graduate School of Advanced Science and Engineering, Hiroshima University, Japan

b Department of Physical Science, Graduate School of Science, Hiroshima University, Japan

c Hiroshima Synchrotron Radiation Center, Hiroshima University, Japan

P25S Spatial inhomogeneity in $Bi_2Sr_2CaCu_2O_{8+\delta}$ investigated by micro photoemission spectroscopy

T. Sugiyama[a] H. Iwasawa[b,c], S. Ozawa[d], H. Oda[d], R. Takahashi[e], T. Kono[d], T. Okuda[c], K. Miyamoto[c], H. Wadachi[e], S. Ishida[f], Y. Yoshida[f], H. Eisaki[f], A. Kimura[a,d]

a Graduate School of Advanced Science and Engineering, Hiroshima Univ., Japan

b National Institutes for Quantum Science and Technology, Japan

c Hiroshima Synchrotron Radiation Center, Hiroshima Univ., Japan

d Graduate School of Science, Hiroshima Univ., Japan

e Graduate School of Science, Univ. of Hyogo, Japan

f National Institute of Advanced Industrial Science and Technology, Japan

P26S Minority-spin Dominated Band Structure Near the Fermi Energy of Fe_4N Film Revealed by Spin- And Angle-Resolved Photoemission Spectroscopy

Karen Nakanishi[a], Kiyotaka Ohwada[b], Kenta Kuroda[b], Kazuki Sumida[c], Koji Miyamoto[d], Taichi Okuda[d], Shinji Isogami[e], Keisuke Masuda[e], Yuya Sakuraba[e], Akio Kimura[a,b]

a Department of Physics, Faculty of Science, Hiroshima University, Japan

b Graduate School of Advanced Science and Engineering, Hiroshima University, Japan

c Materials Sciences Research Center, Japan Atomic Energy Agency, Japan

d Hiroshima Synchrotron Radiation Center, Hiroshima University, Japan

e National Institute for Materials Science, Japan

P27S Many-body Interactions on the Surface of the Topological Insulators

Amit Kumar[a], Shiv Kumar[a,b], Kenya Shimada[a,b]

a Graduate School of Science, Hiroshima University, Japan

b Hiroshima Synchrotron Radiation Center, Hiroshima University, Japan

P28 Observation of Liquid-Liquid Phase Separation of FUS-LC using VUV-CD Spectroscopy

Kentaro Fujii[a], Nobuo Maita[b], Koichi Matsuo[c], Masato Kato[b]

a Institute for Quantum Life Science, National Institutes for Quantum Science and Technology, Japan

b Institute for Quantum Life Science, National Institutes for Quantum Science and Technology, Japan

c Hiroshima Synchrotron Radiation Center, Hiroshima University, Japan

-Poster Session-

The poster number with "S" is eligible for the Best Student Poster Award nomination.

P29S Development of Time-Resolved Vacuum-Ultraviolet Circular Dichroism Spectroscopy and its Application to the Interaction Analysis betweenβ-Lactoglobulin and Lipid Membrane

Satoshi Hashimoto[a], Koichi Matsuo[b]
a Graduate School of Advanced Science and Engineering, Hiroshima University, Japan
b Hiroshima Synchrotron Radiation Center, Hiroshima University, Japan

P30S Direct observation of Dirac nodal-line fermions in P-square net superconductor, $ZrP_{1.24}Se_{0.57}$

S. Ishizaka[a], A. Ino[b,c], T. Kono[a], Y. Miyai[d], S. Kumar[c], K. Shimada[c], H. Kito[e], I. Hase[e], S. Ishida[e], K. Oka[e], H. Fujihisa[e], Y. Gotoh[e], Y. Yoshida[e], A. Iyo[e], H. Ogino[e], H. Eisaki[e], K. Kawashima[f,e], Y. Yanagi[f,e], A. Kimura[a,d]
a Graduate School of Science, Hiroshima University, Japan
b Kurume Institute of Technology, Japan
c Hiroshima Synchrotron Radiation Center, Hiroshima University, Japan
d Graduate School of Advanced Sciences and Engineering, Hiroshima University, Japan
e National Institute of Advanced Industrial Science and Technology (AIST), Japan
f IMRA JAPAN Co., Ltd., Kariya, Japan

P31 Current activities of research and education on BL-5 (FY2021)

T. Yokoya[a,b], T. Wakita[a,b], Y. Muraoka[a,b]
a Research Institute for Interdisciplinary Science, Okayama University, Japan
b Research Laboratory for Surface Science, Okayama University, Japan

P32 Angle resolved resonant photoemission study of Si 3*p* band

T. Wakita[a], Y. Muraoka[a,b], T. Yokoya[a,b]
a Research Institute for Interdisciplinary Science, Okayama University, Japan
b Research Laboratory for Surface Science, Okayama University, Japan

P33S Observation of Fast Dirac Nodal-Line Fermions in a Nonsymmorphic Superconductor, $HfP_{1.55}Se_{0.45}$

Y. Nishioka[a], S. Ishizaka[b], K. Kuroda[c], A. Ino[d,e], S. Kumar[e], K. Shimada[e], H. Kito[f], I. Hase[f], S. Ishida[f], K. Oka[f], H. Fujihisa[f], Y. Gotoh[f], Y. Yoshida[f], A. Iyo[f], H. Ogino[f], H. Eisaki[f], K. Kawashima[f,g], Y. Yanagi[f,g], A. Kimura[a,b,c]
a Faculty of Science, Hiroshima University, Japan
b Graduate School of Science, Hiroshima University, Japan
c Graduate School of Advanced Sciences and Engineering, Hiroshima University, Japan
d Kurume Institute of Technology, Japan
e Hiroshima Synchrotron Radiation Center, Hiroshima University, Japan
f National Institute of Advanced Industrial Science and Technology (AIST), Japan
g IMRA JAPAN Co., Ltd., Japan

Re-examination of the Phase Diagram of $Bi_2Sr_2CaCu_2O_{8+\delta}$ Studied by ARPES

Y. Tsubota[a], S. Kumar[b], Y. Miyai[b], K. Tanaka[c], S. Ishida[d], H. Eisaki[d], S. Nakagawa[e], T. Kashiwagi[e], M. Arita[b], H. Namatame[b], K. Shimada[b] and S. Ideta[b]

[a] *Department of Physics, School of Science, Hiroshima University, Higashi-Hiroshima 739-0046, Japan*
[b] *Hiroshima Synchrotron Radiation Center, Hiroshima University, Higashi-Hiroshima 739-0046, Japan*
[c] *UVSOR, Institute for Molecular Science, Okazaki, Aichi 444-8585, Japan*
[d] *National Institute of Advanced Industrial Science and Technology, Tsukuba, Ibaraki 305-8560, Japan*
[e] *Division of Materials Science, Tsukuba University, Tsukuba, Ibaraki 305-8577, Japan*

Keywords: high-T_c cuprate superconductors, ARPES

In high-T_c cuprate superconductors, the phase diagram plotted as a function of temperature and hole concentration has been elucidated as the universal phase diagram. The phase diagram has been known as a dome-like shape centered at the hole concentration of 16% which was determined in the previous report [1]. In contrast to the empirical and universal phase diagram, recent angle-resolved photoemission spectroscopy (ARPES) study has shown that the electronic structure of the cuprates behaves differently in the superconducting and normal states [2], even though the samples are expected to be the same hole concentration. Therefore, we expect that the phase diagram of the high-T_c cuprate superconductors might be deviated from the universal one and the optimally doped hole concentration should be re-examined.

In this study, we have performed an ARPES measurement to investigate the electric structure of the Bi-based high-T_c cuprate superconductors $Bi_2Sr_2CaCu_2O_{8+\delta}$ (Bi2212), which has two CuO_2 planes in the unit cell, with three compositions: $Bi_{2.1}Sr_{1.9}CaCu_2O_{8+\delta}$, $Bi_{2.3}Sr_{1.7}CaCu_2O_{8+\delta}$, $Bi_{2.1-x}Pb_xSr_2CaCu_2O_{8+\delta}$ (x = 0.66). Figure 1 shows the Fermi surface taken at $h\nu$ = 28 eV and T = 30 K in the superconducting state of $Bi_{2.1}Sr_{1.9}CaCu_2O_{8+\delta}$. The Fermi surfaces are clearly observed in wide momentum space. We have analyzed the ARPES spectra around the nodal region for each sample and determined the Fermi momentum points for each Fermi surface by fitting of momentum-distribution curves (MDCs) with a Lorentzian as shown by red dots (Fig. 1). As a result, we have found that three samples with different compositions show that the distance between two nodal points has a different value. This implies that these samples show a different hole concentration even though the sample has been expected to be optimal doping.

In this poster presentation, we will discuss a possible interpretation to understand the data obtained from the present ARPES study and show an expected phase diagram of Bi2212.

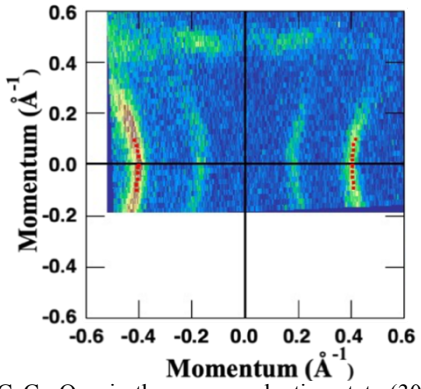

FIGURE 1. Fermi surfaces of $Bi_{2.1}Sr_{1.9}CaCu_2O_{8+\delta}$ in the superconducting state (30 K). Red dots are the Fermi momentum estimated from MDC near the Fermi level.

REFERENCES

1. J. L. Tallon, C. Bernhard, H. Shaked, R. L. Hitterman and J. D. Jorgensen, Generic superconducting phase behavior in high-T_c cuprates: T_c variation with hole concentration in $YBa_2Cu_3O_{7-\delta}$, *Phys. Rev. B* **51**, 12911 (1995).
2. I. M. Vishik, M. Hashimoto, Rui-Hua He, Wei-Sheng Lee, Felix Schmitt, Donghui Lu, R. G. Moore, C. Zhang, W. Meevasana, T. Sasagawa, S. Uchida, Kazuhiro Fujita, S. Ishida, M. Ishikado, Yoshiyuki Yoshida, Hiroshi Eisaki, Zahid Hussain, Thomas P. Devereaux, and Zhi-Xun Shen, *Proc. Nat. Acd. Sci.* **6**, 18332-18337 (2012).

Roles of Surface and Bulk States in Magneto-transport Properties in Antiferromagnetically Ordered $Bi_{1.9}Dy_{0.1}Te_3$ Topological Insulator

Vinod K. Gangwar[a], Shiv Kumar[b], Mahima Singh[a], Zhang Yufeng[c], Chaoyu Chen[d], Eike F. Schwier[b], Kenya Shimada[b], Prashant Shahi[e], Yoshiya Uwatoko[c], Swapnil Patil[a], Anup K. Ghosh[f] and Sandip Chatterjee[a]

[a]*Department of Physics, Indian Institute of Technology (BHU) Varanasi 221005, India*
[b]*Hiroshima Synchrotron Radiation Center, Hiroshima University, 739-0046 Japan*
[c]*Institute for Solid State Physics, University of Tokyo, Kashiwa, Chiba 277-8581, Japan*
[d]*Southern University of Science and Technology, Shenzhen, Guangdong 518-055, China*
[e]*Department of Physics, D.D.U. Gorakhpur University, Gorakhpur 273-009, India*
[f]*Department of Physics, Banaras Hindu University, Varanasi 221-005, India*

Keywords: topological insulator, magneto-transport, ARPES study

Topological insulators (TIs) have attracted much interest for many exciting physical phenomena like quantum anomalous Hall effect (QAHE), Majorana fermions, magnetic monopoles and with great possibilities of application in spintronics and quantum computing [1, 2]. Magnetic TIs provide a route to study the connection between topological surface states (TSS) and magnetism. In addition, finding the anomalous Hall effect (AHE) in topological states of matter is absolutely fascinating. In fact, transition metal-doped TIs have shown QAHE with long-range ferromagnetic ordering, which are suitable source materials for spintronic applications [3, 4]. Antiferromagnetic TIs have been extensively studied due to their application in spintronics and to decrease the critical current density [5]. It was theoretically predicted that antiferromagnetic ordering does not always destroy TSS. It locally breaks the time-reversal symmetry (TRS) but maintains global TRS in combination with the translation symmetry. Therefore, the antiferromagnetic order can coexist with TSS [6].

We have synthesized $Bi_{1.9}Dy_{0.1}Te_3$ single crystals by a two-step melting method [7]. A stoichiometric mixture of highly pure Bi, Dy and Te was sealed in a quartz ampoule at a vacuum level of ~10^{-6} torr. After that, the sealed quartz ampoule was slowly (60 ^{o}C/h) heated up to 950 ^{o}C and kept there for a period of 24 h. Then it was cooled at the rate of 5 ^{o}C/h from 950 ^{o}C to 550 ^{o}C and hold at 550 ^{o}C for 72 h, then slowly (60 ^{o}C/h) cooled down to room temperature.

In order to observe the electronic structure and the effect of magnetic ordering in $Bi_{1.9}Dy_{0.1}Te_3$, we have also carried out ARPES measurements. The high-resolution angle-resolved photoemission spectroscopy (ARPES) measurements have been performed with a focused ultraviolet laser beam (photon energy of 6.3 eV, the beam spot size of ~10 μm) equipped with VG Scienta R4000 electron analyzer at the Hiroshima Synchrotron Radiation Center (HiSOR), Hiroshima University, Japan [8]. Figure 1 shows the electronic structure of $Bi_{1.9}Dy_{0.1}Te_3$ taken along ($\bar{K} - \bar{\Gamma} - \bar{K}$) direction of the hexagonal surface Brillouin zone. The 'V'- shaped, Dirac-like TSS are clearly visible confirming topological non-triviality of the electronic structure of $Bi_{1.9}Dy_{0.1}Te_3$. The broad 'M'- shaped bulk valence band (BVB) is also observed at higher binding energies. The Fermi level (E_F) lies very near to the bulk conduction band (BCB) and the position of DP is observed around −0.305±0.002 eV below the E_F, which lies inside the central wedge of the 'M'- shaped BVB. One can notice the ARPES intensity corresponding to the BCB at E_F in Fig. 1(a) confirming the electron-doped nature of the bulk. Consequently, n-type nature revealed from the ARPES measurement is consistent with Hall and thermoelectric measurements. Figure 1 illustrates two-dimensional constant energy contour plots of the ARPES intensity at different energies (Fig. 1(c-k)). On approaching the DP from the E_F, the constant energy contour plot of the TSS is changed from a hexagram to a hexagonally warped structure, then to a circle of gradually reducing radius, and then finally it shrinks to a point, the DP, as is generally

observed in other TIs [9, 10]. Other than the TSS, the six-fold petal-like intensity pattern at energy -0.24 to -0.305 eV is also visible, which originates from the BVB. The obtained surface carrier density derived from the TSS is $\sim 1.5 \times 10^{13}$ cm^{-2}. In Fig. 1(b) only a single peak appears in the energy distribution curve (EDC) at the DP, which suggests the absence of appreciable gap opening at the DP [9, 10]. ARPES results support that $Bi_{1.9}Dy_{0.1}Te_3$ is a gapless magnetic topological insulator.

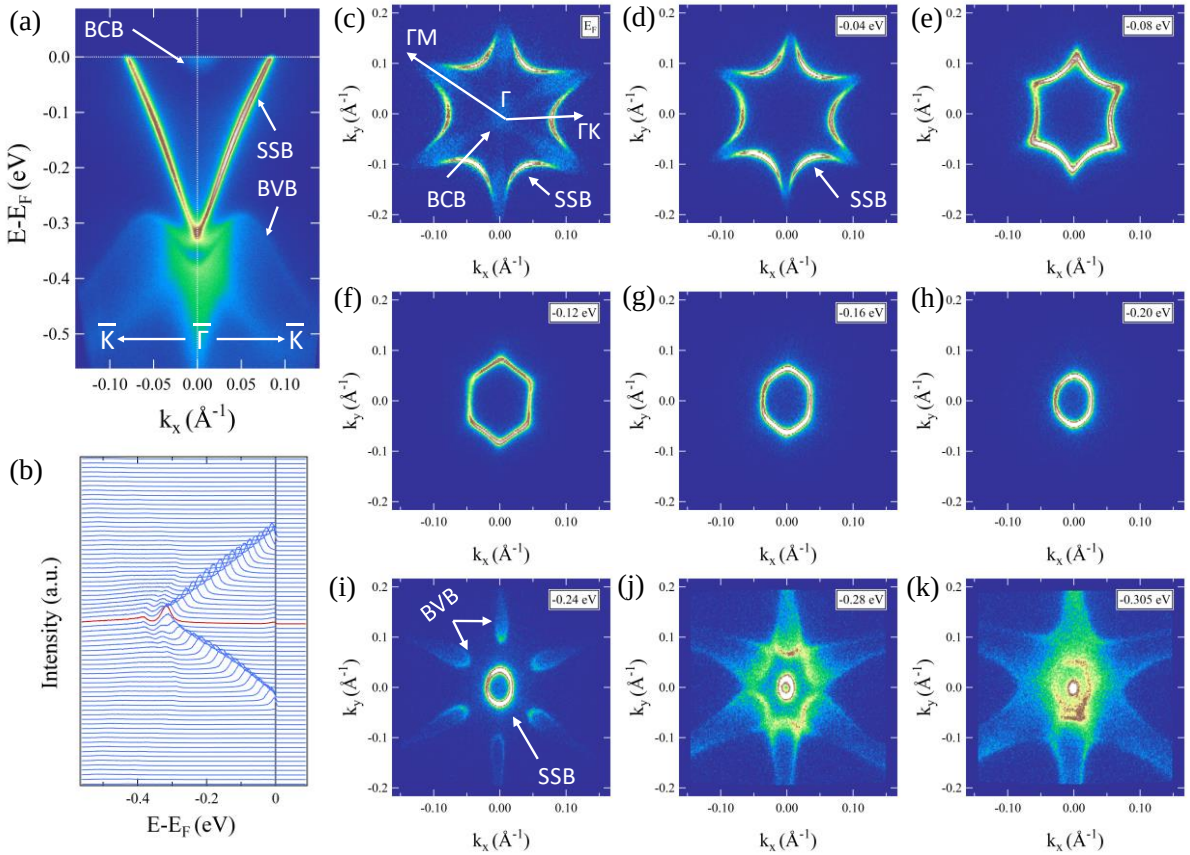

FIGURE 1. (a) Electronic spectra for $Bi_{1.9}Dy_{0.1}Te_3$ taken along ($\bar{K} - \bar{\Gamma} - \bar{K}$) direction (b) Energy distribution curve's (EDC's), (c) - (k) the plots of the iso-energy contours of the ARPES spectra at different energies.

REFERENCES

1. X.-L. Qi, R. Li, J. Zang, S.-C. Zhang, *Science* **323**, 1184-1187 (2009).
2. M. Z. Hasan, C. L. Kane, *Reviews of Modern Physics* **82**, 3045-3067 (2010).
3. C.-Z. Chang *et al.*, *Nature Materials* **14**, 473-477 (2015).
4. J. S. Dyck, P. Hájek, P. Lošt'Ák, C. Uher, *Physical Review B* **65**, (2002).
5. T. Jungwirth, X. Marti, P. Wadley, J. Wunderlich, *Nature Nanotechnology* **11**, 231-241 (2016).
6. R. S. K. Mong, A. M. Essin, J. E. Moore, *Physical Review B* **81**, (2010).
7. A. Singh *et al.*, *Materials Research Bulletin* **98**, 1-7 (2018).
8. H. Iwasawa *et al.*, *Ultramicroscopy* **182**, 85-91 (2017).
9. K. Kuroda *et al.*, *Physical Review Letters* **105**, (2010).
10. Y. L. Chen *et al.*, *Science* **329**, 659-662 (2010).

Hybridization of the Electronic Structure in Triple-layer High-T_c Cuprate Bi2223 Observed by ARPES

S. Ideta[a,b], S. Johnston[c], T. Yoshida[d], K. Tanaka[b], M. Mori[e], H. Anzai[f], A. Ino[a,g], M. Arita[a], H. Namatame[a], M. Taniguchi[a], S. Ishida[h], K. Takashima[l], K. M. Kojima[k], T. P. Devereaux[i], S. Uchida[h,l], and A. Fujimori[l,m]

[a] *Hiroshima Synchrotron Radiation Center, Hiroshima University, Higashi-Hiroshima 739-0046, Japan*
[b] *Institute for Molecular Science, UVSOR-III Synchrotron Okazaki, 444-8585, Japan*
[c] *Department of Physics and Astronomy, The University of Tennessee, Knoxville, Tennessee 37996, USA*
[d] *Department of Human and Environmental studies, Kyoto University, Sakyo-ku, Kyoto 606-8501, Japan*
[e] *Advanced Science Research Center, Japan Atomic Energy Agency, Tokai 319-1195, Japan*
[f] *Graduate School of Engineering, Osaka Prefecture University, Sakai 599-8531, Japan*
[g] *Department of Education and Creation Engineering, Kurume Institute of Technology, Fukuoka 2286-66, Japan*
[h] *National Institute of Advanced Industrial Science and Technology, Tsukuba, Ibaraki 305-8568, Japan*
[i] *Geballe Laboratory for Advanced Materials, Stanford University, Stanford, California 94305, USA Menlo Park, California 94025, USA*
[j] *National Institute of Advanced Industrial Science and Technology, Tsukuba, Ibaraki 305-8568, Japan*
[k] *Centre for Molecular and Materials Science, TRIUMF, 4004 Vancouver, Canada*
[l] *Department of Physics, University of Tokyo, Bunkyo-ku, Tokyo 113-0033, Japan*
[m] *Department of Applied Physics, Waseda University, Shinjuku-ku, Tokyo 169-8555, Japan*

Keywords: Superconductivity, Cuprate, ARPES, Electronic structure.

The energy gap seen in the superconducting (SC) and normal states has been believed to be an important piece of evidence for the mechanism of high SC transition temperature in cuprate superconductors. Bi-based high-T_c cuprate superconductors can be classified by the number of the neighboring CuO_2 planes (n): single-layer (n = 1) $Bi_2Sr_2CuO_{4+\delta}$ (Bi2201), double-layer (n = 2) $Bi_2Sr_2CaCu_2O_{8+\delta}$ (Bi2212), triple-layer (n = 3) $Bi_2Sr_2Ca_2Cu_3O_{10+\delta}$ (Bi2223). In going from n = 1 to 3, the maximum T_c increases: It is 35 K and 95 K for Bi2201 and Bi2212, respectively, and reaches 110 K for Bi2223, which is the highest T_c among the Bi family of cuprates [1]. However, the microscopic origin of this trend has not been clarified yet.

For optimally doped Bi2223, we have revealed the electronic structure using angle-resolved photoemission spectroscopy (ARPES) [2-4]. In the present study, we have performed a high-resolution ARPES study of Bi2223 using synchrotron radiation and observed hybridization between the CuO_2 planes, which shows that an anti-crossing energy gap opens around the off-nodal region. In this poster presentation, we will discuss a possible interpretation of hybridization of the electronic structure in the triple-layer cuprate superconductor and the origin of the high T_c [5].

REFERENCES

1. A. Iyo *et al*., *J. Phys. Soc. Jpn*., **76**, 094711 (2007).
2. S. Ideta et al., *Phys. Rev. Lett.* **104**, 227001 (2010).
3. S. Ideta et al., *Phys. Rev. B* **85**, 104515 (2012).
4. S. Kudo *et al*., *Phys. Rev. B* **92**, 195135 (2015).
5. S. Ideta *et al*., *Phys. Rev. Lett.* **127**, 217004 (2021).

XPS study on DCL films with various film thickness

Yuji Muraoka[a], Takanori Wakita[a] and Takayoshi Yokoya[a]

[a]*Research Institute for Interdisciplinary Science, Okayama University, 3-1-1 Tsushima-naka, Tsushima, Kita-ku, Okayama 700-8530, Japan*

Keywords: Diamond-like carbon, X-ray photoelectron spectroscopy, Raman spectroscopy, sp^3 content, Film thickness

Diamond-like carbon (DLC) is a metastable form of amorphous carbon containing a significant sp^3 content. It shows a high mechanical hardness, chemical inertness and optical transparency [1], depending on the sp^3 content. Thus, the sp^3 content is an important parameter that determines the properties of DLC. X-ray photoemission spectroscopy (XPS) and Raman spectroscopy techniques are widely used to determine the sp^3 contents in DLC films, while XPS is relatively surface sensitive and Raman spectroscopy is more bulk sensitive. There are a number of studies on the sp^3 content in DLC films with film thickness ranging from nanometer to several tens of micrometer order. However, only few studies for the thickness dependence of sp^3 content in DLC films have been shown so far. It is beneficial to know how the sp^3 content changes with the film thickness of DLC films from both viewpoints of fundamental science and applications. In this study, we prepared DLC films with various film thickness and examined the film thickness dependence of sp^3 content in DLC films by means of XPS and Raman spectroscopy.

The amorphous DLC films were fabricated on sapphire $Al_2O_3(0001)$ substrates using a pulsed laser deposition technique with a KrF excimer laser (λ = 248 nm). Before film deposition, the substrates were heated at 573 K for 1.5 h in a vacuum of 4×10^{-7} Pa for the surface cleaning. Film deposition was performed at 300 K in a vacuum of 4×10^{-7} Pa. Laser fluence was 1.1 J/cm^2 and deposition rate was ~6 nm/min. The films thickness was controlled by changing the deposition time and was varied from 20 to 634 nm. Raman spectroscopy measurements of DLC films were performed using a micro-Raman spectrometer with a 532-nm laser (JASCO NRS-5100). X-ray photoemission spectroscopy (XPS) measurements were carried out on the beamline BL-5, at the Hiroshima Synchrotron Radiation Center in Hiroshima University with non-monochromatic Mg Kα X-ray source ($h\nu$ = 1253.6 eV). C 1*s* core-level spectra were measured under an ultrahigh vacuum of ~10^{-7} Pa using a VSW hemispherical analyzer. The total energy resolution was about 1.8 eV. The binding energy of the films was corrected using the peak position of molybdenum spectra. Before measurements, the films were annealed at 373 K under ultrahigh vacuum (~10^{-6} Pa) for 1 h to clean the film surface.

Figure 1(a) shows the Raman spectra of the DLC films. A peak at ~1550 cm^{-1} and shoulder structure at around 1350 cm^{-1} were observed in the spectrum for 24-nm-thick film. The shoulder structure at ~1350 cm^{-1} developed to become a peak as the film thickness increased. For the obtained spectra, spectral fitting was performed using a Gaussian function. The experimental data was correctly fitted with three peaks. The three components had peak positions of 1140-1170, ~1400, and ~1560 cm^{-1}. The peak of 1140-1170 cm^{-1} was assigned to nanocrystalline diamond [2,3]. The peaks of ~1400 and ~1560 cm^{-1} correspond to the so-called D and G peaks, respectively. The sp^3 content in the DLC films was estimated from full-width-half-maximum, FWHM of G peaks [4]. The results are shown Fig. 1(b). The sp^3 content in the DLC films decreased as the film thickness increased; the sp^3 content reduced from approximately 37 % at 24 nm to 0% over 400 nm. In order to check the film thickness dependence of the sp^3 content in the DLC films, XPS measurements of the films were also conducted.

Figure 2 shows the XPS spectra of the C 1*s* core-level for the DLC films with film thickness of 24, 98 and 634 nm. A peak at the binding energy of ~285 eV was observed in the spectra for all the films. The peaks of ~285 eV corresponded to sp^3 C-C bond [5]. The peak position of the films did not move and always located at ~285 eV regardless of film thickness. The results of XPS measurements are inconsistent with those of Raman spectroscopy. The thickness dependence of sp^3 content in DLC was observed in Raman spectroscopy measurements, but it was not in XPS measurements. A possible reason is the difference in the probing depth between the two methods. Raman spectroscopy is a bulk sensitive method and the probing

depth is more than thousands of nm. By Raman spectroscopy measurements, the sp^3 content in the entire film can be evaluated. On the other hand, XPS is a relatively surface sensitive method and the probing depth is estimated to be a few nm near the surface in this study. By XPS measurements, the sp^3 content near the film surface can be examined. If the surface of the DLC films is modified or/and is covered with contaminations which are not easy to remove our cleaning procedure, the XPS spectra for all of the films should be identical regardless of film thickness of DLC. More bulk sensitive XPS measurements help examine this consideration.

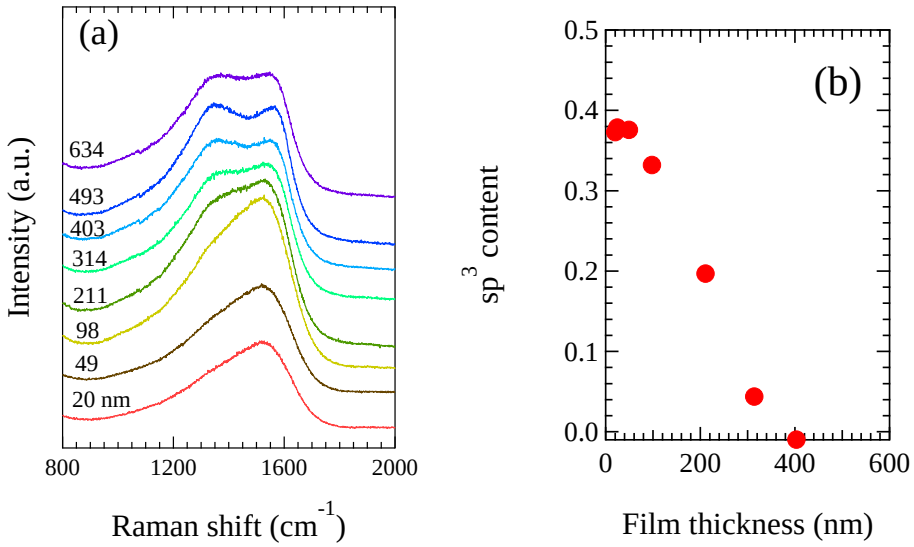

FIGURE 1. (a) Raman spectra for the DLC films with various film thickness. (b) sp^3 content in the DLC films as a function of film thickness.

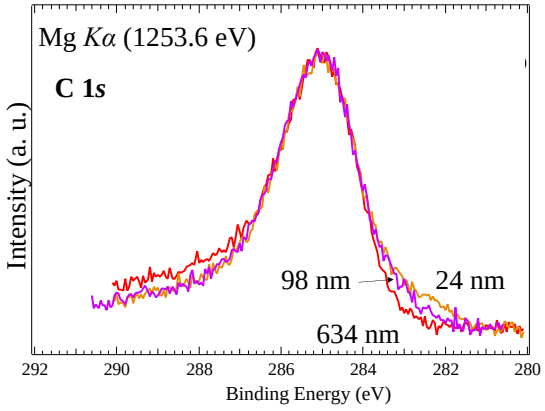

FIGURE 2. C 1s core-level spectra for the DLC films with the film thickness of 24, 98, 634 nm.

REFERENCES

1. J. Robertson, *Mater. Sci. Eng. R* **37**, 129-281 (2002).
2. C. Ziebert *et al.*, *Sur. Coat. Technol*. **200,** 1127-1131 (2005).
3. S. Nakao *et al.*, *Diamond Relat. Mater.* **15,** 884-887 (2006).
4. W. G. Cui *et al.*, *Sur Coatings Technol.* **205,** 1995-1999 (2010).
5. V. Y. Fominski *et al.*, *Diamond Relat. Mater.* **92,** 266-277 (2019).

Electronic structure of half-metallic ferromagnet CrO_2 studied by VUV-ARPES

T. Setoguchi[a], N. Kataoka[a], S. Kumar[b], S. Ideta[b], K. Shimada[b], T. Wakita[c], Y. Muraoka[a, c] and T. Yokoya[a, c]

[a]*Graduate School of Natural Science and Technology, Okayama University, 3-1-1 Tsushima-naka, Kita-ku, Okayama 700-8530, Japan*
[b]*Hiroshima Synchrotron Radiation Center, Hiroshima University, 2-313 Kagamiyama, Higashi-Hiroshima 739-0046, Japan*
[c]*Research Institute for Interdisciplinary Science, Okayama University, 3-1-1 Tsushima-naka, Kita-ku, Okayama 700-8530, Japan*

Keywords: Half-metallic ferromagnet, ARPES

Half-metallic ferromagnets have only one electronic spin state at the Fermi level. Due to this characteristic property, they are expected to be used as the completely spin-polarized sources in the field of spintronics. Among that kind of materials, one of the most promising materials is chromium dioxide(CrO_2). About 100% of spin polarization was observed at 1.8K in CrO_2 by means of Point contact Andreev reflection [1], which means that this is ideal for the completely spin-polarized sources. However, the spin polarization decreases as the temperature increases and it does not obey the temperature dependence of macroscopic magnetization. The reason for this marked decrease was recently attributed to non-quasi particles, which is many body effects originated from the peculiar half metallic electronic structure, from high resolution spin-dependent photoemission spectroscopy [2]. On the other hand, CrO_2 is expected to be a Weyl ferromagnet, which is Weyl topological material with time-reversal symmetry breaking[3]. In Weyl materials, bulk Weyl fermions and surface Fermi arcs can be observed. To experimentally verify these interesting electronic structure angle-resolved photoemission spectroscopy (ARPES) measurement is a powerful tool. Though previous soft-x ray(SX) ARPES studies have reported overall band dispersions [4], the energy resolution of SXARPES is not enough to investigate these electronic structure.

In this study, we have performed vacuum ultraviolet VUV-ARPES of CrO_2 at BL1, HiSOR. Generally, it is said that photoemission spectroscopy by using light with vacuum ultraviolet (VUV) range is relatively surface-sensitive technique. Therefore, cleanness of sample surface is important. However, surface of CrO_2 easily tends to change Cr_2O_3 and this makes it difficult to observe intrinsic electronic state of CrO_2. To solve this problem, we have synthesized high quality films using closed system chemical vapor deposition in evacuated quartz tube [5], prepared those films in a glove box filled with Ar and measured the films without exposing them to atmosphere.

By using this method, we could successfully observe a clear band dispersion and Fermi surface of CrO_2. We will discuss the electronic structure of CrO_2 using obtained high-resolution ARPES data.

REFERENCES

[1] R. J. Soulen Jr., J. M. Byers, M. S. Osofsky, B. Nadgorny, T. Ambrose, S. F. Cheng, P. R. Broussard, C. T. Tanaka, J. Nowak, J. S. Moodera, A. Barry, and J. M. D. Coey, Science **282,** 85 (1998).
[2] Hirokazu Fujiwara, Masanori Sunagawa, Kensei Terashima, Tomoko Kittaka, Takanori Wakita, Yuji

Muraoka, and Takayoshi Yokoya, App. Phys. Lett. **106** 202404 (2015).
[3] R. Wamg, Y. J. Jin, J. Z. Zhao, Z. J. Chen, Y. J. Zhao, and H. Xu, Phys. Rev. B **97,** 195157 (2018).
[4] F. Bisti, V. A. Rogalev, M. Karolak, S. Paul, A. Gupta, T. Schmitt, G. Guntherodt, V.Eyert, G. Sangiovanni, G. Profeta, and V. N. Strocov, Phys. Rev. X **7**, 041067 (2017).
[5] K. Iwai, Y. Muraoka, T. Wakita, M. Hirai, T. Yokoya, Y. Kato, T. Muro, Y. Tamenori, et al. J. Appl. Phys. **108**, 043916 (2010).

Soft X-ray absorption spectroscopy of cyclodextrin compounds including a noble metal atom

Kiminori Baba [a)] and Hiroaki Yoshida [a,b)]

[a] *Physics program, Graduate School of Advanced Science and Engineering, Hiroshima University, 1-3-1 Kagamiyama, Higashi-Hiroshima, 739-8526 Japan.*
[b] *Hiroshima Synchrotron Radiation Center, Hiroshima University, 2-313 Kagamiyama, Higashi-Hiroshima, 739-0046 Japan.*

Keywords: Cyclodextrin, gold, inclusion, potassium, X-ray, absorption

Introduction

An environmentally friendly method for gold recovery is recently proposed as simple as mixing $KAuBr_4$ and cyclodextrins [1]. A 1:2 ratio of $KAuBr_4$ and α-CD forms gold-containing nanowires that precipitate immediately, whereas β- and γ-CD do not. The different binding positions of K to CD is considered to be determine whether nanowire formation occurs or not by the results of crystallographic analysis [1]. To investigate the difference in the binding of K to each CD in aqueous solution, soft X-ray absorption spectroscopy of the K2p absorption edge was performed at the beamline BL-6 of HiSOR.

Experiment

A mixture of $KAuBr_4$ aq. (2 mM) and CD aq. (4 mM) was prepared and the measurements were carried out on drop-dried films. The solution was dropped onto a stainless plate and vacuum dried. This process was repeated several times to obtain a K-containing thin film with sufficient concentration to be used for drain current measurement. The sample was placed in a vacuum chamber, and synchrotron radiation was incident at an angle of 45° to the normal of the sample. The obtained signals were normalized by incident light intensities.

Results and Discussion

First, solid samples of KCl was measured for energy calibration (Figure 1). The obtained spectrum shows two well-resolves peaks for each 2*p* spin-orbit component. Crystal-field splitting, T_{2g} and E_g, in crystals with cubic symmetry is observed in each 2*p* peak. The spectrum is good agreement with the previous study [2] and the energy axis is calibrated at $2p_{3/2} \rightarrow 3d$ (296.461 eV) and $2p_{1/2} \rightarrow 3d$ (299.141 eV) peaks. Figure 1 also shows the spectra of $KAuBr_4$ and a 1:2 mixture of $KAuBr_4$ and α-, β-, and γ-CD in the films.

The spectrum of $KAuBr_4$ has a similar shape to that of KCl. Although the respective peak widths are broadened, the peak energies of $2p_{3/2}$ and $2p_{1/2}$ are almost the same. On the other hand, in the spectrum of the cyclodextrin mixture, the respective spin-orbit peaks become broader. The difference between the α-, β-, and γ-CD spectra is small. This may be due to the formation of bonds between various sites of cyclodextrins and K in the liquid, which disrupted the crystalline field around K.

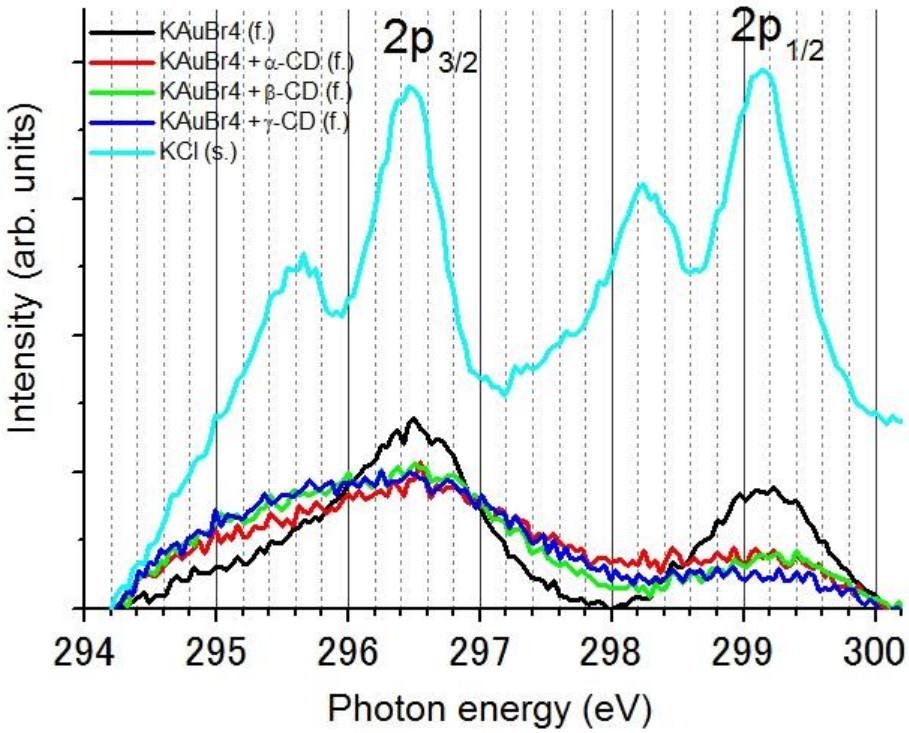

Figure 1 XAS spectra of KCl(solid), $KAuBr_4$(film), $KAuBr_4$+α-CD(film), +β-CD(film), and +γ-CD (film) at the K2p edge.

REFERENCES

[1] Z. Liu et al., *Nat. commun.* **2013**, 1855.
[2] F. Sette et al., *Phys. Rev.* B **39** (1989**)** 11125-11130.

Soft X-ray photoelectron spectroscopy of the metal complex included in cyclodextrin

Kiminori Baba [a)], Hitoshi Sato [b)], and Hiroaki Yoshida [a,b)]

[a] *Physics program, Graduate School of Advanced Science and Engineering, Hiroshima University, 1-3-1 Kagamiyama, Higashi-Hiroshima, 739-8526 Japan.*
[b] *Hiroshima Synchrotron Radiation Center, Hiroshima University, 2-313 Kagamiyama, Higashi-Hiroshima, 739-0046 Japan.*

Keywords: Cyclodextrin, gold, inclusion, X-ray, photoelectron

Introduction

Gold is a finite resource and is currently used for decoration and inside electronic devices. In recent years, there has been an urgent need to recover and reuse gold contained in industrial waste. In this study, we focused on the galvanic substitution reaction as a method to recover gold from $AuBr_4^-$, which is formed by dissolving gold during the recovery process. The galvanic substitution reaction is a spontaneous reaction caused by the difference in standard redox potentials [1]. When a Ni plate is immersed in a $KAuBr_4$ solution, $AuBr_4^-$ undergoes galvanic substitution with Ni and Au is deposited. During this process, the reddish-brown solution turned transparent. In order to obtain information about the precipitates on Ni, photoelectron spectroscopy experiments were performed at BL7 in HiSOR, and the photoelectron spectra in the Au 4*f* region were discussed.

Experiment

Ni discs (0.1 mm thick, φ = 3 mm) were immersed in 20 mM $KAuBr_4$ solution in a vial to precipitate the Au complex; if CD was added, the equivalent of 40 mM was added. After immersing the Ni plate in each solution for more than 24 hours, the sample was removed onto filter paper, washed three times with milli-Q water, and transferred to a vacuum chamber to dry. The sample holder was made of oxygen-free copper and silver paste was used to bond the holder to the sample. To investigate the electronic structure of the deposited gold, photoelectron spectroscopy was performed at HiSOR BL-7 using SR in the incident light energy range from 50 eV to 400 eV.

Results and Discussion

Figure 1 shows the soft x-ray photoelectron spectra in the Au 4f region of the precipitates. The incident light energy is 200 eV. Neutral Au (Au^0; 0-valent) has $4f_{7/2}$ and $4f_{5/2}$ peaks at 83.8 and 87.1 eV, respectively. On the other hand, when ionized, each peak shifts to the higher binding energy side, with peaks at Au^{1+} (85.6 and 89.1 eV) and Au^{3+} (87.3 and 90.4 eV), respectively [2]. Gold bromide (present as Au_2Br_6) is also stable as a neutral compound containing gold and bromine. It may precipitate and in this case, Au^{3+} would be observed. Comparison of the Au 4*f* photoelectron spectra of the fresh Au^0 film already installed at BL-7 and the present precipitates on the Ni plate surface shows that the peak energies of the respective 4f peaks are almost same between them. It is, thus, indicating that the precipitated material is not Au_2Br_6 but neutral gold Au^0. The peak position does not shift when cyclodextrin was added. These results confirm that the galvanic substitution reaction occurred under the present experimental conditions. In the future, we plan to obtain

information on the reaction rate by examining the time variation of the UV spectra, and to try to control the reaction by using inclusion by cyclodextrins.

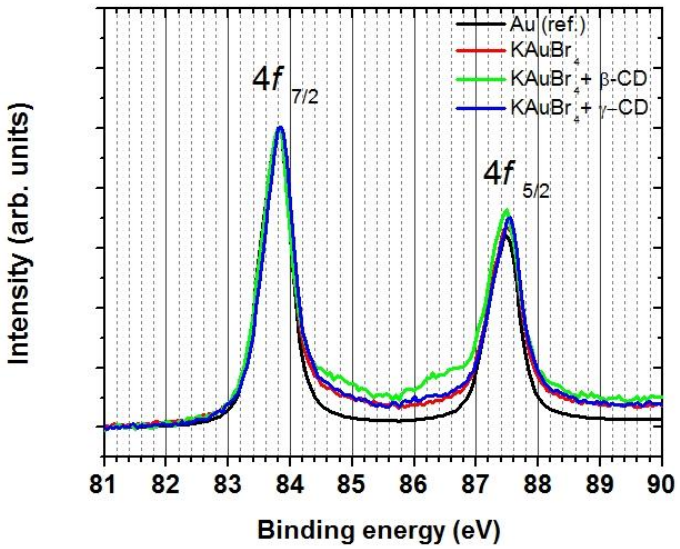

Figure 1 Comparison of the soft x-ray photoelectron spectra in the Au 4*f* region between a fresh Au film and the respective precipitates; $KAuBr_4$, $KAuBr_4$+β-CD, and $KAuBr_4$+γ-CD films.

REFERENCES

[1] A. Volta, *Phil. Trans. Royal Soc.* **90** (1800) 403–431.

[2] J.-P. Sylverstre et al., *J. Phys. Chem.* B **108** (2004) 16864-16869.

Hard X-ray absorption spectroscopy of a gold complex included by cyclodextrin

Kiminori Baba [a)], Shinjiro Hayakawa [b)], and Hiroaki Yoshida [a,c)]

[a] *Physics program, Graduate School of Advanced Science and Engineering, Hiroshima University, 1-3-1 Kagamiyama, Higashi-Hiroshima, 739-8526 Japan.*
[b] *Applied Chemistry program, Graduate School of Advanced Science and Engineering, Hiroshima University, 1-4-1 Kagamiyama, Higashi-Hiroshima, 739-8527 Japan.*
[c] *Hiroshima Synchrotron Radiation Center, Hiroshima University, 2-313 Kagamiyama, Higashi-Hiroshima, 739-0046 Japan.*

Keywords: Cyclodextrin, gold, inclusion, potassium, X-ray, absorption

Introduction

Gold recovery using the inclusion of cyclodextrins (CDs) has been proposed as an environmentally friendly method [1]. This method is as simple as mixing $KAuBr_4$ and CD in a 1:2 ratio; α-CD forms gold-containing nanowires that precipitate immediately, whereas β- and γ-CD do not. Crystallographic analysis suggests that the different binding positions of K to CD determine whether nanowire formation occurs or not. To investigate the difference in the binding of K to each CD in aqueous solution, X-ray absorption spectroscopy of the K1s absorption edge was performed at the beamline BL-11 of HiSOR.

Experiment

A mixture of $KAuBr_4$ aq. (20 mM) and CD aq. (40 mM) was prepared and the measurements were carried out on drop-dried films. 20 μl of the solution was dropped onto a potassium-free quartz glass and vacuum dried. This process was repeated five times to obtain a K-containing thin film with sufficient concentration to be used for fluorescence measurement. A special holder was used for the measurement as a solution and the concentration of $KAuBr_4$ aq. was 50 mM. The sample was placed in the He chamber, and synchrotron radiation was incident at an angle of 45° to the normal of the sample. The incident light intensity for normalization was measured by filling the ion chamber with He-N_2 mixed gas.

Results and Discussion

First, solid samples of KCl and KBr were measured for energy calibration (Figure 1). The obtained spectrum of KCl is good agreement with the previous study [2] and the energy axis was calibrated at the Pre-edge peak 3610.2 eV and Post-edge peak 3614.2 eV. Figure 2 shows the spectra of $KAuBr_4$ in film and liquid and a 1:2 mixture of $KAuBr_4$ and α-CD in the film. In the drop-dried film of $KAuBr_4$ aq., K^+ and $AuBr_4^-$ are considered to be ionically bonded and not expected to form molecular orbitals by coordination bonds. Therefore, the K^+ 1s→4p transition appears strongly at 3611.5 eV. On the other hand, the spectrum of $KAuBr_4$@α-CD is similar to that of liquid $KAuBr_4$ due to the coordination of some H_2O to K^+. In Figure 3, the spectra of drop-dried films when various CDs are mixed with $KAuBr_4$ solution. Comparing each spectrum, there is a difference especially in the intensity around 3610 eV. The spectra were fit and separated by the components for each peak and the difference in the peak intensities is discussed in point of the binding of K to each CDs.

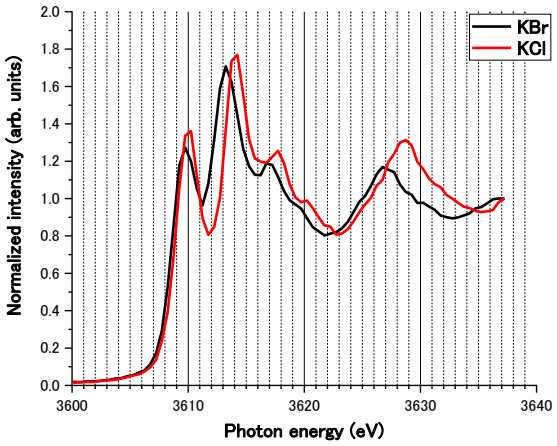

Figure 1 XAS spectra of KCl and KBr at the K1s edge.

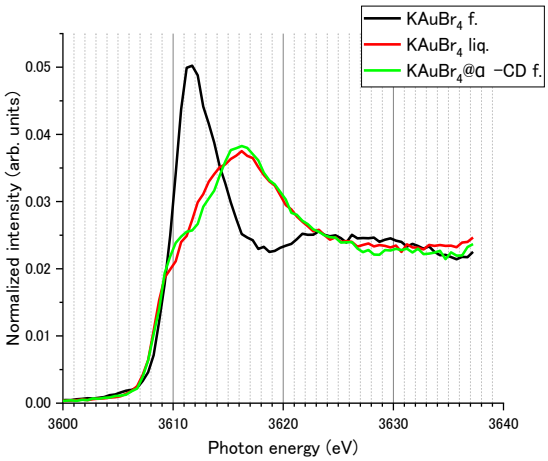

Figure 2 XAS spectra of $KAuBr_4$ (film), $KAuBr_4$ (liquid), and $KAuBr_4$@α-CD (film) at the K1s edge.

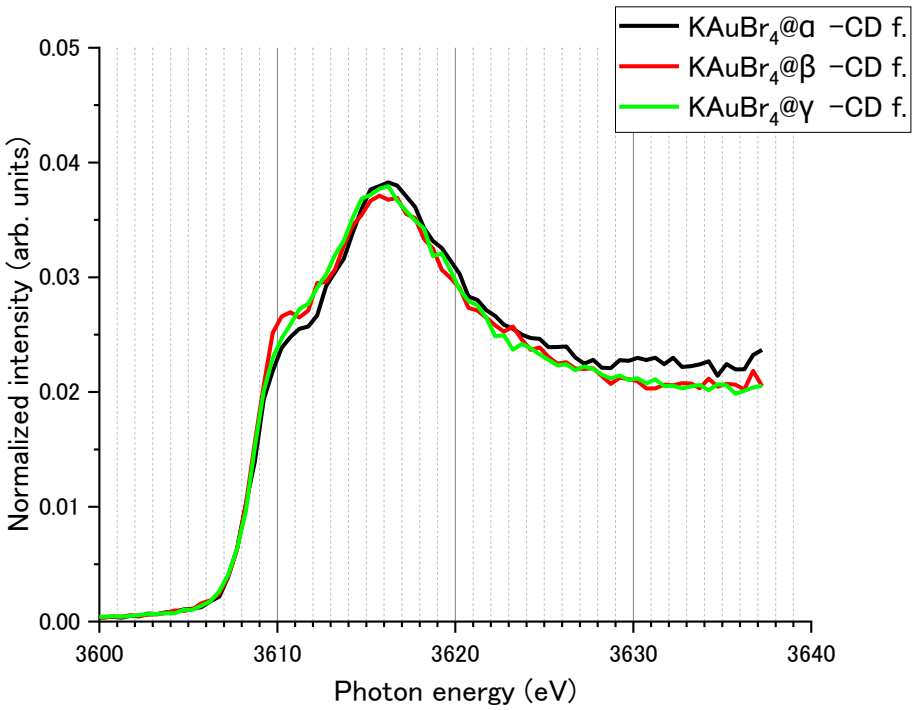

Figure 3 XAS spectra of $KAuBr_4$@α-CD, @β-CD, and @γ-CD (film) at the K1s edge.

REFERENCES

[1] Z. Liu et al., *Nat. commun.* **2013**, 1855
[2] W. Li et al., *Geosatand. Geoanal. Res.*, **44** (2020**)** 805-819

Investigation of the Origin of Photo-Induced Doping on $TlBiSe_2$

R. Itaya[a], Y. Toichi[a], R. Nakanishi[a], Y. Nakata[b], K. Kasai[b], K. Kuroda[c], M. Arita[d], I. Yamamoto[e], K. Fukutani[f] and K. Sakamoto[a]

[a] *Graduate School of Engineering, Osaka University, Osaka 565-0871 Japan*
[b] *Graduate School of Science and Engineering, Chiba University, Chiba 263-8522 Japan*
[c] *Graduate School of Advanced Science and Engineering, Hiroshima University, Higashi-Hiroshima 739-0046, Japan*
[d] *Hiroshima Synchrotron Radiation Center, Hiroshima University, Higashi-Hiroshima 739-0046, Japan*
[e] *Synchrotron Light Application Center, Saga University, Saga 840-8502, Japan*
[f] *Institute for Molecular Science, National Institutes of Natural Sciences, Okazaki, 444-8585, Japan*

Keywords: Topological insulators, hole-doping, photo-induced reaction.

Topological insulators (TIs) are promising materials for spintronics applications owing to their spin-polarized metallic electronic states that prohibit the 180° backscattering. This peculiar spin-polarized states also shows the possibility to control the direction of spin current by switching the TI from p-type to n-type or vice versa. In order to make this switching, one need to tune the Fermi level. This means that developing an easy way to dope charge into TIs is highly recommended to fabricate highly functional spintronics devices such as topological p-n junctions. In addition, this doping will make the bulk, which is metallic in most TIs due to the presence of defect, insulating, that is another key to make TIs possible for spintronics device materials. Doping of TIs has been studied, for example, by doping Ca in bulk Bi_2Se_3 and making $Bi_{2-\delta}Ca_\delta Se_3$ [1] or adsorbing O_2 molecules on Bi_2Se_3 [2], but these doping methods have problems in terms of stability.

Photo-induced doping is a process of holding the bulk of Bi_2Se_3 and Bi_2Te_3 insulating by H_2O exposure followed by VUV and/or SX light irradiation [3]. This method has the possibility of creating devices such as topological p-n junctions by using kind of photomasks like in photolithography. However, Bi_2Se_3 and Bi_2Te_3 have no chance to be bulk insulating p-type TI, because the Dirac point is located below the bulk valence band [4]. In contrast to these TIs, $TlBiSe_2$ has its Dirac point at almost the center of its wide bulk band gap (ca. 300 meV), and thus is one of the most suitable TIs for device applications [4]. Based on these, we tried to do photo-induced doping on $TlBiSe_2$ in our former study. As a result, we succeeded to dope hole into $TlBiSe_2$ by photo irradiation, and making both n-type and p-type $TlBiSe_2$.

In the present study, we performed photon energy-dependent ARPES measurements, at BL-9A of HiSOR, in order to investigate the origin of photo-induced doping on $TlBiSe_2$. In case of Bi_2Se_3 and Bi_2Te_3, the hole-doping were reported to originate by exciting the core-level of the outermost atom, i.e., Se or Te [3]. The surface structure of $TlBiSe_2$ is different from Bi_2Se_3 and Bi_2Te_3, and thus the doping might occur with a different process. As shown in Fig. 1(a), the surface of $TlBiSe_2$ is half covered by Tl islands [5]. $TlBiSe_2$ was cleaved under a UHV condition, exposed to H_2O, and then irradiated with synchrotron radiation light of 10, 20, and 35 eV. As can be seen in Fig. 1(b), 35 eV photon energy allows to excite the Bi core-level, and 20 eV photon energy to excite the Tl core-level. Figures 2(b) and (c) show the results of ARPES measurements after H_2O exposure followed by photo-irradiation at 20 eV and 35 eV, respectively. Compared with the clean $TlBiSe_2$ surface (Fig. 2(a)), the binding energy of the Dirac point (indicated by red line) is shifted to the low binding energy in both cases. However, this shift is smaller than that of the $TlBiSe_2$ surface irradiated at 100 eV(Fig. 2(d)) with the same amount of H_2O exposure. The small shift would originate from the removal of residual gas adsorption, which causes the aging effect, by photo-irradiation [3]. In the present talk, we will explain the mechanism of photo-induced hole doping on $TlBiSe_2$ in more details.

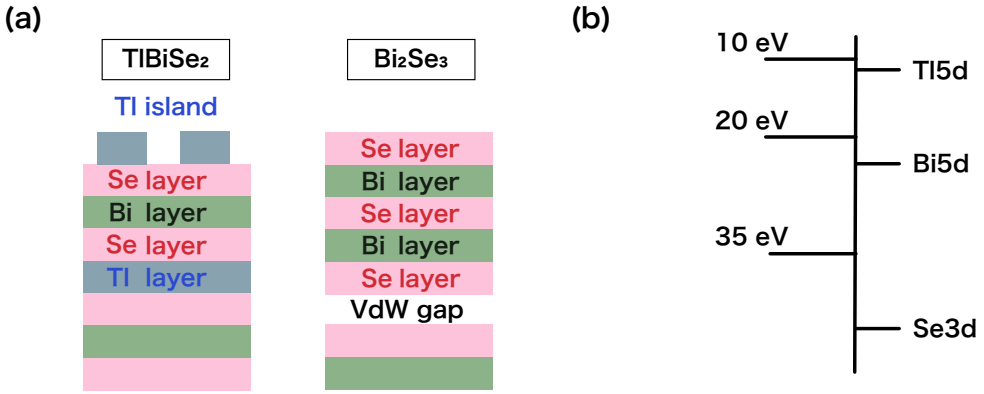

FIGURE 1. (a) Schematic diagram of the surfaces of two different Tis, $TlBiSe_2$ and Bi_2Se_3. (b) Schematic diagram of the relation between the binding energies of Tl5d, Bi5d, and Se3d and the photon energies used in the present study.

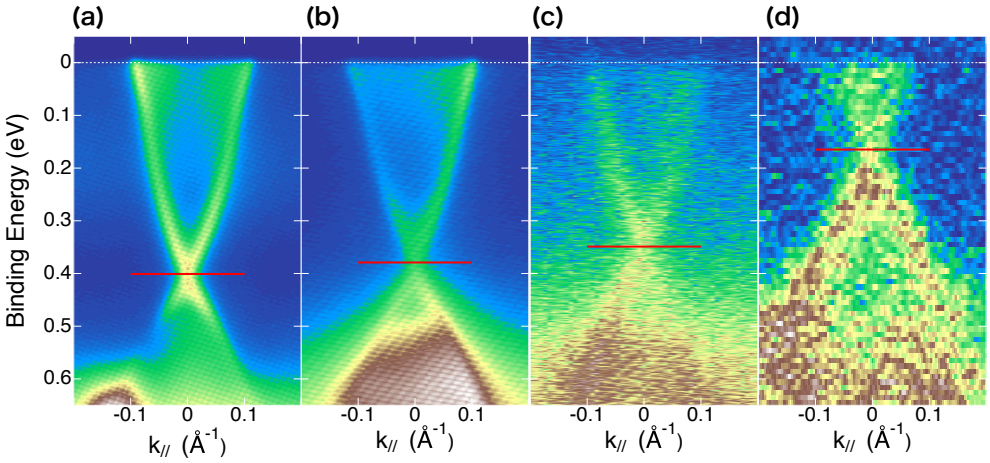

FIGURE 2. Valence bands of (a) a pristine $TlBiSe_2$ ($h\nu$=20 eV), and 5 ML of H_2O exposure followed by (b) $h\nu$= 20 eV, (c) 35 eV, and (d) 100 eV photo-irradiation. (d) has been obtained at the BL13 VLS station of Saga Light Source. Red lines indicate the position of Dirac point.

REFERENCES

1. D. Hsieh,Y. Xia, D. Qian, L. Wray, J. H. Dil, F. Meier, J. Osterwalder, L. Patthey, J. G. Checkelsky, N. P. Ong, A. V. Fedorov, H. Lin, A. Bansil, D. Grauer, Y. S. Hor, R. J. Cava and M. Z. Hasan , Nature **460**, 1101 (2009).
2. Y. Chen, J.-H. Chu, J. G. Analytis, Z. K. Liu, K. Igarashi, H.-H. Kuo, X. L. Qi, S. K. Mo, R. G. Moore, D. H. Lu, M. Hashimoto, T. Sasagawa, S. C. Zhang, I. R. Fisher, Z. Hussain, Z. X. Shen, Science **329** 659 (2010).
3. K. Sakamoto, H. Ishikawa, T. Wake, C. Ishimoto, J. Fujii, H. Bentmann, M. Ohtaka, K. Kuroda, N. Inoue, T. Hattori, T. Miyamachi, F. Komori, I. Yamamoto, C. Fan, P. Krüger, H. Ota, F. Matsui, F. Reinert, J. Avila, and M. C. Asensio, Nano Lett. **21**, 4415 (2021).
4. O. V. Yazyev, J. E. Moore, and S. G. Louie, Phys. Rev. Lett. **105**, 266806 (2010).
5. K. Kuroda, M. Ye, A. Kimura, S. V. Eremeev, E. E. Krasovskii, E. V. Chulkov, Y. Ueda, K. Miyamoto, T. Okuda, K. Shimada, H. Namatame, and M. Taniguchi, Phys. Rev. Lett. **105**, 146801 (2010).

Structure of a Novel Amorphous Organic-Inorganic Hybrid Tin Cluster Exhibiting Nonlinear Optical Effects by Low-Energy XAFS Measurements

Jens R. Stellhorn[a], Shinjiro Hayakawa[a], Benedict Paulus[b], Benjamin D. Klee[b], Wolf-Christian Pilgrim[b], Stefanie Dehnen[b]

[a] *Department of Applied Chemistry, Graduate School of Advanced Science and Engineering, Hiroshima University, Higashi-Hiroshima, Hiroshima 739-8527, Japan*
[b] *Department of Chemistry, Philipps University of Marburg, Marburg 35032, Germany*

Keywords: non-linear optical properties, white-light generation, amorphous compound, local structure, EXAFS.

Tailored light sources have greatly advanced technological and scientific progress by optimizing colour and brilliance, improving energy efficiencies or the quantum properties of light. So called supercontinuum generators are premier examples for media with nonlinear optical (NLO) effects – far superior in some respects to other sources such as phosphorescent white light-emitting diodes (LEDs). However, unlike LEDs, most of these advanced light sources are only used for scientific purposes, as they require extreme electric field strengths which are commonly realized by high-power pulsed lasers. In contrast, the materials of interest for this research project represent a new generation of supercontinuum emitters that are readily obtained from ubiquitous resources in a simple synthesis.

In our study [1], we investigated the local structure of 4 different amorphous organotin sulfide [$(R\text{-}Sn)_4S_6$] compounds by X-ray absorption spectroscopy. These compounds exhibit a non-linear optical response upon irradiation with a continuous-wave near-infrared laser.[2-4] Their basic structural motif is a hetero-adamantane cluster with different organic substituents R. The nature of the NLO response depends strongly on the morphology of the material, which is influenced by the choice of the organic substituents, leading to either a second harmonic generation or the generation of a supercontinuum, potentially appearing as white light.

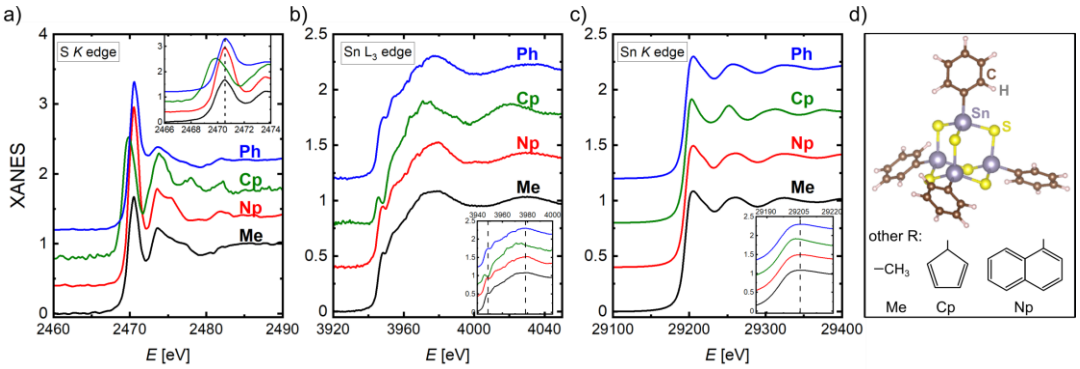

Fig. 1: XANES data for the 4 organotin sulfide samples (Me: black, Np: red, Cp: green, Ph: blue, shifted upwards for clarity) at the S *K* (a), the Sn L_3 (b) and the Sn *K* edge (c). The insets highlight the regions close the first maxima of the respective edges. A model of the Ph-Cluster from a DFT simulation[2] is illustrated in (d), along with schematic illustrations of the other organic substituents.

Due to the amorphous nature of the materials, their structural properties, and thereby the apparent origin of this effect, is difficult to determine [3]. Despite these difficulties, our results provide experimental evidence that the nature of the NLO properties is tied to distortions occurring at the cluster core, with almost ideal clusters in compounds that show second harmonic generation, and strongly distorted clusters in the case of compounds that generate a supercontinuum. These distortions may enable a closer proximity of the cluster cores, and thereby influence the NLO response by altering the intermolecular order.

As an example, Figure 1 illustrates the near-edge structure of the absorption spectrum (XANES) around the S *K*, Sn L_3 and Sn *K* edges (the latter was measured at P65 of the PETRA-III synchrotron). In all datasets, the edge of the cluster with R=Cyclopentadienyl (Cp) is shifted to lower energies (see insets in Fig. 1), indicating a change in the oxidization state of the cluster core. As we will show in the analysis of the XAFS data, this leads to a significant distortion of the cluster relative to the other compounds.

All in all, the XAFS experiments at the S *K* edge performed at BL11 of HiSOR provide key information about the potential proximity of neighboring clusters, and therefore contain information on the intermolecular order of the system.

REFERENCES

[1] J.R. Stellhorn et al., in preparation.
[2] N.W. Rosemann et al., Science 6291, 1301 (2016).
[3] B. D. Klee, et al., Phys. Stat. Solidi B 255, 1800083 (2018).
[4] K. Hanau et al., Angew.Chem. Int. Ed. 60, 1176-1186 (2021).

Development Of A New Device For Angular Dependent Conversion Electron Yield XAFS Measurements

Shinjiro Hayakawa [a], Haruka Yoshimoto[a], Jens R. Stellhorn[a], Kenji Komaguchi[a]

a *Applied Chemistry program, Graduate School of Applied Science and Engineering,, Hiroshima University, Higashi-Hiroshima, Hiroshima 739-8527, Japan*

Keywords: XAFS, conversion electron yield, angular dependence, polythiophene

Introduction

X-ray absorption fine structure (XAFS) measurements in the soft X-ray region are widely conducted with X-ray fluorescence yield (XFY) method and electron yield method owing to the difficulties in preparing samples of appropriate optical thickness for the transmission method. We have been employing conversion electron yield (CEY) method [1] that utilizes the ionization of surrounding gas molecules by the energetic Auger electrons from a sample. CEY is advantageous in the sense of S/N compared to XFY owing to the extremely small fluorescence yield in the soft X-ray region. However, the use of an electrode that prevents created electron-ion pairs from the recombination has made the angular dependent measurements difficult. We have developed a new device that can make the angular dependent XAFS measurements using CEY method. The device was applied to the fractional determination of orientations in polythiophene thin films.

2. Experimental

2.1 CEY device

Principles of the CEY measurements are similar to those of X-ray detection with an ionization chamber except for the ionization source of gas molecules. Typically He gas is employed to reduce the direct ionization with X-rays, and a planer electrode has been adopted in BL-11 to avoided the recombination of the created electron-ion pair. To overcome the interference of the electrode with incident X-rays, we have adapted a rod-shaped electrode that is similar to the proportional counter (PC) for X-ray detection, and the PC could be utilized for measuring CEY from the sample placed in the counter when operated with the mixture of He and methane [2].

Figs.1 show schematic side view and the photograph of the new device. Two electrodes of semicircle rod shape were arranged below and above the beam height. The diameter of the electrode, *b*, was 6 mm, and the

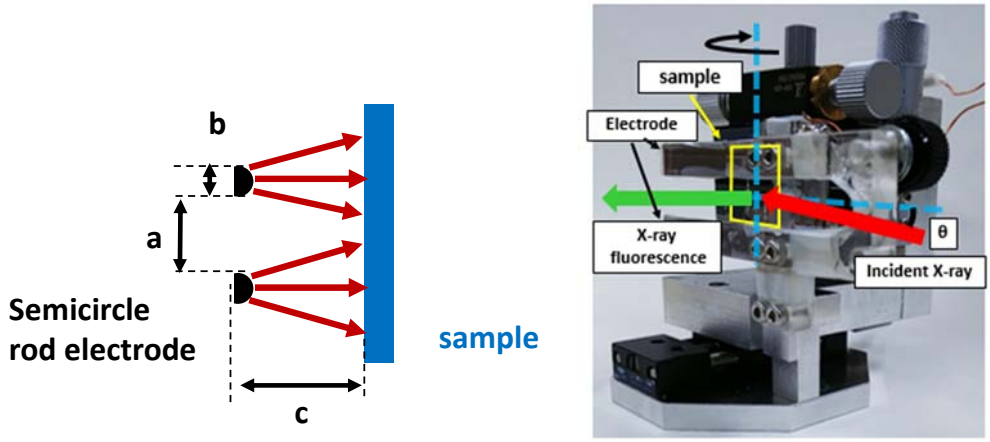

FIGURES 1. Schematic side view around the electrodes and the photograph of the new device

size was determined to make the strength of the electric field around the sample relatively uniform within the region of the ionization chamber while the electron cascade around the electrode was prevented. The clearance between the electrodes, *a*, was 8 mm, and the distance between the sample surface and the center of the electrode, *c*, was 8 mm. A sample was mounted on the rotational stage or a rotational axis of a motor for in plane rotation.

2.2 P3HT samples

Several types of poly (3-hexylthiophene-2,5-diyl) (P3HT) were spin coated onto Si or ITO glass substrates. Among them a special P3HT sample was prepared with a commercial P3HT reagent, and the surface of the ITO substrate was previously brushed with a velvet fabric. The sample showed uniaxial edge-on orientation, and the majority of the backbone of P3HT molecules were aligned along the brushing direction [3].

XAFS measurements were performed on BL-11, and both XFY and CEY were measured simultaneously. The developed new device was utilized for the XAFS measurements with the various glancing and azimuthal angles.

3. Results and discussion

Fig. 2 shows a series of sulfur K-edge XAFS spectra from the uniaxial edge-on sample. The glancing angle was 80 deg, and the incident beam was almost normal to the surface. It was clear that the XAFS spectra have azimuthal angular dependence, and the uniaxial character of the film could be explained with the angular dependences of σ* and π* peaks in the spectra.

Figs. 3 and 4 show azimuthal angular dependence of σ* and π* peak intensities. Fitting procedures with the theoretical model provided fractions of orientations in the sample.

In this presentation the principles and the advantages of the new device will be explained、and the results of the fractional determination of the P3HT orientations will be presented.

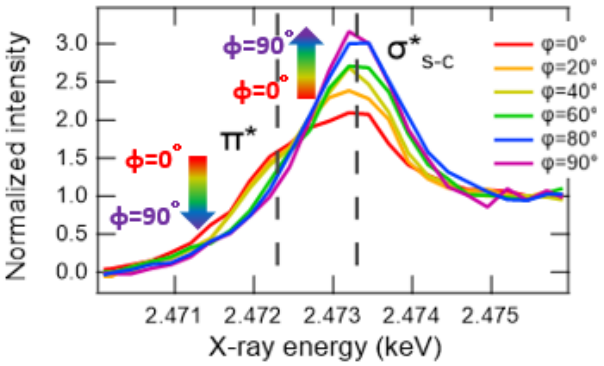

FIGURE 2. Polarization (azimuthal angle) dependence of Sulfur K-edge XAFS spectra of a P3HT film of uni-axial edge-on orientation.

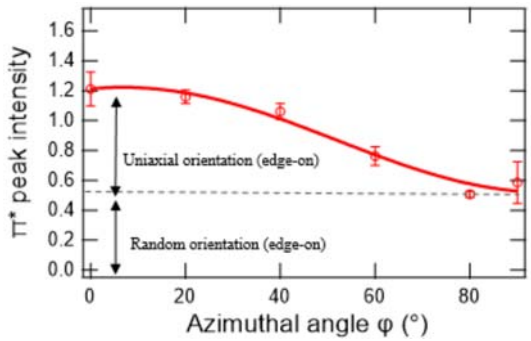

Figure 3. Azimuthal angle dependence of π* peak intensities

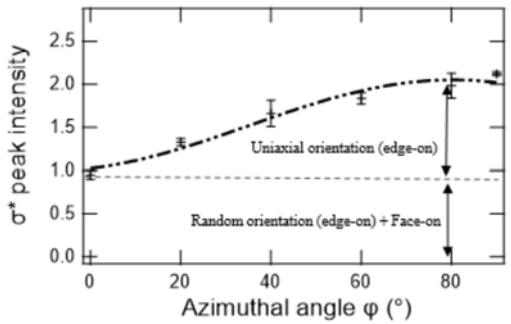

Figure 4. Azimuthal angle dependence of σ* peak intensities

REFERENCES

1. S. Hayakawa et al., Spectrochim. Acta. B , 54B (1999) 235-240.
2. S. Hayakawa et al., Jpn. J. Appl. Phys.,38 (1999) 2161-2163.
3. M Imanishi et al., Sci.Rep.,7(2017)514,

C K-edge XAFS measurements for detection of unsaturated bonds in organically bridged silica materials

Shinjiro Hayakawa [a], Joji Oshita[a,b], Kei Oshima[a,b], Shogo Tendo[c],

Toshinori Tsuru[d], Shinichi Wada[c]

a *Applied Chemistry program, Graduate School of Applied Science and Engineering,, Hiroshima University, Higashi-Hiroshima, Hiroshima 739-8527, Japan*
b *Smart Innovation program, Graduate School of Applied Science and Engineering,, Hiroshima University, Higashi-Hiroshima, Hiroshima 739-8527, Japan*
c *Physics program, Graduate School of Applied Science and Engineering,, Hiroshima University, Higashi-Hiroshima, Hiroshima 739-8526, Japan*
d *Chemical Engineering program, Graduate School of Applied Science and Engineering,, Hiroshima University, Higashi-Hiroshima, Hiroshima 739-8527, Japan*

Keywords: XAFS, unsaturated bond, organosilica, carbon K-edge

Introduction

Microporous organosilica membranes are attractive because of unique features such as a high surface area, improved hydrothermal stabilities, and applications of them are widely expanding [1]. Most of researches have been focused on bis-(triethoxysilyl)ethane (BTESE) and characteristics of BTESE derived materials. To expand the possibilities of organosilica membranes we have been exploring different precursors to introduce ethylene and acetylene bridges into the organosilica membranes. Though the properties of the synthesized organosilica were characterized by the many analytical methods, there exists no method that provide the evidence of the unsaturated carbon bond. Moreover, the quantification of the amount of the unsaturated bonds is quite difficult. We have utilized C K-edge XAFS spectroscopy for detecting remained unsaturated bonds in PMOs, and the possibilities of quantification will be discussed.

2. Experimental

2.1 Samples

Table 1 shows precursors used for synthesis of organically bridged silica materials. Three types of precursor were utilized including bis-(triethoxysilyl)ethane, bis-(triethoxysilyl)ethylene and bis-(triethoxysilyl)acetylene, and their ethoxysil groups were converted into siloxane or silanor groups via the hydrolysis and polymerization. Ethanol solutions of samples (5 wt %) were prepared for each, and a 30 μL of the solution was dropped three times onto a Si substrate of approximately 15 mm square under atmospheric condition.

TABLE 1. Samples and their precursors of the organically bridged silica materials investigated.

Sample name	Precursor	Approximate mass fraction of carbon
BTES-E1 ethane bridge	$(EtO)_3SiCH_2CH_2Si(OEt)_3$	18.17 %
BTES-E2 ethylene bridge	$(EtO)_3SiCHCHSi(OEt)_3$	18.45 %
BTES -E3 acetylene bridge	$(EtO)_3SiCCSi(OEt)_3$	18.74 %

2.2 XAFS measurements

Experiments were carried out on the beamline BL13 [2]. Incident X-rays were monochromatized with a grating monochromator, and the incident X-ray intensity was monitored from a Au coated grid of stainless steel. The beam size at the sample position was approximately 1 mm square, and the glancing angle of 20 deg. was employed for X-ray absorption fine structure (XAFS) measurements. Total electron yield (TEY) from a sample was monitored, and the normalized spectra were utilized for the further analysis. To avoid the inhomogeneity of the sample on the substrate, several positions on the sample were selected for measurements. Incident X-ray energy was calibrated with the main peak obtained with PMMA, and the observed spectra were shifted to 1.44 eV minus to let the peak energy of PMMA be 288.34 eV.

3. Results and discussion

Figure 1 shows C K-edge XAFS spectra of organically bridged silica materials. Obtained main peak with ethane bridged silica material (BTES-E1) showed a main peak around 290.2 eV, and the spectrum was almost identical to that obtained with the blank (Si substrate). On the other hand two spectra of ethylene bridged silica material (BTES-E2) showed the characteristic peak around 285.04 eV. The peak energy was similar to the reported value of 1s to π* transition (around 285 eV) obtained from the adsorbed ethylene on the Si substrate [3]. Though the similar peak corresponding to1s to π* transition was expected with acetylene bridged silica, no clear peak was observed while the broadened peaks remained in the present experiment. It was clear that the direct evidence of the remaining unsaturated carbon bond in the organically bridged silica material could be monitored with the C K-edge XAFS spectroscopy. While the contribution of the surface contamination with the hydrocarbon should be considered for determination of the portion of the unsaturated bond in the sample.

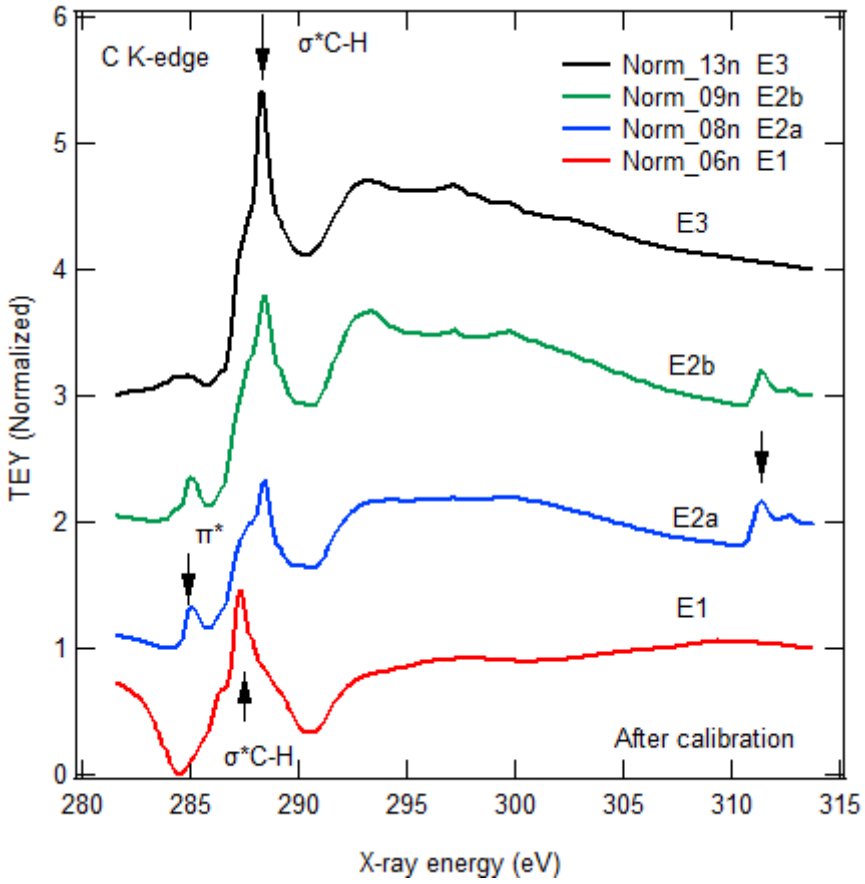

REFERENCES

1. R. Xuet al., Appl. Mater. Interfaces 6(2014) 9357-9364.
2. S. Wada et al., Surf. Sci. 601 (2007) 3833-3837.
3. F. Matsui et al., Surf. Sci. 401 (1998) L413-419.

Desiccation-Induced Conformational Change of Group 3 LEA Protein in the presence of Membrane Characterized by Vacuum-Ultraviolet Circular Dichroism Spectroscopy

Shun Sawada[a], Munehiro Kumashiro[b], Ryota Imaura[b], and Koichi Matsuo[c]

[a] *Faculty of Science, Hiroshima University*
[b] *Graduate School of Science, Hiroshima University,*
[c] *Hiroshima Synchrotron Radiation Center, Hiroshima University*

Keywords: circular dichroism, G3LEA protein, membrane, phase transition, secondary structure, trehalose, water

Elucidating the molecular mechanisms of cell desiccation tolerance is necessary for engineering the biological stability of mammalian cells in dry state and for developing countermeasures against foodborne illnesses caused by dry foods. Recent studies have reported that organisms, including sleeping chironomid, survive severe dehydration by accumulating saccharides and proteins, such as trehalose and group 3 late embryogenesis abundant (G3LEA) protein, inside their cells [3]. Although the trehalose protects cell structure and function via the well-understood mechanisms of water replacement and glass formation, the molecular mechanism of desiccation protection by the G3LEA protein remains to be further explored. In this study, to characterize the desiccation protection mechanism of G3LEA protein, we measured vacuum-ultraviolet circular dichroism (VUVCD) spectra of two tandem repeats of 11-mer consensus motif of G3LEA protein in the presence of lipid membranes under aqueous and dry conditions. We also investigated the conformation of G3LEA peptide in the presence of trehalose to reveal the synergistic effect of G3LEA protein and trehalose on the desiccation protection.

G3LEA peptide was synthesized in GL Biochem (Shanghai, China). 1,2-Dimyristoyl-sn-glycero-3-phosphatidylcholine (DMPC), 1,2-dimyristoyl-sn-glycero3-phosphatidylglycerol (DMPG), and 1-palmitoyl-2-oleoyl-snglycerol-3-phosphatidylcholine (POPC) lipids were purchased from Avanti. D-(+)-trehalose was obtained from Sigma. Each molecule was dissolved in 10 mM phosphate buffer (pH 7.4). Liposome suspension was prepared using extrusion technique with 100 nm polycarbonate filter, and then mixed with peptide solution at lipid-to-peptide molar ratio of 10. A 100 µl droplet was dried on a CaF_2 window in a vacuum overnight. The VUVCD spectra of G3LEA peptide were measured at HiSOR BL-12. The artefacts from linear dichroism and linear birefringence in VUVCD spectra of dry samples were eliminated by averaging the VUVCD spectra measured at four rotation angles (θ , ϕ) = (0°, 0°) (0°, 180°), (90°, 0°), and (90°, 180°), where θ is the angle around axis parallel to the incident light and φ is the angle around axis vertical to the incident light. The content of secondary structures of G3LEA protein was estimated by using SELCON3 software and VUVCD dataset.

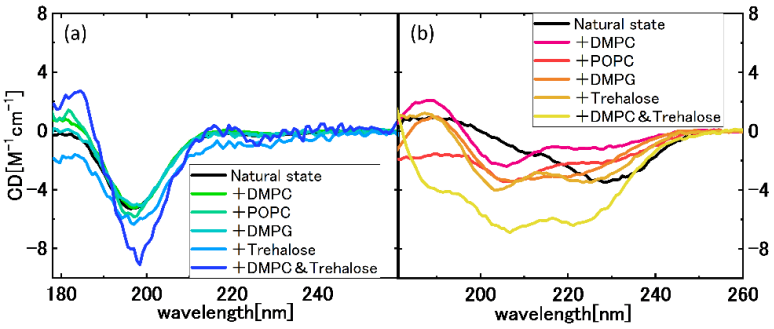

FIGURE 1. VUVCD spectra of G3LEA peptide under (a) aqueous and (b) dry conditions at 25° C.

Figure 1 (a) shows the VUVCD spectra of G3LEA peptide in the presence and absence of DMPC, DMPG, and POPC liposomes under aqueous condition. Native G3LEA peptide shows a negative peak CD at 200 nm, which is characteristic for random coil structure of proteins. The spectral shapes of G3LEA peptide in DMPC, DMPG, and POPC liposomes were consistent with that of native G3LEA peptide, indicating that G3LEA peptide did not interact with liposomes in aqueous solution. Figure 1 (b) shows the VUVCD spectra of G3LEA peptide in the presence of DMPC, DMPG, and POPC liposomes under dry condition. G3LEA peptide in DMPC liposome in dry state shows two negative peaks around 222 and 208 nm and a positive peak at 190 nm, which are characteristics for α-helix structure of proteins. This indicates that the formation of α-helix in G3LEA peptide contributes to the function to preserve the membrane from desiccation. Further, the peak intensities of VUVCD spectra of G3LEA peptide in DMPG liposome are about 2-fold greater than that in DMPC liposome, implying the importance of electrostatic interaction between positively charged residues of G3LEA peptide and negatively charged headgroups of phospholipid membrane. We also found that the spectral intensities of G3LEA peptide in DMPC liposome in the presence of trehalose was 4-fold greater than that in the absence of trehalose (Figure 1 (b)). These results suggest that G3LEA protein protects cell structure by interacting with the headgroups of phospholipid membranes, and that trehalose enhances the function of G3LEA protein to protect membrane.

REFERENCES

1. Juliana Sakamoto Yoneda, Andew J.Miles, Ana Paula Ulian Araujo, and B.A. Wallace , Differential dehydration effects on globular proteins and intrinsically disordered proteins during film formation , Protein Sci Vol.26 pp718-726(2017)
2. Daixi Li ,and Xiaoming He ,Desiccation Induced Structural Alterations in a 66-Amino Acid Fragment of an Anhydrobiotic Nematode Late Embryogenesis Abundant (LEA) Protein ,Biomacromolecules Vol.10 No.6 pp1469-1477(2009)
3. Takao Furuki, Takahiro Watanabe, Tadaomi Furuta, Kiyoshi Takano, Ryo Shirakashi , and Minoru Sakurai, The Dry Preservation of Giant Vesicles Using a Group 3 LEA Protein Model Peptide and Its Molecular Mechanism, Bull.Chem.Soc.Jpn. Vol.89 No.12 pp1493-1499(2016)

Orientation Analysis of Antimicrobial Peptide Magainin 2 Bound to Phospholipid Membrane by Synchrotron-Radiation Linear Dichroism Spectroscopy

Munehiro Kumashiro[a], Ryoga Tsuji[b], Shoma Suenaga[a], and Koichi Matsuo[c]

[a]*Department of Physical Science, Graduate School of Science, Hiroshima University, 1-3-1 Kagamiyama, Higashi-Hiroshima, Hiroshima 739-8526, Japan*
[b]*Physics Program, Graduate School of Advanced Science and Engineering, Hiroshima University, 1-4-1 Kagamiyama, Higashi-Hiroshima, Hiroshima 739-8527, Japan*
[c]*Hiroshima Synchrotron Radiation Center, Hiroshima University, 2-313 Kagamiyama, Higashi-Hiroshima, Hiroshima 739-0046, Japan*

Keywords: antimicrobial peptide; magainin 2; synchrotron-radiation linear dichroism; peptide-membrane interaction.

Antimicrobial peptide (AMP) interacts with and induces the damages to the cell membrane of antimicrobial-resistant microorganisms via the complicated mechanisms that remain to be further explored. Recently, we have investigated the interaction mechanism between a model AMP or magainin 2 (M2) and dipalmitoyl-phosphatidylglycerol (DPPG) lipid membrane using a synchrotron-radiation circular dichroism spectroscopy and revealed that α-helix monomers of M2 assembled and transformed into β-strand oligomers with increasing peptide-to-lipid (L/P) molar ratio at 25 °C [1]. However, it is still unclear whether the β-strand oligomers insert into the membrane and are involved in the disruption of cell membrane. In this study, we measured synchrotron-radiation linear dichroism (LD) spectrum of M2 to characterize the orientation of the β-strand oligomers in the membrane.

M2 peptide was synthesized in GL Biochem (Shanghai, China), and DPPG phospholipid was purchased from Avanti Polar Lipids, Inc. Each sample was dissolved in 10 mM phosphate buffer (pH 7.0). DPPG liposome with 100 nm diameter was prepared by an extrusion technique, and then mixed with M2 solution at the L/P molar ratio of 4, which corresponds to the experimental condition mainly occupied by the β-strand oligomeric state [1]. The LD spectrum of M2 in DPPG liposome was measured at BL-12 beamline in HiSOR. The details of the flow LD measurement system are described elsewhere [2].

Figure 1 shows the LD spectrum of M2 in DPPG liposome at L/P = 4. The β-strand oligomers of M2 in the DPPG liposomes showed the peak around 200 nm with a small shoulder at 220 nm. According to previous research [3], the net electric or magnetic dipole moments of β-strand around 195 nm and 220 nm are vertical to the strand axis. The β-strand polarized parallel and perpendicular to the membrane normal shows positive and negative LDs at 195 and 220 nm, respectively [3]. Hence, the positive peak LD around 200 nm means that the axis of the β-strands of M2 was parallel to the membrane normal on average, suggesting that the β-strand oligomers of M2 may insert into the membrane and contribute to the formation of pores in the membrane to induce the membrane disruption. Fluorescence anisotropy measurements supported the discussion (data not shown).

In this presentation, we will discuss the antimicrobial mechanism of M2 based on our paper [4].

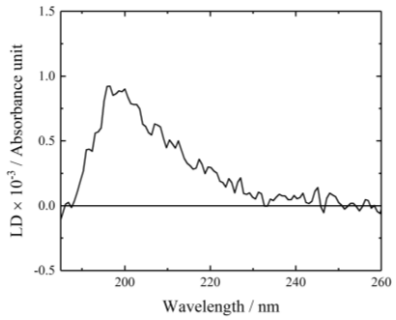

FIGURE 1. LD spectrum of M2 in DPPG liposome at L/P = 4. The LD was recorded at 25 °C with the flow velocity of 1.0 mL min^{-1}.

REFERENCES

1. M. Kumashiro and K. Matsuo, *The 25th Hiroshima International Symposium on Synchrotron Radiation*, Hiroshima, Japan, Mar 2021.
2. K. Matsuo, et al., *Proteins* **84**, 349-59 (2016).
3. A. Rodger, et al., *Phys. Chem. Chem. Phys.* **4**, 4051–7 (2002).
4. M. Kumashiro, et al., *Membranes* **12**, 131 (2022).

Analysis of structural change of XRCC4 by pseudo-phosphorylation using VUV-CD and SAXS

Kai Nishikubo[a,b], Maho Hasegawa[a,b], Yudai Izumi[b], Kentaro Fujii[b], Koichi Matsuo[c], Yoshihisa Matsumoto[d], Akinari Yokoya[b,a]

[a]*Graduate School of Science and Engineering, Ibaraki University, Japan*
[b] *Institute for Quantum Life Science, Quantum Life and Medical Science Directorate, National Institutes of Quantum Sciences and Technology (QST), Japan*
[c]*Hiroshima Synchrotron Radiation Center, Hiroshima University, Japan*
[d]Tokyo Institute of Technology

Keywords: VUV-CD, SAXS, XRCC4, DNA repair, phosphorylation

XRCC4 is a key protein to repair severe DNA damage of double strand breaks (1). The XRCC4 dimer has been reported to form a multimer scaffold with another repair protein, the XRCC4-like factor (XLF). Enzymatically induced phosphorylation at several amino acid residues in XRCC4, such as serine (2), might cause a local change of statically electric charge, resulting conformational alteration to activate the protein. However, the correlation between the structural change and activation has not been understood yet. Full-length XRCC4 was not able to be crystallized because of its intrinsically disordered C-terminal region including several phosphorylation sites. Previously, we have applied circular dichroism (CD) spectral analysis for the full length of wild type XRCC4 (denoted as WT) in an aqueous solution and reported its characteristic secondary structure (3).

In the present study, we focused further the structural change by phosphorylation. We prepared a dimer and multimers of WT XRCC4 as well as mutated ones in which serine residues were substituted to an aspartic acid (denoted as S260D and S327D) to mimic phosphorylation in terms of statically electric charge. Spectra of XRCC4 dimer proteins were similar irrespective of phosphorylation. On the other hand, spectra of multimers were significantly different between WT and mutated proteins (**FIGURE 1**). The composition ratios of the secondary structures were calculated for each sample using a software, SELCON3 (**TABLE 1**). The results indicate that the multimerization and pseudo-phosphorylation increase β-strands. Small angle X-ray scattering (SAXS) at BL6A at the Photon Factory in KEK was also applied to further obtain structural information of XRCC4. The results suggest that the XRCC4S260D dimer has a slightly larger radius of inertia (Rg) than WT (**TABLE 2**),

which may correspond to the slight increase in β-strands shown in the CD analysis. The β-strand formation by the phosphorylation at the C-terminal might stabilize the NHEJ machinery after DSB repair completion.

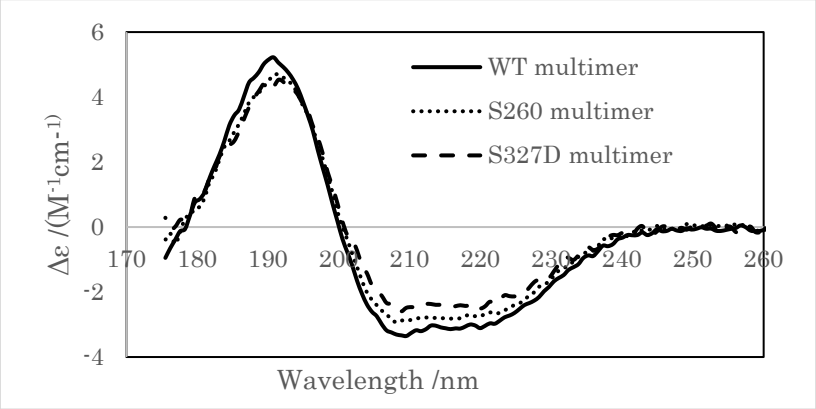

FIGURE 1. Typical CD spectra of wild type and mutated XRCC4 multimers.
The solid, dotted and broken lines represent the spectrum of the wild type, XRCC4S260D and XRCC4S327D dimers, respectively.

TABLE1. Contents of secondary structures of dimer of WT and multimers of WT and mutant of XRCC4.

Structure content (%)		α-Helix	β-Strand	Turn	Unordered
Wild type	dimer	50.8±0.9	5.8±0.8	20.1±2.2	23.2±2.1
	multimer	36.4±1.0	15.7±0.8	22.5±1.4	25.4±0.6
S260D	dimer	50.2±1.9	7.1±3.6	19.7±2.7	23.0±1.2
	multimer	34.2±0.5	17.3±0.9	23.1±0.3	25.5±1.1
S327D	dimer	47.4±2.1	11.5±4.5	18.4±4.1	22.8±1.3
	multimer	32.0±1.7	19.6±0.8	22.7±0.2	25.7±1.2

TABLE 2. Radius of inertia of dimer of WT and mutant of XRCC4.

	WT	S260D	S327D
Rg (Å)	56.25± 0.77	58.02 ± 0.07	57.75 ± 1.04

REFERENCES

1. R. P. Kamdar and Y. Matsumoto, Radiation-induced XRCC4 Association with Chromatin DNA Analyzed by Biochemical Fractionation. *J. Radiat. Res.* **51**, 303-313 (2010).
2. M. Hammel, M. Rey, Y. Yu, R. C. Mani, S. Classen, M. Liu, M. E. Pique, S. Fang, B. L. Mahaney, M. Weinfeld, D. C. Schriemer, S. P. Lees-Miller and J. A. Tainer, XRCC4 protein interactions with XRCC4-like factor (XLF) create an extended grooved scaffold for DNA ligation and double strand break repair. *J. Biol. Chem.* **286**, 32638-23650 (2011).
3. K. Nishikubo, Y. Izumi, Y. Matsumoto, K. Fujii, K. Matsuo and A. Yokoya, Structural analysis of DNA repair protein XRCC4 applying circular dichroism in an aqueous solution. *Radiat. Prot. Dosim*. **183**, 36-39 (2019).

NEXAFS Study of Fullerene Adsorbed on Aminothiophenol Self-Assembled Monolayer

K. Kono[a] , S. Wada[b,c] and T. Sekitani[b,c]

[a]*Faculty of Science, Hiroshima University*
[b]*Graduate School of Advanced Science and Engineering, Hiroshima University*
[c]*Hiroshima Synchrotron Radiation Center, Hiroshima University*

Keywords: fullerene, self-assembled monolayer, NEXAFS

Controlling the microstructure of organic materials to nanometer scale has motivated scientific studies of molecular structure and molecular interactions on various surfaces. Among the various techniques for the preparation of ordered thin organic films, the self-assembled films provide the desired control of molecular order at the interface and also introduce various functional groups into the molecular systems with a high degree of control over the orientation of those groups. The adsorption of thiols onto gold surfaces has attracted considerable interest, as it has been shown that such adsorption can result in formation of well-organized self-assembled monolayer (SAM) [1]. The organothiol self-assembly on metal surface have attracted much interest in a facile manipulating of surface functionality. The SAM have successfully employed as components in molecular electronic devices. Self-assembly of aromatic thiols are particularly interesting due to the interaction of delocalized π orbital of phenyl ring.

The unique electronic, spectroscopic, and structural properties of fullerene and fullerene derivative are very useful to the various application of the material. C_{60} is characterized by the delocalized and highly degenerate orbitals due to π bonding and I_h symmetry. C_{60} is also served as an excellent electron acceptor in molecularly designed donor-acceptor systems, such as molecular photovoltaics [2]. Attachment of C_{60} to the tail groups of SAM provides discrete monolayers of C_{60} and also organized assembly where C_{60} will remain immobilized on the surface.

In this study, the adsorbed state of C_{60} on SAM was examined by NEXAFS spectroscopy. 4-aminothiophenol was used as SAM. The aminothiophenol SAM was prepared by immersing the gold coated Si substrate to 1 mM solution in ethanol for 24 h. The aminothiophenol SAM was cleaned with ethanol and dipped further in 1 mM C_{60} solution in benzene and kept for 24 h. The SAMs thus formed were washed with benzene, ethanol, and dichloromethane. C_{60} multilayer was formed by dropping benzene solution to gold coated substrate and drying in air. NEXAFS measurements were performed at BL13 of Hiroshima Synchrotron Radiation Center.

C K-edge NEXAFS spectra were measured for $C_{60,}$ aminothiophenol SAM and C_{60} adsorbed aminothiophenol SAM. Since NEXAFS spectrum of C_{60} adsorbed SAM includes contribution of aminothiophenol, the component of C_{60} in the C_{60}-SAM was obtained by subtraction of aminothiophenol SAM spectrum from C_{60}-SAM spectrum. The obtained difference spectrum shows similar feature as C_{60} spectrum, but shows peak shifts and peak broadening compared with C_{60} spectrum. Particularly, LUMO peak is shifted to higher photon energy and overlapped with LUMO+1 peak. A higher photon energy shift of LUMO is observed at C_{60} adsorbed on 11-amino-1-undecane thiol SAM [3]. The results suggest that C_{60} is chemisorbed on amino thiolate SAM by hybridization between N Pz of amino group and π* orbital of C_{60}.

REFERENCES

1. J. C. Love, L. A. Estroff, J. K. Kriebel, R. G. Nuzzo, G. M. Whitesides, *Chem. Rev*. **105**, 1103 (2005)
2. H.Imahori, Y.Kashiwagi, T. Hasebe, M. Kimura, T. Hanada, Y. Nishimura, I. Yamazaki, Y. Araki, O. Ito, S. Fukuzumi, *Thin Solid Films*. **451-452**, 580 (2004)
3. A.Patnaik, K.Okudaira, S.Kera, H.Setoyama, K.Mase, N.Ueno, *J. Chem. Phys*. **122**, 154703 (2005)

Characterization of self-assembled monolayers of methyl-ester terminated naphthalenethiol

A. Niozu[a], H. Sunohara[b], S. Tendo[a], M. Tabuse[a], and Shin-ichi Wada[a,c]

[a]*Graduate school of advanced science and engineering, Hiroshima University, Higashi-Hiroshima 739-8526, Japan*
[b] *Faculty of science, Hiroshima University, Higashi-Hiroshima 739-8526, Japan*
[c]*Hiroshima Synchrotron Radiation Center, Hiroshima University, Higashi-Hiroshima 739-0046, Japan*

Keywords: Self-assembled monolayers (SAMs), Near edge X-ray absorption fine structure (NEXAFS)

Core-electron excitations by soft X-ray radiation possess several unique properties that differ from those of valence excitations. Core-excitation energy depends on the element and its chemical environment, which allows selective excitation of a specific atom in a molecule. In general, core excitation is followed by Auger decay on a time scale of a few femtoseconds, resulting in final states with large excess energy. Thereafter, the excited molecule follows a rich variety of relaxation pathways, e.g. desorption of ion and neutral species and charge transfer within the molecule.

An interesting phenomenon that reflects the selective nature of core excitation is site-selective bond breaking of molecules, i.e. the so-called “molecular scalpel” [1,2]. In particular, it has been reported that highly site-selective bond scission can be achieved in self-assembled monolayers (SAMs) of molecules absorbed on metal surfaces [1,2]. Furthermore, our recent experiments on aliphatic and aromatic SAMs have suggested that the degree of site-selective bond scission depends on the molecular structure of backbone between the excitation cite and the metal substrate. This implies the key role of energy transfer between the excitation cite and the substrate for the manifestation of site-selective bond scission. To corroborate this picture, a systematic experimental study about the fragmentation dynamics dependent on the molecular structure is helpful.

In this study, we investigated the ion desorption dynamics of SAMs of methyl-ester terminated naphthalenethiol molecules. The SAM samples were prepared by immersing Au substrates in 1.0 mM ethanol solution of the sample molecules for 24 hs. We characterized the prepared SAM samples by near-edge X-ray absorption fine structure (NEXAFS) measurements. The experiment was performed at the BL 13 of HiSOR. The C K-edge NEXAFS spectra were measured by the total electron yield (TEY) method via the sample drain current. The measurements were performed at different incident beam angles, and polarization dependence of the NEXAFS intensity was investigated. The obtained NEXAFS spectra (Fig. 1) show peaks corresponding to excitations to individual unoccupied molecular orbitals and provided precise values of their excitation energies. In addition, the spectra exhibit a clear polarization dependence, which supports the formation of well-oriented SAMs on the substrate.

The measurements of desorbed ions were performed at BL 2B of photon factory (PF) in KEK. PF was operated in the hybrid operation mode, and the single-bunch component of the X-ray beam was skimmed and used in the experiment. Partial ion yield (PIY) spectra were recorded with a time-of-flight ion spectrometer. The PIY of CH_n^+ (n=0,1,2,3) ions showed a prominent enhancement at the C1s(OCH_3)→ σ^*(O-CH_3) resonant excitation, which have been observed in previous experiments on methyl-ester terminated SAMs [1,2]. From the PIY spectra, we evaluated the degree of site-selective desorption by analyzing the relative yield of CH_n^+ ions. The degree of site-selectivity for the present molecule with naphthalene backbone was evaluated to be between those for molecules with benzene and biphenyl (with two benzene rings) backbones. The present results corroborate the correlation between the molecular conductivity and the site selectivity in ion desorption.

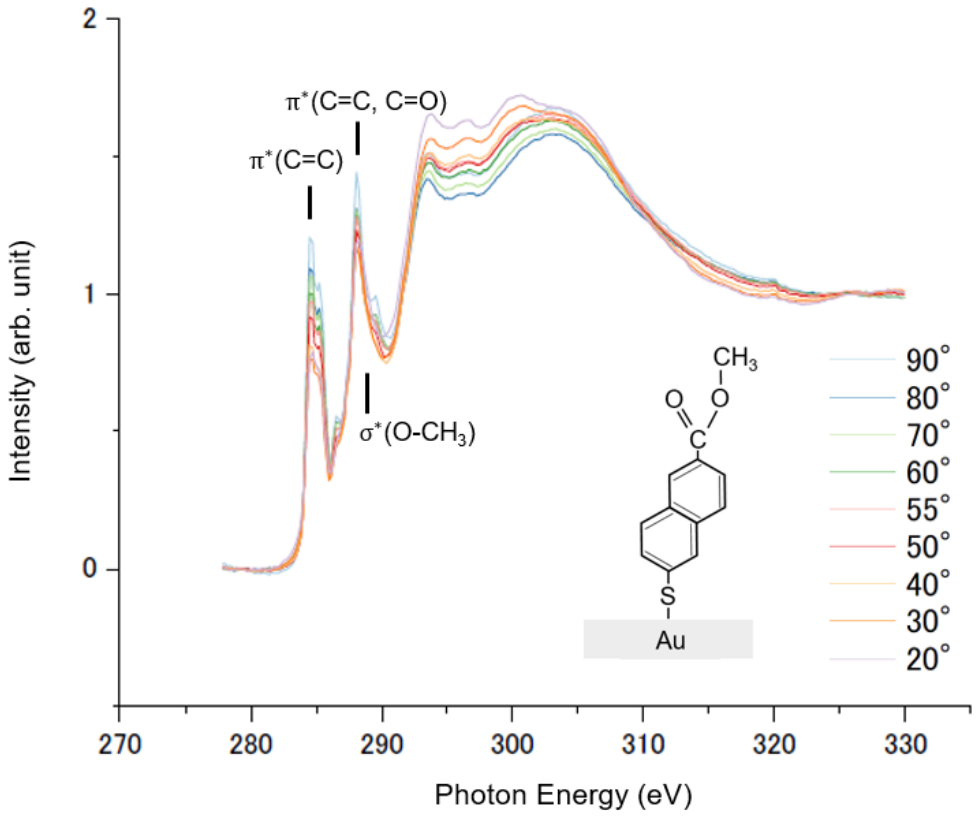

FIGURE 1. TEY spectra for methyl-ester terminated naphthalenethiol SAMs. The spectra exhibit peaks corresponding to excitations to individual π^* and σ^* orbitals. The spectra show a clear polarization dependence, which supports the formation of ordered SAMs on the Au substrate.

REFERENCES

1. S. Wada, H. Kizaki, Y. Matsumoto, R. Sumii, and K. Tanaka, J. Phys. Condens. Matter **18**, 1 (2006).
2. S. Wada, and K.Tanaka, J. Mass Spectrom. Soc. Jpn **58**, 17 (2010).

Soft X-ray Polarization Measurements of Phospholipid Multilayers Supported on Hydrophilic Si Surfaces

Masataka Tabuse[a], Akinobu Niozu[a], and Shin-ichi Wada[a,b]

[a]*Graduate School of Advanced Science and Engineering, Hiroshima University*
[b]*Hiroshima Synchrotron Radiation Center, Hiroshima University*

Keywords: Linear Polarization, XAS (X-ray absorption spectroscopy), NEXAFS (near edge X-ray absorption fine structure), Phospholipids, DCCP, DOPC.

Lipid membranes supported on substrates are promising systems for use in biological sensing, biocompatibility, bioelectronics [1]. The idea that ordered lipid molecules can be prepared by several convenient methods, like freeze-thaw and spin-coating methods [2]. We also confirmed that the phospholipid multilayers made by simple dropping of acetone solution onto hydrophilic Si substrates under atmospheric pressure and moisture and room temperature conditions forms well-ordered multilamellar structures. But the quality of ordering as well as formation process of ordered lamellar structure during such a short period is not well understood.

X-ray absorption spectroscopy (XAS) is one of powerful tools to investigate local structural and dynamical information because of its element selectivity. Especially, one can easily get orientation structure around X-ray absorption center by using linearly polarized X-ray beam. In this study, polarization dependence of XAS measured for phospholipid multilayers supported on hydrophilic Si surfaces was investigated in order to quantify the orientation quality.

Measurements of near edge X-ray absorption fine structure (NEXAFS) have been performed at BL-13 of HiSOR, where is a soft X-ray beamline with a Dragon-type spherical grating monochromator developed to investigate soft X-ray spectroscopy for surface organic materials. During measurements, the experimental chamber had a base pressure less than 1×10^{-9} Torr. NEXAFS spectra around the C K-edge were recorded in total electron yield (TEY) mode by measuring a sample drain current by changing incident angle of synchrotron radiation. Polarization at BL-13 is horizontal due to bremsstrahlung from a bending magnet and the polarization factor P was determined to be 0.95 [3] by measuring azimuthal angle-dependent NEXAFS spectra of a highly oriented pyrolytic graphite (HOPG) [4].

DPPC and DOPC phospholipid molecules were used to form supported lipid membranes from 10 to 1000 multilayer by changing the dropping volume of lipid solution onto hydrophilic Si substrates, and moreover for getting the bilayer membranes, multilayers on substrates were considerably washed by immersing Milli-Q water. DPPC and DOPC molecules are shown in Fig. 1, consisting of a polar zwitterionic hydrophilic group and two non-polar carbon chains. So, molecules in aqueous solution form bilayers with the carbon chains facing each other due to hydrophobic interaction. It is understood that bilayers of DPPC with saturated carbon chains form crystalline-like gel phase at room temperature, while DOPC with unsaturated chains composes liquid crystalline phase. Fig. 2 shows typical polarization dependent NEXAFS spectra measured for (a) DPPC and (b) DOPC on Si surfaces at C K-edge. Although DPPC shows clear polarization dependence, the dependence of DOPC in not so dominant. Tendency of such polarization dependence does not depend on the layer number of lipids. So, the different degree of

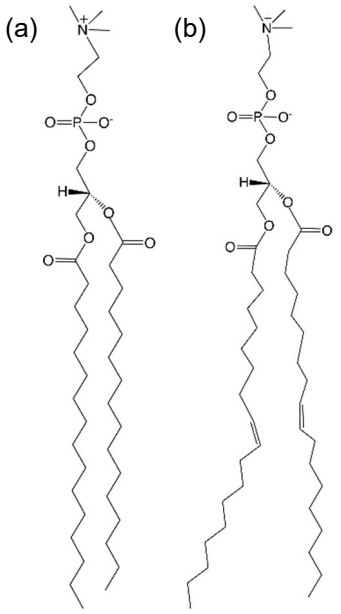

FIGURE 1. Molecular structures of phospholipids (a) DPPC and (b) DOPC.

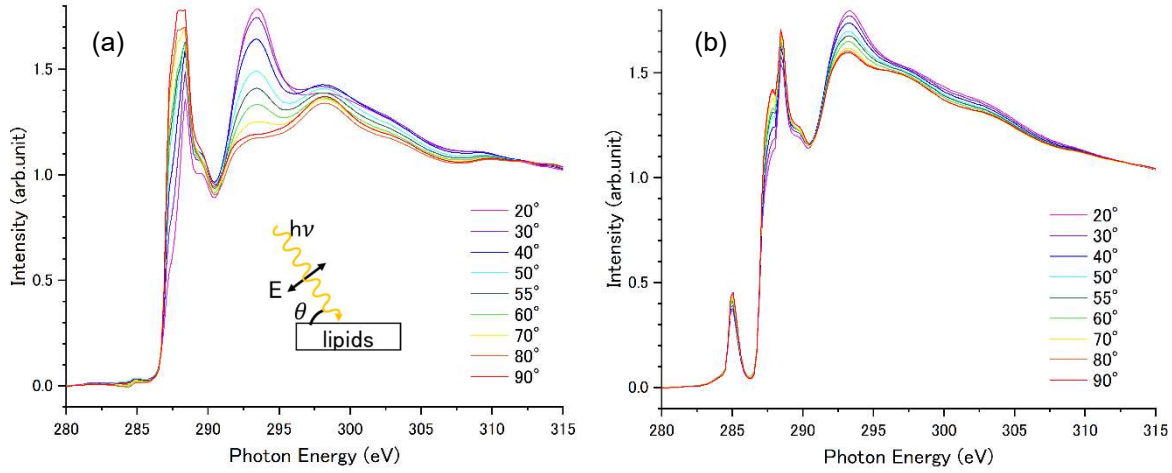

FIGURE 2. Polarization dependent NEXAFS spectra of (a) DPPC and (b) DOPC phospholipids multilamellar membranes measured at C K-edge. These membranes consist of about 100 bilayers, which are confirmed by simple molar consideration and interference of reflected visible light. Incident angle θ from the surface, and therefore the angle of electric vector from the surface normal, is defined like inset.

polarization dependence reflects not only the orientation angles themselves but also the different phase (ordering quality) of lipid membranes. On the basis of above consideration and the careful analysis of polarization dependence of each resonant peaks, DPPC bilayers (that is gel phase) consist of 60% ordered component and 40% non-ordered one, while DOPC bilayers (liquid phase) contain 80% non-ordered carbon chains. This is the first quantitative analysis of phospholipid bilayers of DPPC and DOPC by means of strong advantage of polarization quality and element selectivity of soft-X ray synchrotron radiation.

REFERENCES

1. Z.Zhi, I.Y. Hasan, A. Mechler, *Biotechnol. J.* **13**, 1800101 (2018).
2. A.C. Simonsen and L.A. Bagatolli, *Langmuir* **20**, 9720-9728 (2004).
3. M. Tabuse, K. Yamamoto, S. Wada, *HiSOR Activity Report 2019*, 124 (2020).
4. B. Watts, L. Thomsen and P.C. Dastoor, *J. Electron Spectrosc. Relat. Phenom.* 151, 208 (2006).

Interface structure of Co ultrathin films evaporated on h-BN/Ni(111) studied by LEED Intensity Analysis

Wataru Nishizawa[a] and Masahiro Sawada[b]

[a]*Graduate School of Science, Hiroshima University*
[b]*Hiroshima Synchrotron Radiation Center, Hiroshima University*

Keywords: epitaxial growth, hexagonal boron nitride, low energy electron diffraction

Magnetic tunneling junction (MTJ) structures, where ferromagnetic electrode layers sandwich an insulating barrier layer, show tunnel magnetic resistance (TMR) effect that is widely applied for spintronics devices such as magnetic random access memory. One of important performance factors of TMR element is magnetic resistance (MR) ratio, which is sensitive to not only electronic and magnetic status in the magnetic electrode layers but also the interface structure. Conventional metal oxide layers have been utilized for the barrier layer in the device structures, where improvement of MR ratio is limited because of disorder of the interfacial crystal structures, arises from lattice mismatch, inter-diffusion or defect formation. In recent years, much attention and intensive studies have been devoted to hexagonal boron nitride (h-BN) whose structure is two-dimensional honeycomb formed by stable chemical bonding. Monolayer h-BN is one of good candidates for the ideal burrier layer of TMR devices because the h-BN layer is expected to form an abrupt and pinhole-less interface with magnetic layers. Although a coherent growth of h-BN/Ni(111) is established and the ideal sandwich structure is also expected for Co/h-BN/Ni(111), the growth mode and interface structure for Co overlayer has not been clarified up to now.

In this study, we have investigated growth mode of Co ultrathin films on h-BN/Ni(111) in manner of Auger electron spectroscopy (AES) and intensity analysis of low energy electron diffraction (LEED). The sample of Co/h-BN/Ni(111) was prepared in ultra-high vacuum by means of MBE evaporation of Co on h-BN/Ni(111), where high quality h-BN monolayer was preliminarily prepared on the clean surface of Ni(111) by cracking of borazine ($B_3N_3H_6$) [1]. Thickness dependence of AES intensity ratio of Co (LMM) to Ni (LMM) shows a clear deviation from simple exponential expansion with increasing thickness, meaning a failure of complete layer-by-layer growth. From the LEED I-V curves obtained from the (0,1) diffraction spot of Co/h-BN/Ni(111), peak shifts are found around 80 and 120 eV within the thickness of 1.5~3ML, while no change in the I-V curves is observed above 3ML. According to this result, we can suggest initial island growth followed by two-dimensional epitaxial growth above 3 ML.

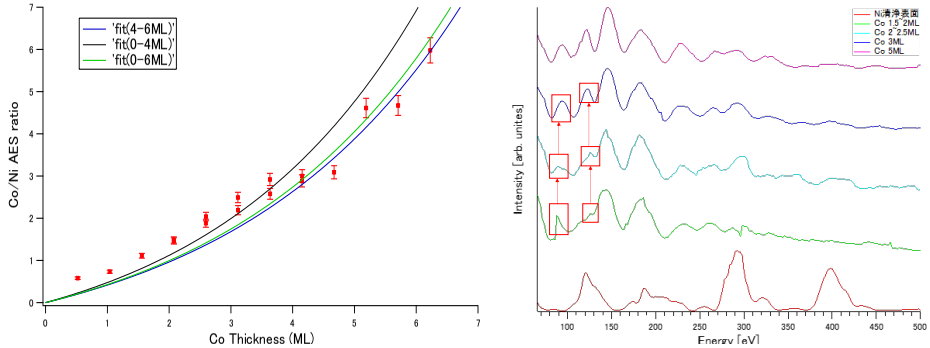

FIGURE. Co thickness dependence of intensity ratio of Auger electron of Co (LMM) to Ni (LMM) obtained from differential Auger electron spectra from Co/h-BN/Ni(111) (left), and LEED I-V curves of the (0,1) diffraction spot (right).

REFERENCES

1. A. Nagashima *et al.*, Phys. Rev. B51, 4606 (1995).

Evolution of c-f hybridization in valence transition compound $YbInCu_4$ observed by ARPES

R. Kamimori[a], Y. Tanimoto[b], H. Sato[c], M. Arita[c], S. Kumar[c], K. Shimada[c], K. T. Matsumoto[d], K. Hiraoka[d]

[a]*Graduate School of Advanced Science and Engineering, Hiroshima University, Higashi-Hiroshima 739-8526, Japan*
[b]*Faculty of Science, Hiroshima University, Higashi-Hiroshima 739-8526, Japan*
[c]*Hiroshima Synchrotron Radiation Center, Hiroshima University, Higashi-Hiroshima 739-0046, Japan*
[d]*Graduate School of Science and Engineering, Ehime University, Matsuyama 790-8577, Japan*

Keywords: valence transition, *c-f* hybridization, angle resolved photoemission spectroscopy

Yb compounds shows rich variety of interesting phenomena originated from the hybridization between the delocalized conduction electrons and localized Yb 4*f* electrons (*c* - *f* hybridization). The Yb valence in the compounds often fluctuates between divalent state (Yb^{2+}:$4f^{14}$) and trivalent state (Yb^{3+}:$4f^{13}$) and has a non-integer value averaged over the compounds. $YbInCu_4$ shows a first order valence transition at T_v = 42 K. The mean Yb valences were estimated to be ~2.90 in the high temperature phase and ~ 2.74 in the low temperature phase by means of the hard x-ray photoemission spectroscopy for the Yb 3*d* core states [1]. The magnetic susceptibility changes sharply from the Curie-Weiss behavior above T_v to Pauli paramagnetic behavior below T_v. The Kondo temperature also varies from T_K ~ 25 to ~ 400 K, which indicates that a degree of *c* - *f* hybridization is enhanced in the low temperature phase. A number of studies of electronic structure of $YbInCu_4$ by means of angle-integrated photoemission spectroscopy have been reported [1-3]. We successfully observed the increase of the *c* - *f* hybridization strength below T_v by means of the low-energy excited photoemission spectroscopy at $h\nu$ = 7 eV [3]. On the other hand, angle-resolved photoemission spectroscopy (ARPES) study for $YbInCu_4$ has been limited because it is difficult to prepare a clean and flat surface to obtain the clear ARPES spectra by the usual fracturing method. Only two ARPES results have been reported so far, where the signature of the *c* - *f* hybridization is reported [4, 5]. To observe the evolution of the *c* - *f* hybridization in the low temperature phase of $YbInCu_4$ by ARPES, the preparation of the clean and flat surface is indispensable.

In this study, we prepared the clean and flat $YbInCu_4$(001) surface suitable for ARPES measurements as follows. First, the $YbInCu_4$ single crystal was polished *ex situ* until a mirror-like (001) surface plane was obtained. Then, the polished surface was *in situ* cleaned by repeating Ar ion sputtering and heating at about 400 °C. The cleanliness and flatness of the prepared surface are confirmed by means of the Auger electron spectroscopy and low-energy electron diffraction. Single crystals of $YbInCu_4$ were synthesized by the flux-method. The ARPES experiments on $YbInCu_4$(001) were performed at undulator beamlines BL-1 and BL-9A of Hiroshima Synchrotron Radiation Center (HSRC).

First, we measured incident photon energy dependence of the ARPES spectra of $YbInCu_4$(001) between $h\nu$ = 30 and 172 eV taken at 23 K along [100] direction to observe the k_z dispersion. Figures 1(a) and 1(b) show ARPES intensity plots at $h\nu$ = 64 and 96 eV, respectively. A vertical axis represents binding energy (E_B) relative to the Fermi energy (E_F). The dispersive Cu 3*d* bands are clearly observed around E_B ~ 3 eV. The flat bands due to the bulk-derived Yb^{2+} $4f_{7/2}$ and $4f_{5/2}$ states are found near E_F and 1.35 eV, respectively. From the periodicity of the $h\nu$ dependent ARPES spectra, the inner potential is determined to be about 13 eV. The ARPES spectra at $h\nu$ = 64 and 96 eV (Figs. 1 (a) and 1 (b)) are those along *X* - *U* and *Γ* - *K* directions, respectively.

Figures 2 (a) and (b) present the ARPES spectra measured along [110] direction at 120 K (high temperature phase) and 10 K (low temperature phase), respectively. The excitation energy is $h\nu$ = 14 eV and the ARPES spectra are measured along the *X* - *W* direction. The flat band due to the Yb^{2+} $4f_{7/2}$ states

are observed at $E_B \sim 0.03$ eV and two dispersive upward bands due to the conduction electrons are also detected (*c* and *c'* in Figs. 2(a) and 2(b)). The two conduction electron bands are well reproduced by the band-structure calculation for $LuInCu_4$ using the WIEN2k code [6]. It is noted that the inner conduction electron band (*c*) bents downward just below the Yb^{2+} $4f_{7/2}$ band, indicating the gap formation originated from the *c* - *f* hybridization. The splitting between the two bands is increased at 10 K as shown with "Δ" in Figs. 2(a) and 2(b) for a guide, which indicates that the *c* - *f* hybridization is enhanced in the low temperature phase. The enhanced splitting is clearly seen in the ARPES spectra at $k = 0.17$ Å^{-1} in Fig. 2(c).

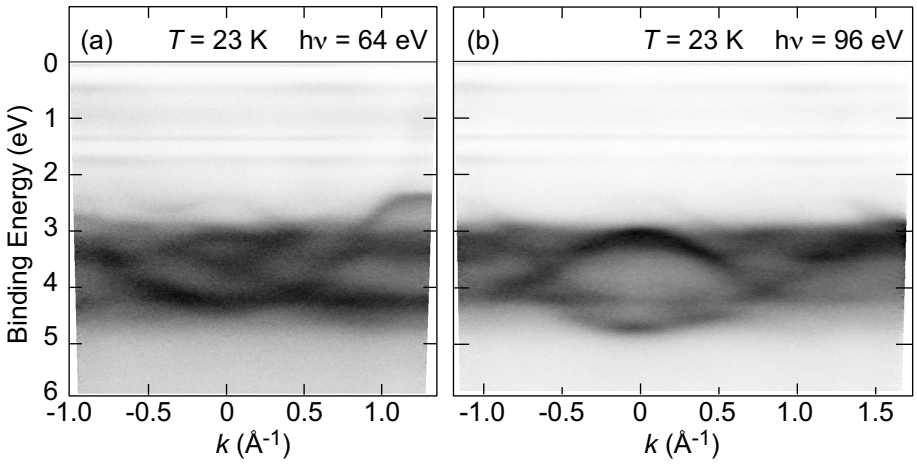

FIGURE 1. ARPES intensity plots of $YbInCu_4$(001) along [100] direction measured at 23 K with (a) $h\nu = 64$ eV and (b) $h\nu = 96$ eV.

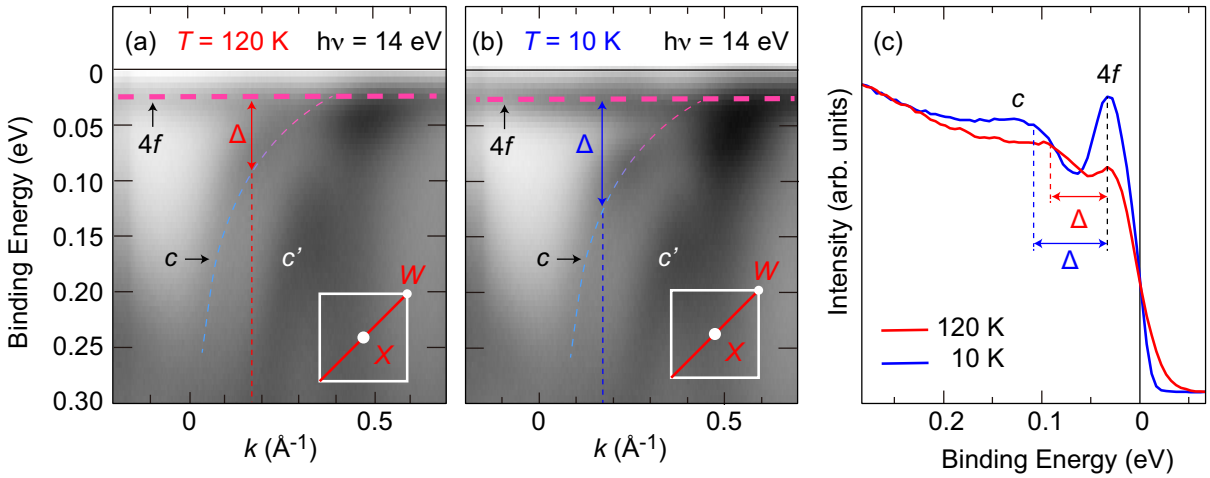

FIGURE 2. ARPES intensity plots of $YbInCu_4$(001) along *X* - *W* directions measured between 120 and 10 K with $h\nu = 14$ eV.

REFERENCES

1. H. Sato, K. Shimada, M. Arita, K. Hiraoka, K. Kojima, Y. Takeda, K. Yoshikawa, M. Sawada, M. Nakatake, H. Namatame, M. Taniguchi, Y. Takata, E. Ikenaga, S. Shin, K. Kobayashi, K. Tamasaku, Y. Nishino, D. Miwa, M. Yabashi and T. Ishikawa, Phys. Rev. Lett. **93**, 246404 (2004).
2. For example, F. Reinert, R. Claessen, G. Nicolay, D. Ehm, S. Hüfner, W. P. Ellis, G.-H. Gweon, J. W. Allen, B. Kindler and W. Asmus, Phys. Rev. B **58**, 12808 (1998).
3. K. Yoshikawa, H. Sato, M. Arita, Y. Takeda, K. Hiraoka, K. Kojima, K. Tsuji, H. Namatame and M. Taniguchi, Phys. Rev. B **72**, 165106 (2005).
4. S. Ishihara, K. Ichiki, K. Abe, T. Matsumoto, K. Mimura, H. Sato, M. Arita, E. F. Schwier, H. Iwasawa, K. Shimada, H. Namatame, M. Taniguchi, T. Zhuang, K. Hiraoka and H. Anzai, J. Electr. Spectrosc. Relat. Phenom. **220**, 66 (2017).
5. H. Anzai, S. Ishihara, K. Mimura, H. Sato, M. Arita, T. Zhuang and K. Hiraoka, Phys. Rev. Research **2**, 033408 (2020).
6. P. Blaha, K. Schwarz, G. Madsen, D. Kvasicka and J. Luitz, WIEN2k, *An Augmented Plane Wave Plus Local Orbitals Program for Calculating Crystal Properties* (TU Vienna, Vienna, 2001).

Evaluation of Self-Energy in Overdoped Bi2201 by Angle-Resolved Photoemission Spectroscopy

Y. Miyai[a], Shiv Kumar[b], T. Kurosawa[c], M. Oda[d], S. Ideta[b], K. Shimada[b]

[a]*Graduate School of Science, Hiroshima University, Kagamiyama 1-3-1, Higashi-Hiroshima 739-8526, Japan*
[b] *Hiroshima Synchrotron Radiation Center, Hiroshima University, Kagamiyama 1-3-1, Higashi-Hiroshima 739-8526, Japan*
[c] *Fuculty of Science and Engineearing, Muroran Institute of Technology, 27-1 Mizumoto-cho, Muroran, Hokkaido, 050-8585, Japan*
[d] *Department of Physics, Hokkaido University, Sapporo 060-0809, Japan*

Keywords: High-T_C Superconductor, ARPES, Many-body interactions

High transition-temperature (T_C) cuprate superconductors have attracted much interest since their discovery in 1986 for their high superconducting transition temperature as well as unusual physical properties such as bad metal state and formation of density waves [1,2]. To understand these physical properties, it is necessary to quantitatively evaluate the electron-electron interaction and the electron-boson interaction and to experimentally clarify a quasiparticle state near the Fermi level. Angle-Resolved Photoemission Spectroscopy (ARPES) is an effective and direct way to investigate electronic states in solids. The ARPES spectrum is associated with the imaginary part of one-particle Green's function and gives the quasiparticle excitation spectrum of the quasiparticle. By analyzing ARPES spectral lineshape quantitatively, it is possible to extract the self-energy that includes information of the electron-electron and the electron-boson interactions. Most of the previous ARPES studies of cuprates have focused on the investigation of the electron-boson interaction at the vicinity of the Fermi level. As the self-energy contains the contributions from the electron-electron interaction, it was subtracted based on the empirical assumptions. On the other hand, the water-fall-like spectral feature which is peculiar to the strong correlation system has been observed in the valence band of cuprates in the wide energy range [3]. To understand the mechanism of the high Tc superconductivity in cuprates, it is important to clarify the electron-boson interaction as well as electron-electron interaction. For this purpose, it is necessary to analyze the electronic states from small energy scale near the Fermi level to large energy scale throughout the entire valance band, but this kind of study has not been sufficiently done so far.

To quantitatively evaluate the electron-boson interaction and the electron-electron interaction, we have focused on the Bi-based high-T_C cuprate, $(Bi,Pb)_2Sr_2CuO_{6+\delta}$ (Pb-Bi2201) and performed high-resolution ARPES. Bi2201 having a single CuO_2 plane in the unit cell is expected to eliminate complexity derived from plural CuO_2 planes, and using the overdoped sample that is expected to behave like metals enable us to extract normal self-energy. Figures 1(a) and (b) show the experimentally extracted real part and imaginary part of the self-energy. The solid lines show fitting to a model self-energy. One can see that the real part of the self-energy crosses the zero line and the imaginary part of self-energy has the maximum at $\omega \sim -0.5$ eV. Figure 1(c) shows the simulation of the ARPES spectrum using the model self-energy. Because the imaginary part of the self-energy gives the spectral width, the water-fall-like structure is caused by the suppression of the spectral intensity due to the significant linewidth broadening at $\omega \sim -0.5$ eV due to the electron-electron interaction.

In addition, we extracted the self-energy due to the electron-boson interaction near the Fermi level using the laser-based μARPES system by subtracting the contribution from the electron-electron interaction estimated above. The coupling parameter of the electron-boson interaction is $\lambda_{EB} \sim 1.5$ at low temperature and decreases with increasing temperature (Figure 1(d)). This behavior is similar to the temperature dependence of the coupling parameter of the electron-phonon interaction [4]. It should be also noted that the total coupling parameter of the electron-electron interaction and the electron boson interaction is $\lambda \sim 2.8$

(strong coupling) at low temperature, and the electron-electron interaction is also significant near the Fermi level.

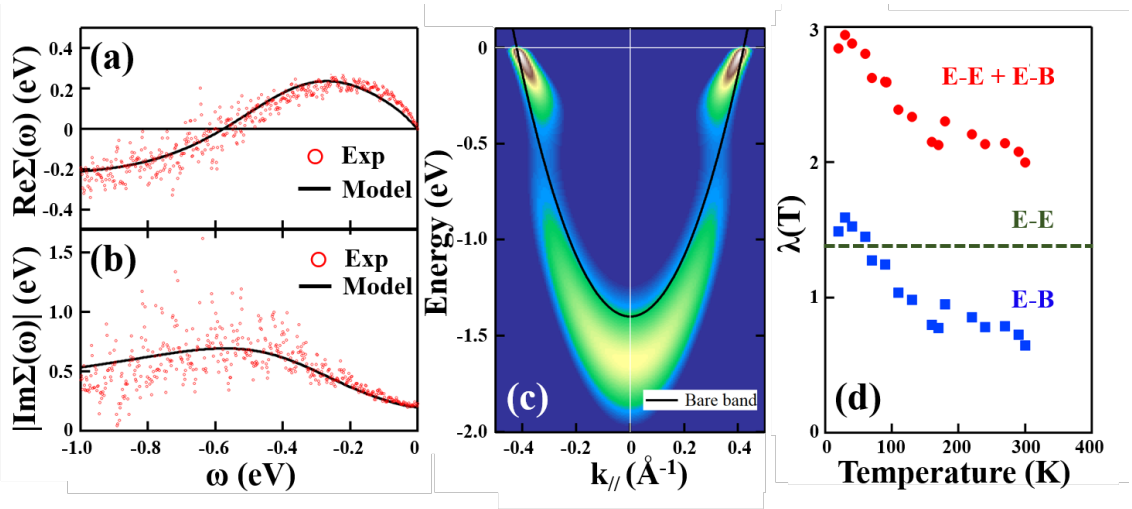

FIGURE 1. (a)(b) Circles indicate experimentally evaluated real and imaginary parts of the self-energy. Solid lines indicate fits to the model self-energy. (c) ARPES simulation using the model self-energy. (d) The temperature dependence of the coupling parameter.

REFERENCES

1. P. Choubey *et al.*, Proceedings of National Academy of Sciences, 117, 14805 (2020).
2. Y.Y. Peng *et al.*, Nature Materials 17, 697 (2018).
3. D.S.Inosov, et al, Phys. Rev. Lett **99**, 237002, (2007).
4. J.Jiang, et al., Phys. Rev. B **84**, 155124, (2011).

Direct Observation of the Three-dimensional Electronic Structure of RMnSi (R=La, Ce) with Noncentrosymmetic Antiferromagnetic Order

Kaito Shiraishi[a], Takuma Iwata[b], Kenta Kuroda[a], Munisa Nurmamat[a], Karen Nakanishi[b], Shiv Kumar[c], Kenya Shimada[c], Masashi Arita[c], Yoshinori Kotani[d], Keisuke Mitsumoto[e], Hiroshi Tanida[e], Akio Kimura[a]

[a]*Graduate School of Advanced Science and Engneering, Hiroshima University, 1-3-1 Kagamiyama Higashi-hiroshima, Hiroshima, Japan*
[b]*Faculty of Science, Hiroshima University, 1-3-1 Kagamiyama Higashi-hiroshima, Hiroshima, Japan*
[c]*Hiroshima Synchrotron Radiation Center, Hiroshima University, 2-313 Kagamiyama Higashi-hiroshima, Hiroshima, Japan*
[d]*Japan Synchrotron Radiation Reseach Institute, 1-1-1 Koto, Sayo-cho, Sayo-gun, Hyogo, Japan*
[e]*Liberal Arts and Sciences, Toyama Prefectural University, 5180 Kurokawa, Imizu, Toyama, Japan*

Keywords: ARPES, Antiferromagnet, Rare-earth compound, Nonsymmorphic, Cluster magnetic multipole

Utilizing antiferromagnets for spintronics has recently attracted attentions. It is generally believed that it is difficult to control the physical properties of antiferromagnets by external fields due to the absence of macroscopic magnetization. However the magnetic multipole order hidden in the antiferromagnetism induces dramatic cross-correlational phenomena between electric and magnetic responses. Recently, a spintronic application using such antiferromagnetic order with hidden magnetic multipole has been proposed and has attracted considerable attention [1].

LaMnSi (CeMnSi) is an antiferromagnet with a Néel temperature of T_N ~ 293 K (~ 240 K). The crystal structure of RMnSi (R=La, Ce) belongs to the nonsymmorphic space group P4/nmm, as shown in Fig. 1(a) [2]. It contains a buckling layer composed of Mn and Si atoms as shown in Fig. 1(b). In the paramagnetic (PM) phase, the crystal does not have local inversion symmetry at each atomic site, leading to a sublattice connected by the spatial inversion symmetry operation [Fig. 1(c), Left]. Once the antiferromagnetic (AFM) order with q = 0 appears [Fig. 1(c), Right], the sublattice becomes inequivalent, and the global spatial inversion symmetry is spontaneously broken. This is prerequisite for the emergence of magnetic multipoles, which may lead to Rashba-type spin splitting and wavenumber-shifted asymmetric bands in the electronic structure [1], and may induce exotic external field responses [3]. In fact, magnetic piezoelectric effects have been observed in the antiferromagnets $BaMn_2As_2$ [4] and $EuMnBi_2$ [5], incorporating a buckling layer similar to that in Fig. 1(b), and the origin of the effects could be possibly ascribed to magnetic multipole order. In RMnSi, an anomaly in the electrical resistivity near T_N has been reported [2], suggesting a change in the electronic structure upon the AFM transition. It is noteworthy that RMnSi is different from ordinary antiferromagnets in that the magnetic moments are arranged in a q = 0 configuration without changing the size of the unit cell through the transition from the AFM phase with respect to the PM phase. This delivers an ideal stage to study

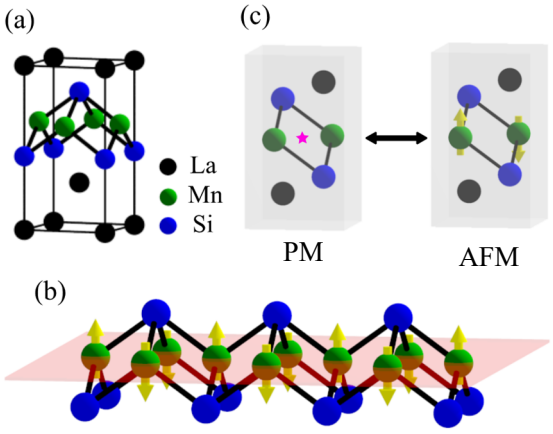

Fig. 1 (a) Crystal structure of LaMnSi. (b) MnSi layer in antiferromagnetic phase. (c) Structures of paramagnetic (Left) and antiferromagnetic states (Right).

the effect of magnetic ordering on the electronic structure. However, there are no experimental reports on the electronic structure of LaMnSi and CeMnSi, and it remains to be clarified whether the electronic structure reflects the symmetry due to the magnetic structure.

In this study, we performed angle-resolved photoemission spectroscopy (ARPES) using synchrotron radiation in the soft X-ray (SX) and vacuum ultraviolet (VUV) regions at SPring-8 BL25SU and HiSOR BL-1 / 9A, respectively, to clarify the effect of the symmetry of the AFM order on the electronic state in RMnSi (R = La, Ce). First, we observed the three-dimensional electronic structure including the band dispersion relation in the k_z direction using SX-ARPES, taking advantage of the tunable incident photon energy of synchrotron radiation. As shown in Fig. 2(a), the Fermi surface in the k_x-k_y plane including the Γ-X high symmetry line in the Brillouin zone was observed at T = 50 K below T_N. The band dispersion along the Γ-X line [cut in Fig. 2(a)] is shown in the left panel of Fig. 2(c). At the X point of the Brillouin zone boundary, a downward-convex parabolic band is clearly observed from the ARPES, and at the Γ point, the intersection of downward and upward dispersions is observed [Fig. 2(c), Right]. These features were also seen by the measurement using *p*-polarized VUV synchrotron radiation [Fig. 2(d)]. Similar dispersion was also observed for CeMnSi at 50 K (< T_N). Both of these experimental results were well reproduced by the first-principles calculation considering the antiferromagnetic order in LaMnSi than that for the PM phase [Fig. 2(c), Right]. These bands are mainly dominated by the Mn 3*d* orbital component, which implies that the Mn 3*d* electronic state responsible for antiferromagnetism has an itinerant character. Thus, the electronic states corresponding to the q = 0 AFM order in RMnSi (R = La, Ce) have been experimentally clarified for the first time.

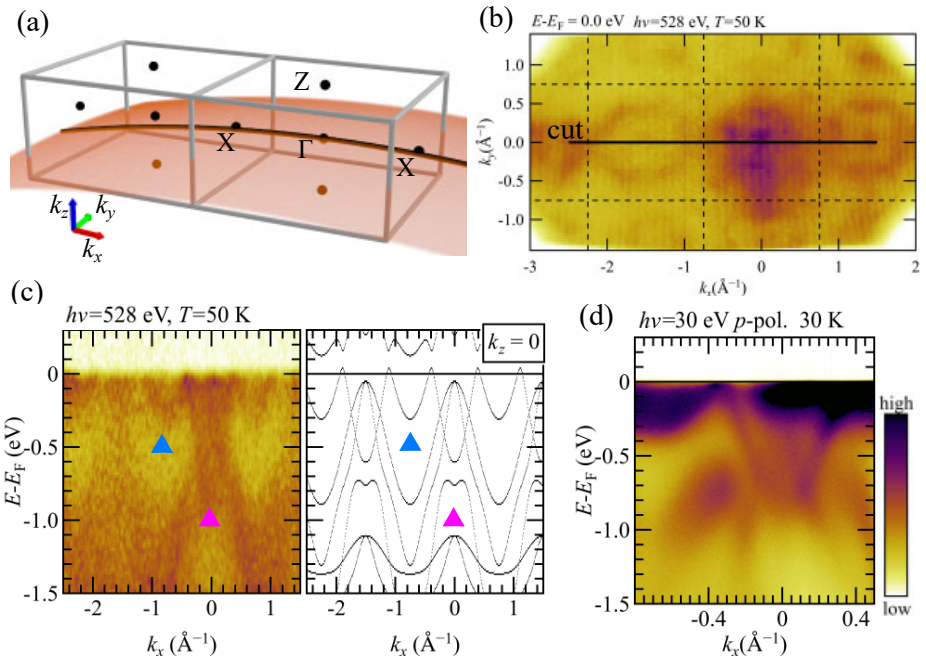

Fig. 2 (a) Brillouin zone of RMnSi. The red plane is the k_x-k_y cut plane at the incident photon energy $h\nu$=528 eV. (b) ARPES k_x-k_y inplane mapping of LaMnSi at 50 K (< T_N) at $h\nu$ = 528 eV at Fermi level. (c) Experimentally obtained energy dispersion ($h\nu$=528 eV) and first-principles calculation results in the Γ-X direction. (d) ARPES energy dispersion in the Γ-X direction for LaMnSi at $h\nu$ = 30 eV at 30 K (< T_N).

REFERENCES

[1] S. Hayami *et.al.*, Phys. Rev. B **98**, 165110 (2018).
[2] H. Tanida *et. al.*, J. Phys. Soc. Jpn. **91**, 013704 (2022).
[3] H. Watanabe *et. al.*, Phys. Rev. B **98**, 245129 (2018).
[4] H. Watanabe *et. al.*, Phys. Rev. B **96**, 064432 (2017).
[5] Y. Shiomi *et. al.*, Phys. Rev. Lett. **122**, 127207 (2019).

Membrane-Bound Conformations of Magainin 2 Depending on the Inherent Characteristics of Membrane Revealed by Synchrotron-Radiation Circular-Dichroism Spectroscopy

Ryoga Tsuji[a], Munehiro Kumashiro[b], Koichi Matsuo[c]

[a]*Physics Program, Graduate School of Advanced Science and Engineering, Hiroshima University, 1-3-1 Kagamiyama, Higashi-Hiroshima, Hiroshima 739-8526, Japan*
[b]*Department of Physical Science, Graduate School of Science, Hiroshima University, 1-3-1 Kagamiyama, Higashi-Hiroshima, Hiroshima 739-8526, Japan*
[c]*Hiroshima Synchrotron Radiation Center, Hiroshima University, 2-313 Kagamiyama, Higashi-Hiroshima, Hiroshima 739-0046, Japan*

Keywords: Antimicrobial Peptide, Circular dichroism, Lipid membrane

Magainin 2 (MG2) is an antimicrobial peptide, and its activity occurs due to the interaction with membranes followed by the formation of transmembrane pores. The antimicrobial activity closely relates to the membrane-bound conformation of MG2, which largely depends on the constitutions of membrane or lipid molecules. Recently, it was found that the characteristics such as the spontaneous curvature of lipid molecule and the fluidity of membrane contributed to the membrane interaction of proteins [1, 2]. Hence, to clarify the contribution of these membrane characteristics to the MG2-membrane interaction, the membrane-bound conformations of MG2 in the presence of four types of lipid membranes (DLPC: dilauroyl phosphatidylcholine, DMPC: dimyristoyl phosphatidylcholine, DPPC: dipalmitoyl phosphatidylcholine, or DSPC: distearoyl phosphatidylcholine) were analyzed by a synchrotron-radiation circular-dichroism (SRCD) spectroscopy at various peptide-lipid concentration ratios and temperatures.

The results showed that MG2 formed a random coil structure in native state (without membrane) but changed to a helical structure in the presence of DLPC and DMPC lipid membranes at 25°C, showing that MG2 interacted with the both membranes (**FIGURE1**). On the other hand, MG2 retained its random coil structure in the presence of DPPC and DSPC lipid membranes, implying no membrane interaction (**FIGURE2**). Since the phase transition temperature (T_m) of these lipid molecules are -2°C for DLPC, 24°C for DMPC, 41°C for DPPC, and 55°C for DSPC, it was suggested that MG2 could interact with the membrane of liquid phase. To enhance the fluidity of DPPC and DSPC lipid membranes or to see the M2 conformation at their liquid phases, the temperature increased above T_m of the lipid molecules and decreased

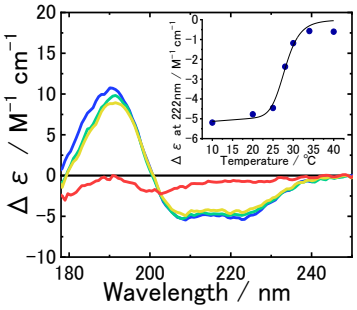

FIGURE1 SRCD spectra of MG2 in the presence of DMPC lipid membranes at 10°C (blue), 20°C (green), 25°C (yellow), 40°C (red).

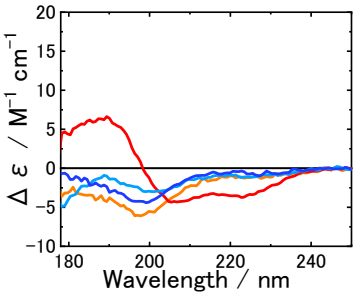

FIGURE2 SRCD spectra of MG2 in the presence of DPPC at 25°C (orange) and after annealing (red), and in the presence of DSPC (light blue) at 25°C and after annealing (blue).

until 25°C. After the annealing, MG2 formed helix structure in the DPPC lipid membrane but retained the random coil structure in the DSPC lipid membrane (**FIGURE2**). The DPPC and DSPC lipid membranes have the positive and negative spontaneous curvatures, respectively. Hence, these results suggest that in the membrane with the positive spontaneous curvature, MG2 could adsorb onto the membrane surface when its fluidity was enhanced, and penetrate when the temperature decreased. On the other hand, in the membrane with the negative spontaneous curvature, MG2 could not access the membrane surface even in the high temperature and retain its random coil structure in the low temperature. These differences mean that the lipid characteristics such as the spontaneous curvature and the fluidity would affect the membrane-bound conformation of MG2.

REFERENCES

1. E. Strandberg, J. Zerweck, P. Wadhwani, and A. S. Ulirich, *Biophysical Journal*, March 2013, pp. L09-L011
2. L. Ma, Y. Luo, Y-H. Ma and X. Lu, *Langmuir,* 2021, 37, 1613-1621

Spatial inhomogeneity in $Bi_2Sr_2CaCu_2O_{8+\delta}$ investigated by micro photoemission spectroscopy

T. Sugiyama[a] H. Iwasawa[b,c], S. Ozawa[d], H. Oda[d], R. Takahashi[e], T. Kono[d], T. Okuda[c], K. Miyamoto[c], H. Wadachi[e], S. Ishida[f], Y. Yoshida[f], H. Eisaki[f] and A. Kimura[a,d]

[a] *Graduate School of Advanced Science and Engineering, Hiroshima Univ., Hiroshima 739-8526 Japan*
[b] *National Institutes for Quantum Science and Technology, Hyogo 679-5184, Japan*
[c] *Hiroshima Synchrotron Radiation Center, Hiroshima Univ., Hiroshima 739-0046, Japan*
[d] *Graduate School of Science, Hiroshima Univ., Hiroshima 739-8526 Japan*
[e] *Graduate School of Science, Univ. of Hyogo, Hyogo 678-1205, Japan*
[f] *National Institute of Advanced Industrial Science and Technology, Ibaraki 305-8568, Japan*

Keywords: micro-ARPES, micro-XPS, high-T_c superconductivity, Bi2212

In recent years strongly correlated electron systems have attracted a great deal of attention because they exhibit interesting phenomena such as high-T_c superconductivity and giant magnetoresistive effect. These properties are caused by the competition and/or coexistence of multiple interactions (many-body interactions), such as those between electrons and bosons (phonons, magnons, etc.), due to strong electron correlation. In addition, it has recently become clear that the physical properties of such complex electron systems are based on "the self-organization of electrons", in which the electron system is ordered on a specific spatial scale and size of relevant interaction [1]. On the other hand, the theoretical treatment of many-body interactions is always an enormous challenge. It is otherwise approximated with the mean field and sometimes leads to wrong interpretations. Therefore, it is necessary to investigate electronic states and their many-body interactions experimentally. Photoelectron spectroscopy is a powerful experimental technique that can satisfy such requirements. In the past, the spatial resolution of photoemission spectroscopy was as low as about a millimeter, but in recent years, micro photoemission spectroscopy with well-improved spatial resolution has been developed worldwide [2,3]. In fact, in Cr-V_2O_3, a prototypical strongly correlated electron system, the inhomogeneous distribution of metallic and insulating electronic phases on a scale of several tens of microns has been observed by micro photoemission spectroscopy [4]. Such electronic phase separation is an essential phenomenon of strongly correlated electron systems, which is not found in conventional metals, insulators, and semiconductors. Therefore, it is essential to observe the electronic state with high spatial resolution in order to understand the physical properties of strongly correlated electron systems.

In this study, we have developed a micro angle-resolved photoemission spectroscopy (micro-ARPES) system at the Hiroshima Synchrotron Radiation Center, Hiroshima University, and investigated the real-space behavior of the electronic state of the cuprate high-T_c superconductor $Bi_2Sr_2CaCu_2O_{8+\delta}$ (Bi2212). In addition to the valence band information, we also carried out micro X-ray photoelectron spectroscopy (micro-XPS) measurements to analyze the chemical state. Also, we analyzed the spatial mapping data using a clustering method based on machine learning to handle big data, usually obtained in microscopy.

Figure 1(a) shows the band dispersion of Bi2212 measured by micro-ARPES. In this study, we evaluated the position dependence of the ARPES spectra by measuring the band dispersion at each position with small changes in the measurement position. Next, the momentum dependence of the band dispersion was measured at two points (A and B) where the sample positions were slightly different (0.2 mm), and the different sizes of the superconducting gap were observed [Fig. 1(b)]. This result suggests that the doping level differs depending on the position, and there is a small but finite difference in the observed size of the Fermi surface. On the other hand, it is still not realistic to examine the spatial dependence of such detailed and fine electronic structures by high-resolution ARPES because of time constraints. Therefore, we have performed micro-XPS measurements enabling microscopic measurements in a wider range with finer steps.

In this study, two-dimensional spatial mapping of the O 1s spectrum was performed by micro-XPS. The mapping range and step were respectively set to 1 mm and 5 μm each in horizontal and vertical directions, providing 40,000 O1s spectra in total. Since the total measurement time had to be limited to suppress the spectral change due to the surface degradation, the statistical accuracy of the experimental data at each measurement point was insufficient, making peak analysis difficult [FIG. 2(a)]. In addition, it is difficult to understand the characteristics of the electronic state only from the two-dimensional spatial distribution of the integrated intensity of the O 1s spectrum, as shown in FIG 2(c). Therefore, we performed a clustering analysis using machine learning on the spatial mapping data. The two-dimensional spatial distribution of each cluster obtained by clustering is shown in FIG. 2(d). At first glance, it is clear that each cluster is distributed inhomogeneously near the center of the sample, unlike the spatial distribution of the integrated intensity. By integrating the whole data classified into the same cluster, the obtained spectrum has enough statistical accuracy for peak analysis, making it possible to extract the electronic features, as exemplarily shown in FIG. 2(b). The subsequently performed peak analysis on each integrated spectrum [FIG. 2(e)] revealed that the peak positions shifted by more than 0.1 eV between clusters. This result clearly indicates that the chemical potential shift depending on the position, demonstrating the presence of spatial inhomogeneity in the doping level.

The present micro-ARPES and micro-XPS studies consistently showed that cuprate high-T_c superconductor Bi2212 exhibits micro-scale electronic inhomogeneity. Our results provide an important guideline for understanding the phase transition phenomena in high-T_c superconductivity.

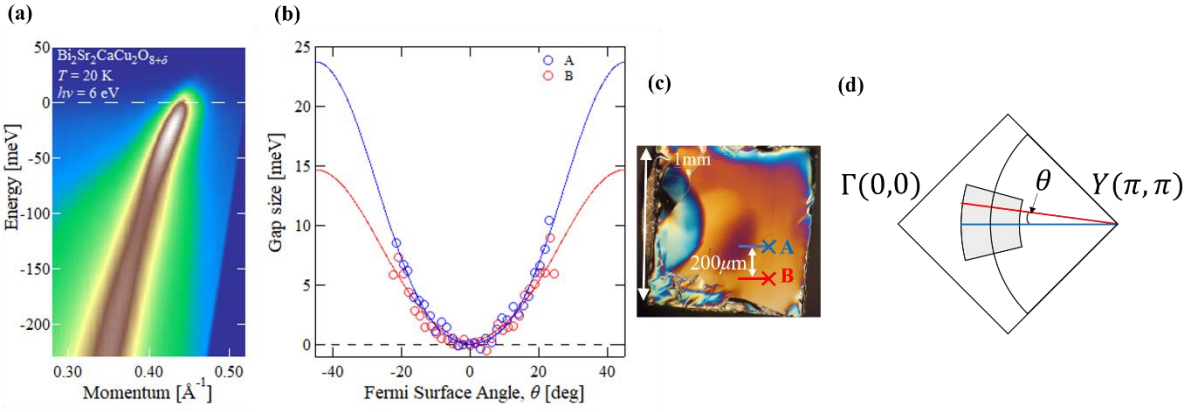

FIGURE 1. (a) ARPES image along the nodal direction (ΓY direction: blue line in FIG. 1(d)). (b) Momentum dependence of the superconducting gap measured at two points A and B (see FIG. 1(c)). (c) Optical microscope image observed ex-situ after ARPES measurements. (d) A quarter Brillouin zone of Bi2212, where θ is the Fermi surface angle defined by two segments starting from the Y point (π, π). Here, θ = 0 corresponds to the nodal direction.

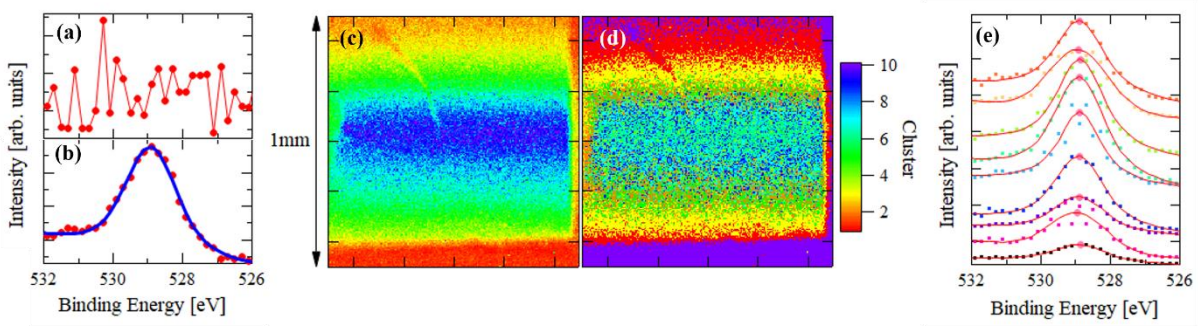

FIGURE 2. (a) Raw O 1s spectrum at one measurement point acquired by two-dimensional spatial mapping. (b) O 1s spectrum obtained by integrating data classified into the same cluster by clustering analysis. (c) Two-dimensional spatial distribution of the integrated intensity of the O 1s spectrum. (d) Two-dimensional spatial distribution of clusters. (e) Integrated spectra of each cluster (squares) and results of peak analysis (lines). The circles represent the peak position determined by fitting.

REFERENCES

1. E. Dagotto, Science **309**, 257-262 (2005).
2. E. Rotenberg and A. Bostwick, J. Synchrotron Radiat. **21**, 1048-1056 (2014).
3. H. Iwasawa, Electron. Struct. **2**, 043001 (2020).
4. S. Lupi *et al.*, Nat. Commun. **1**, 105 (2010).

Minority-spin Dominated Band Structure Near the Fermi Energy of Fe_4N Film Revealed by Spin- And Angle-Resolved Photoemission Spectroscopy

Karen Nakanishi[a], Kiyotaka Ohwada[b], Kenta Kuroda[b], Kazuki Sumida[c], Koji Miyamoto[d], Taichi Okuda[d], Shinji Isogami[e], Keisuke Masuda[e], Yuya Sakuraba[e], Akio Kimura[a,b]

[a]*Department of Physics, Faculty of Science, Hiroshima University, Higashi-Hiroshima 739-8526, Japan*
[b]*Graduate School of Advanced Science and Engineering, Hiroshima University, 1-3-1 Kagamiyama, Higashi-hiroshima 739-8526, Japan*
[c]*Materials Sciences Research Center, Japan Atomic Energy Agency, Hyogo 679-5148, Japan*
[d]*Hiroshima Synchrotron Radiation Center, Hiroshima University, 2-313 Kagamiyama, Higashi-Hiroshima 739-0046, Japan*
[e]*National Institute for Materials Science, 1-2-1 Sengen, Tsukuba 305-0047, Japan*

Keywords: Fe_4N thin film, Vacuum suitcase, Spin-dependent band structures, Spin-ARPES

Fe_4N has attracted a great deal of attention as a strong candidate for spintronic materials because of the inverse tunneling magnetoresistance (TMR) effect [1], the negative anisotropic magnetoresistance [2], and an enhanced spin-pumping efficiency [3,4]. An almost 100% negative spin polarization in the conductivity has been predicted for Fe_4N, where the hybridization between Fe 4*sp* and N 2*sp* orbitals plays an important role [5], while the spin polarization in the density of states at the Fermi level (E_F) is as small as -0.6. The spin polarization for Fe_4N film was measured by the point-contact Andreev reflection experiment, while its sign remained undetermined [6]. The TMR was often used to estimate the spin-polarization using Jullier's model [7], which was significantly influenced by the film-substrate interface. It is reminded that the unexpectedly high magnetoresistance at room temperature was reported for Fe/MgO/Fe magnetic tunneling junction, where the band-selective electron conductivity takes place in 'non-half-metallic' ferromagnetic layers [8]. It tells us that an experimental determination of spin- and wavenumber-dependent band structures are quite important.

Spin- and angle-resolved photoemission spectroscopy (spin-ARPES) is one of the most powerful experimental tools to clarify the spin-dependent electronic band structures. It requires a single crystal with remanent magnetization. In fact, there have been no direct experimental observations of the electronic band structures for the bulk Fe_4N due to the lack of cleavage plane and the non-saturating magnetization in the absence of an external magnetic field. The previous spin- resolved photoemission study on the Fe_4N film reported the negative spin polarization near E_F. However, the ion-sputtering of *ex-situ* grown film caused the deficiency of N atoms and the measured spin polarization remained inaccurate [9].

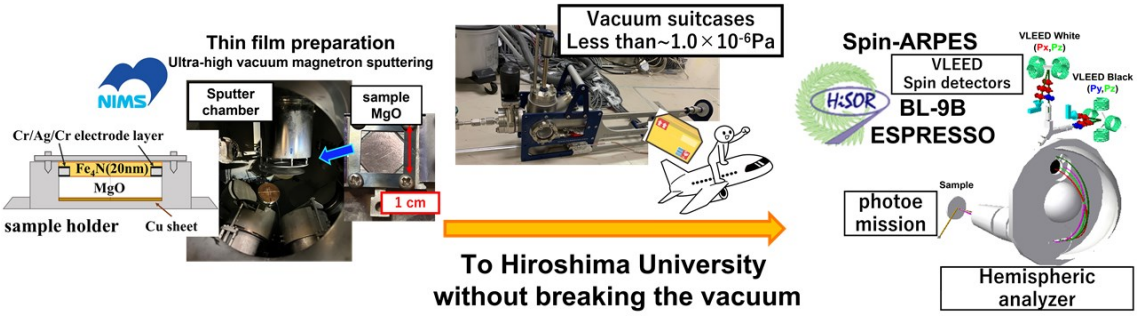

FIGURE 1. Growth of Fe_4N thin film and in-vacuum transportation to HiSOR.

To overcome this problem, we have grown the Fe_4N thin film and *in situ* performed spin-ARPES. The thin film samples were grown on MgO substrates by an ultrahigh-vacuum magnetron sputtering method at the National Institute for Materials Science (NIMS). The degree of order for nitrogen atoms in the film was evaluated to be 0.95 by the in-plane X-ray diffraction. An electrode layer of Cr/Ag/Cr was inserted to increase the electrical conductivity between the thin film and the sample holder, being indispensable for the spin-ARPES measurement.

The film samples were transported from NIMS to the preparation chamber of the spin-ARPES apparatus at HiSOR *via* the vacuum suitcase chamber. The thin films were reheated to 390~400°C to remove the contaminants adsorbed during the transportation. No nitrogen deficiency and no other impurities were detected by the Auger electron spectroscopy and the flat (001) surface was ensured by the sharp LEED spots. Spin-ARPES measurement was performed utilizing the ESPRESSO machine composed of the hemispherical analyzer and the VLEED-type spin detector with *s*- and *p*- polarized undulator radiation at BL-9B of HiSOR [7]. The photoelectron spin polarization (P) was estimated from the measured intensity asymmetry $A = (I^+ - I^-)/(I^+ + I^-)$ with the effective Sherman function ($S_{\text{eff}} = 0.3$) through the relation $P = A/S_{\text{eff}}$, where $I^+(I^-)$represents the reflected electron intensity at the positively (negatively) magnetized Fe(001)-p(1×1)O target of the spin detector.

Figure 2(a) shows the ARPES image of Fe_4N thin film in the ΓM direction of the bulk Brillouin zone (Fig.2(c)). We have observed three band structures that cross E_F at $k_{\parallel}$ = -1.0, -0.5 and +0.5 Å^{-1}. Figure 2(b) shows the spin-resolved energy distribution curves deduced by $I_{\uparrow\downarrow} = 0.5I(1 \pm P)$ at the fixed wavenumber of the red line in Fig.2(a), where $I_{\uparrow}$ ($I_{\downarrow}$) corresponds to the photoelectron intensity in the majority (minority) spin channel and $I = I_{\uparrow} + I_{\downarrow}$. We find that $I_{\uparrow}$ is dominant in the energy (E-E_F) from -1.6 eV to -0.5 eV, while $I_{\downarrow}$ gradually increases with increasing energy and get much higher than $I_{\uparrow}$ in the vicinity of E_F.

In summary, the minority-spin dominated character of the band structures in the vicinity of E_F has been unveiled experimentally for Fe_4N thin film. Our finding provides deep insights into the mechanism of the inverse tunneling magnetoresistance effect, the negative anisotropic magnetoresistance, and the enhanced spin pumping in Fe_4N, which will help the development of spintronics devices.

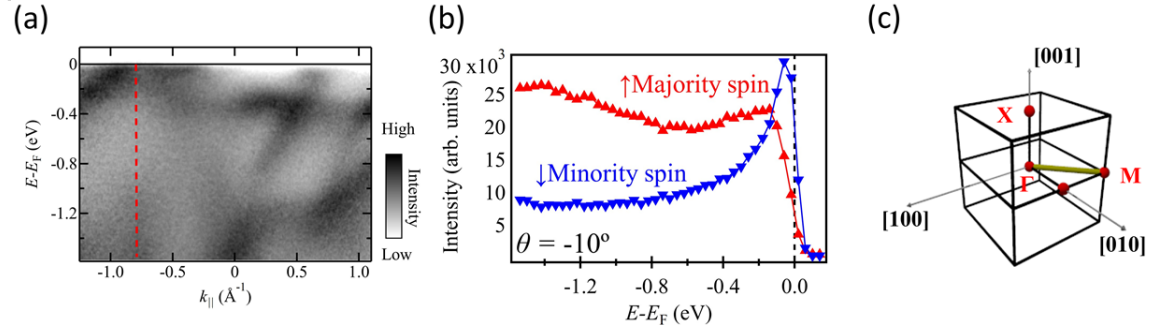

FIGURE 2. (a) ARPES energy dispersions curves along the ΓM line. (b) Spin-resolved energy distribution curves acquired at a wavenumber position denoted with red dashed line in panel (a). (c)Bulk Brillouin zone of Fe_4N.

REFERENCES

1. K. Sunaga, M. Tsunoda, and K. Komagaki *et al*, J. Appl. Phys. **102**, 013917 (2007).
2. M. Tsunoda, Y. Komasaki, S. Kokado, S. Isogami, C.-C. Chen, and M. Takahashi, Appl. Phys. Express **2**, 083001 (2009).
3. S. Isogami, M. Tsunoda, M. Oogane, A. Sakuma, and M. Takahasi, Appl. Phys. Exp. **6**, 063004 (2013).
4. S. Isogami, and M. Tsunoda, Jpn. J. Appl. Phys. **55**, 043001 (2016).
5. S. Kokado, N. Fujima, K. Harigaya, H. Shimizu, and A. Sakuma, Phys. Rev. B.**73**,172410 (2006).
6. A. Narahara, K. Ito, T. Suemasu, Y. K. Takahashi, A. Rajanikanth, and K. Hono, Appl. Phys. Lett. **94**, 202502 (2009).
7. M. Julliere, Phys. Lett. **54A**, 225 (1975).
8. S. Yuasa, T. Nagahama, A. Fukushima, Y. Suzuki, and K. Ando, Nat. Mater. **3**, 868 (2004).
9. K. Ito, K. Okamoto, K. Harada, T. Sanai, K. Toko, S. Ueda, Y. Imai, T. Okuda, K. Miyamoto, A. Kimura, and T. Suemasu, J. Appl. Phys. **112**, 013911 (2012).
10. T. Okuda *et al*, Rev. Sci. Instrum. **82**, 103302 (2011).

Many-body Interactions on the Surface of the Topological Insulators

Amit Kumar[a], Shiv Kumar[a,b], Kenya Shimada[a,b]
[a] *Graduate School of Science, Hiroshima University, Kagamiyama 1-3-1, Higashi-Hiroshima 739-8526, Japan*
[b] *Hiroshima Synchrotron Radiation Center, Hiroshima University, Kagamiyama 2-313, Higashi-Hiroshima 739-0046, Japan*

Keywords: Topological Insulators, ARPES, Many-body interactions, Spintronics

Three-dimensional (3D) topological insulators (TIs) have attracted great attention in condensed matter physics for the past decade because of their fascinating fundamental physical properties and promising applications in the "*spintronics*"[1]. The 3D TIs are remarkable because there exist topological surface states (TSSs) with linear Dirac-cone-like dispersion. The TSSs are metallic and the backscattering is reduced due to the helical spin texture, which is robust against weak non-magnetic disorder or crystal defects as far as the topological property is conserved. These unusual physical properties of the TIs would have potential applications in high-speed dissipationless electronic devices such as quantum computers in the future[2]. Based on the Fermi liquid theory, the transport properties are directly related to the quasiparticles (electrons or holes under the influence of the many-body interactions, such as the electron-phonon and electron-electron interactions) near the Fermi level (E_F). Therefore, quantifying these many-body interactions in the TIs is essentially important for spintronic applications.

In this study, we have examined detailed many-body interactions in the prototypical TIs such as Bi_2Se_3 and Bi_2Te_3 using a laser-based high-resolution angle-resolved photoemission spectroscopy (ARPES)[3]. We have done temperature-dependent ARPES measurements with the *s*-polarization geometry. We cleaved the single crystals below 20 K in the ultrahigh vacuum to get clean surfaces. Figures 1(a1) and 1(b1) show the ARPES results of Bi_2Se_3 and Bi_2Te_3. One can see that they are both n-type semiconductors (the conduction band is closer to the Fermi level) and linearly dispersive Dirac-cone-like spectral feature at the $\overline{\Gamma}$ point ($k_{//}=0$Å^{-1}). The high symmetry directions in the surface Brillouin zone can be determined by measuring the Fermi surface (FS) shapes [see Figs. 1(a2) and (b2)]. Figures 1(a3) and (b3) show the enlarged view of selected regions [rectangle box in Figs. 1(a1) and (b1)] near the E_F. The peak positions were obtained by fitting the peak in the momentum distribution curves (MDCs) to a Lorentzian, as illustrated in Figs. 1(a3) and 1(b3) by the solid black line. One can see clearly in Figs. 1(a3) and 1(b3), no band renormalization (so-called kink, which is the whole mark of electron-phonon interaction), indicating weak electron-phonon interaction in the TSS.

In this poster, I will discuss the magnitudes of the electron-phonon and electron-electron interactions in more detail based on the quantitative ARPES lineshape analyses.

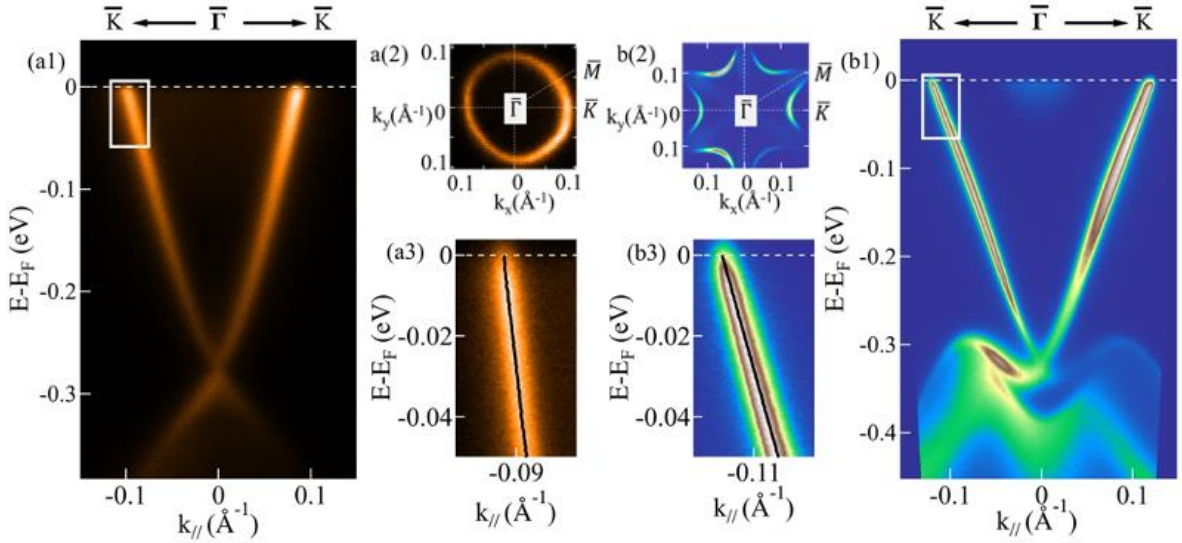

Figure 1. ARPES spectrum measured at 17 K. (a1)-(a3) from Bi_2Se_3 (BS) and (b1)-(b3) from Bi_2Te_3 (BT) respectively. (a1) and (b1) band dispersion along $\overline{\Gamma}$-$\overline{K}$ direction in the surface Brillouin zone. (a2) and (b2) Fermi surface (FS) at E_F. (a3) and (b3) Enlarged view of ARPES spectrum near E_F corresponding to the rectangles in (a1) and (b1), respectively. Solid lines (black) represent peak positions obtained from the MDC lineshape analyses.

References-

[1] M. Z. Hasan and C. L. Kane, Reviews of Modern Physics **82**, 3045 (2010).
[2] D. Pesin and A. H. MacDonald, Nat. Mater. **11**, 409 (2012).
[3] H. Iwasawa, E. F. Schwier, M. Arita, A. Ino, H. Namatame, M. Taniguchi, Y. Aiura, and K. Shimada, Ultramicroscopy **182**, 85 (2017).

Observation of Liquid-Liquid Phase Separation of FUS-LC using VUV-CD Spectroscopy

Kentaro Fujii[a], Nobuo Maita[b], Koichi Matsuo[c], and Masato Kato[b]

[a]*Institute for Quantum Life Science, National Institutes for Quantum Science and Technology, 6-6-11-901 Aoba, Aramaki, Aoba-ku, Sendai-city, Miyagi, 980-8579 JAPAN*
[b]*Institute for Quantum Life Science, National Institutes for Quantum Science and Technology, 4-9-1 Anagawa, Inage-ku, Chiba-city, Chiba, 263-8555 JAPAN*
[c]*Hiroshima Synchrotron Radiation Center, Hiroshima-university, 2-313 Kagamiyama, Higashihiroshima-city, Hiroshima, 739-0046 JAPAN*

Keywords: Liquid-Liquid Phase Separation, FUS-LC, VUV-CD.

Aggregation of the RNA-binding protein FUS (Fused in Sarcoma) has been implicated in the neurodegenerative diseases such as ALS (amyotrophic lateral sclerosis) and FTD (frontotemporal dementia) [1]. The low-complexity domain of the FUS (FUS-LC) mediated liquid-liquid phase separation (LLPS) [2], but the structural mechanism is not known in detail. To address the revealing the mechanism, several structural analyses such as NMR or x-ray crystallography were examined [2, 3]. Reentry, Murakami and co-authors were performed Raman microscopy to analyze LLPS local structure [4]. They revealed that the FUS LC have extremely high concentrations which could not achieved in vitro experiments. In order to reveal the process to form LLPS such a high concentration, we examined the spectroscopic study using VUV-CD measurement, which can analyze the secondary structure of the proteins.

VUV-CD measurements were performed at BL12 VUV-CD station [5]. To increase S/N ratio of CD intensity around VUV energy region; 180-190nm, we prepared the chloride free buffer of FUS LC sample. The LLPS of our prepared FUS LC sample were observed by changing the sample temperature from room temperature to 5℃ in microfuge tube. 40μL of the sample was encapsulated in a CaF_2 cell (path length, 100μm). The cell was attached to peltier controlled cooling holder to control the temperature of the sample [6]. CD spectra were measured between 185 and 260 nm. The temperature of the samples were controlled from room temperature to 5℃ to obtain the LLPS of the FUS LC.

Obtained CD spectra are shown in Figure 1. The CD spectrum obtained by measuring at room temperature has large peak at nm and small shoulder peak near nm. This shows the major structure is random coil since the spectrum were similar to that of STI which is mainly unordered structure. This result is consistent with that obtained from NMR measurement. The peak intensity around 195 nm decreased by cooling the sample temperature.

We thought that the reasons of the obtained spectral changes as follows; 1) LLPS showed secondary structural changes, 2) LLPS make an effect to decreasing the transmission light intensity by scattering of suspension. We try to examine the measurement by changing the relative distance between the cell and the photo-multiplier detector. This may clarify the contribution of the scattering effect on the obtained spectrum.

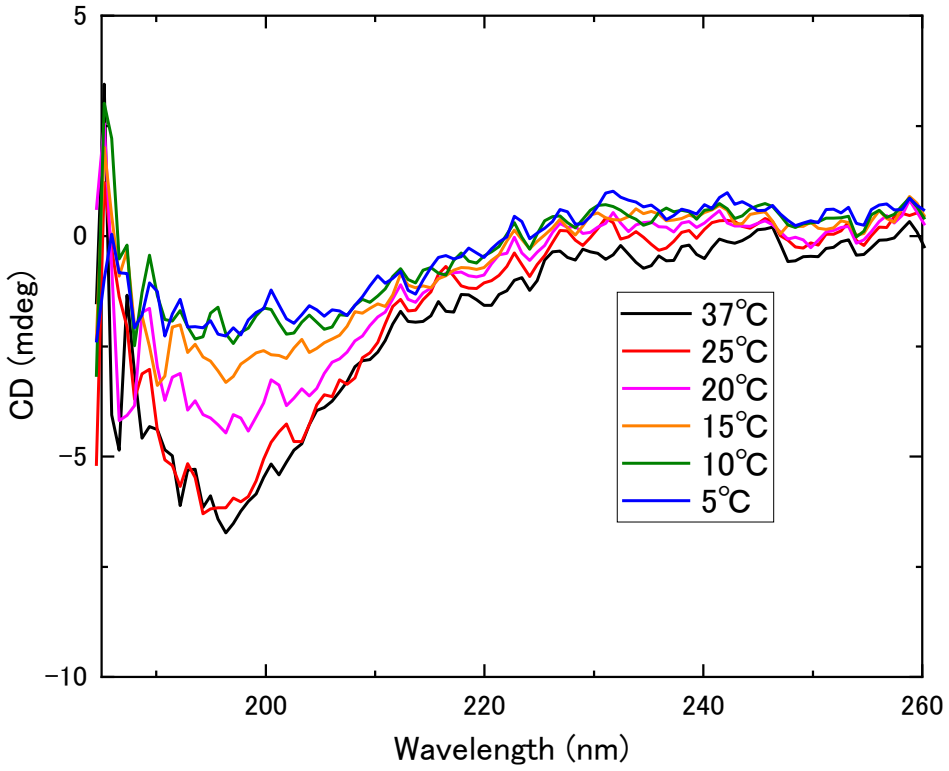

FIGURE 1. The obtained spectra of FUS LC in phosphate buffer pH. 12. By cooling the temperature of the sample, the CD intensity around 195 nm were decreased.

REFERENCES

1. M. Nolan, K. Talbot, O. Ansorge, *Acta. Neuropathologica Communications* **4** (2016) 99.
2. D.T. Murray, M. Kato, Y. Lin, K.R. Thurber, I. Hung, S.L. McKnight, T. Tycko, *Cell* **171** (2017) 615-627.
3. F. Luo, X. Gui, H. Zhou, J. Gu, Y. Ki, X. Liu, M. Zhao, D. Li, X. Li, C. Liu, *Nat. Struct. Mol. Biol.* **25** (2018) 341-346.
4. K. Murakami, S. Kajimoto, D. Shibata, K. Kuroi, F. Fujii, T. Nakabayashi, *Chem. Sci.* **21** (2021) 7411-7418.
5. M. Sawada, H. Namatame, M. Taniguchi, *J. Phys. Conf. Ser.* **425** (2013) 162010.
6. K. Matsuo, K. Sakai, Y. Matsushima, T. Fukuyama, K. Gekko, *Anal. Sci.* **19** (2003) 129-132.

Development of Time-Resolved Vacuum-Ultraviolet Circular Dichroism Spectroscopy and its Application to the Interaction Analysis betweenβ-Lactoglobulin and Lipid Membrane

Satoshi Hashimoto[a], Koichi Matsuo[b]

[a]*Graduate School of Advanced Science and Engineering, Hiroshima University, 1-3-1 Kagamiyama, Higashi-Hiroshima, Hiroshima 739-8526, Japan*
[b]*Hiroshima Synchrotron Radiation Center, Hiroshima University, 2-313 Kagamiyama, Higashi-Hiroshima 739-0046, Japan*

Keywords: Circular dichroism, β-Lactoglobulin, Membrane interaction, Secondary structures, Time-resolved measurement

Structure of protein changes depending on the solvent environments including the presence or absence of membrane, leading various physicochemical phenomena. In this study, vacuum-ultraviolet circular dichroism (VUVCD) spectroscopy combined with time-resolved measurement was used for the analysis of conformational changes of protein induced by membrane interactions. In the time-resolved measurement, we have made a microfluidic cell that can efficiently mix protein solution and lipid membrane solution at a low flow velocity [1-2], and installed it in the VUVCD system equipped with a Schwarzschild focusing system that can miniaturize the synchrotron radiation light below 100 micrometers.

β-Lactoglobulin (βLG) was used as a model protein being capable of interacting with membrane such as lysophosphatidylglycerol lipids (LysoDMPG). Time-resolved VUVCD spectra were measured from 260-180 nm in the range of time resolution from 1 to 15sec at the lipid/protein concentration ratio = 50. After a liner dichroism has no effect on the CD spectrum at the low flow situation, the time-resolved spectra of βLG were analyzed. The result shows that the secondary structure of βLG changes from β-strand to α-helix structures as the time after the mixing passes, indicating that βLG forms a membrane-bound structure within a few seconds. The time-dependent VUVCD spectra were analyzed by singular value decomposition method, and it was found that the structural change was composed of two states.

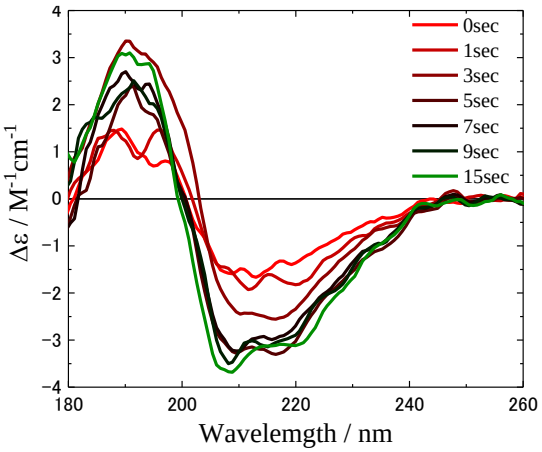

FIGURE 1. Time-resolved VUVCD spectra of βLG for interaction with LysoDMPG in the range of 260-180 nm at the lipid/protein concentration ratio = 50

References

1. A. S. Stroock, S. K. W. Dertinger, A. Ajdari, I. Mezic, H. A. Stone, G. M. whitesides, Chaotic Mixer for Microchannels, *Science*, **295** 647-651 (2002).
2. T. J. Kwak, Y. G. Nam, M. A. Najera, A. W. Lee, J. R. Strickler, W. J. Chang, Convex Grooves in Staggered Herringbone Mixer Improve Mixing Efficiency of Laminar Flow in Microchannel, *PLOS ONE*, e0166068 (2016)

Direct observation of Dirac nodal-line fermions in P-square net superconductor, $ZrP_{1.24}Se_{0.57}$

S. Ishizaka[a], A. Ino[b,c], T. Kono[a], Y. Miyai[d], S. Kumar[c], K. Shimada[c], H. Kito[e], I. Hase[e], S. Ishida[e], K. Oka[e], H. Fujihisa[e], Y. Gotoh[e], Y. Yoshida[e], A. Iyo[e], H. Ogino[e], H. Eisaki[e], K. Kawashima[f,e], Y. Yanagi[f,e], A. Kimura[a,d]

[a]*Graduate School of Science, Hiroshima University, Higashi-Hiroshima 739-8526*
[b]*Kurume Institute of Technology, 2228-66 Kamitsu, Kurume, Fukuoka 830-0052*
[c]*Hiroshima Synchrotron Radiation Center, Hiroshima University, Higashi-Hiroshima 739-0046, Japan*
[d]*Graduate School of Advanced Sciences and Engineering, Hiroshima University, Higashi-Hiroshima 739-8526, Japan*
[e]*National Institute of Advanced Industrial Science and Technology (AIST), Tsukuba, Ibaraki 305-8568, Japan*
[f]*IMRA JAPAN Co., Ltd., Kariya, Aichi 448-8650, Japan*

Keywords: Dirac nodal-line fermion, nonsymmorphic space group, superconductor, ARPES, Dirac velocity, nodal loop

In recent years, Dirac nodal-line fermions in superconducting materials have attracted much attention due to expectation for novel transport properties [1]. For instance, a Dirac nodal-line semimetal (DNLS), $PbTaSe_2$, exhibits Dirac velocity of 4.0×10^5 m/s and superconductivity with critical temperature (T_c) of 3.8 K [2]. However, in order to realize low-loss and fast electronics, the nodal-line superconductors which exhibit higher Dirac velocity and higher T_c are desired. Here, we focus on a recently-discovered layered-phosphide-chalcogenide superconductor, $ZrP_{2-x}Se_x$ (T_c = 6.2 K) [3]. This material is isostructural with ZrSiS, which is known as a typical DNLS. While the first-principles calculation has predicted that a nodal line is present in the band structure of $ZrP_{2-x}Se_x$ [4], no experimental evidence has been reported so far. In this study, we performed an angle-resolved photoemission spectroscopy (ARPES) study of high-quality single crystals of $ZrP_{1.24}Se_{0.57}$, using soft X-ray (SX) and vacuum ultraviolet (VUV) synchrotron radiations at BL25SU of SPring-8 and BL-1of HiSOR, respectively.

The band dispersions of $ZrP_{1.24}Se_{0.57}$ observed by VUV-ARPES along the X-Γ-X and M-Γ-M lines are shown in Figs. 1(a) and (b), respectively. Two electron pockets, γ and δ, centered at the Γ point, and an electron pocket, ε, centered at the X point are observed, as shown in Fig. 1(a). We observed that two steep and straight dispersions cross with each other at -1.3 eV with Dirac velocity of 1.2×10^6 m/s, and that the crossing point forms a closed nodal-loop in the k_x-k_y plane. The experimental band structures is well reproduced by tight-binding calculation of a free-standing P square net.

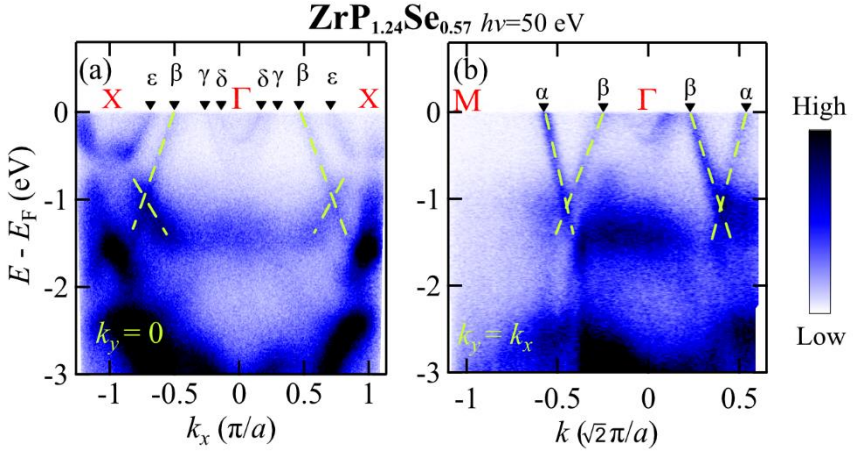

FIGURE 1. Experimental *E*-*k* plots along the (a) X-Γ-X and (b) M-Γ-M, respectively, with $h\nu$ = 50 eV for $ZrP_{1.24}Se_{0.57}$.

In summary, we have demonstrated that $ZrP_{1.24}Se_{0.57}$ is a nodal-line superconductor. The fast Dirac fermions of 1.2×10^6 m/s in $ZrP_{1.24}Se_{0.57}$ arises from the nonsymmorphic P square net, and surpass the velocity record held by the point-node Dirac fermions in graphene. Our finding provides a new playground for emergent exotic phenomena, and will lead to a discovery of elusive Majorana fermions.

REFERENCES

1. C. Chen *et al*., Phy. Rev. B **90**, 205136 (2014).
2. G. Bian *et al*., Nat. Commun. **7**, 10556 (2016).
3. H. Kito *et al*., J. Phys. Soc. Jpn. **83**, 074713 (2014).
4. I. Hase *et al*., J. Phys. Conf. Ser. **1590**, 012008 (2020).

Current activities of research and education on BL-5 (FY2021)

T. Yokoya[a,b], T. Wakita[a,b] and Y. Muraoka[a,b]

[a]*Research Institute for Interdisciplinary Science, Okayama University*
[b]*Research Laboratory for Surface Science, Okayama University, Okayama 700-8530, Japan*

Keywords: Photoemission spectroscopy, photoelectron emission microscopy

We present an overview of our resent research and educational activities on beamline 5 (BL5) in the fiscal year 2021. Our beamline has two experimental stations in a tandem way. The first station is equipped with an angle-resolved photoemission spectrometer (ARPES), a low energy electron diffraction (LEED) apparatus and an X-ray source. The hemispherical analyzer of ARPES spectrometer (HA54, VSW) has a mean radius of 50 mm and is mounted on a twin axis goniometer in ultra-high vacuum chamber. Using this goniometer, one can perform ARPES and photoelectron diffraction (PED) measurements. It is also possible to perform resonant photoemission spectroscopy (RPES) measurements by using photon energy tunability of synchrotron radiation with X-ray absorption spectroscopy (XAS) measurement. With the X-ray source (XR2E2, FISONS), we can perform an X-ray photoelectron spectroscopy (XPS) measurement for the chemical state analysis and the PED. At the second station, we have installed a photoelectron emission microscope (PEEM, 'PEEM III', Elmitec). PEEM provides a magnified image of lateral intensity distribution of photo-emitted electrons from a sample surface. The spatial resolutions are several ten nanometers with Hg lamp and a few micrometers with synchrotron radiation. The sample is transferred between the ARPES and the PEEM chamber in-situ, and one can perform measurements at both stations for the same sample.

In the recent researches on BL-5, we have studied the electronic structure of potassium doped aromatic molecule (K_x picene) [1], iron-based superconductor ($FeSe_xTe_{1-x}$) [2], transition metal di-oxide films such as VO2 thin films which exhibits a first-order metal-to-insulator transition at 340 K [3], CrO_2 thin films which are known as a half-metallic material [4], and TaO_2 film which is stabilized with a new technique developed in our group [5]. We have also studied the electronic structures of a high-quality boron-doped diamond film which shows a signature of the highest superconducting transition temperature of 25 K [6] and a high quality single crystal of $YbFe_2O_4$ which is one of multiferroic materials [7], by utilizing RPES at B *K*- and Fe $M_{2,3}$-edges, respectively. In this fiscal year, we have studied the sp^3 content in diamond-like carbon films by using photoemission spectroscopy in order to optimize the conditions to produce Q-carbon (quenched carbon) which is a newly discovered amorphous phase of carbon with several exotic properties [8], as presented in this symposium.

At present, we are preparing an auto-measurement system for photoemission holography (PEH). PEH is a method that has been greatly developed in Japan in recent years as a measurement method for elucidating the local structure of materials with an atomic resolution [9]. In particular, various results have been reported in the study of the three-dimensional atomic configurational structure around the dopants in crystals [10]. However, the opportunity to use state-of-the-art apparatuses (for example, DA30 analyzer and RFA of BL25SU at SPring-8) are limited. Although our photoelectron energy analyzer is an old model and it is difficult to separate and observe small shifts in core levels because of the energy resolution of 1-2 eV of the system, preliminary experiments on undoped materials can be carried out with our apparatus before the experiment using the latest ones. It can also be used for educational purposes such as experiencing photoelectron holography experiments and learning the analysis methods.

We have used the BL-5 for education activity as well, for example, practical education for undergraduate students of Okayama University. The students have an opportunity to study the synchrotron radiation mechanism and to experience XPS measurement which is very useful for the surface science research. We accepted more than 100 students from 2006 to 2012. From 2014, we have started to join the practical lecture for experiments using the beamline end stations in HiSOR for both graduate school students of Hiroshima

and Okayama Universities. In 2018, we have had a new project for education under a Japan-Asia youth exchange program in science supported by Japan Science and Technology Agency (JST), “Sakura Exchange Program in Science”. We have accepted six students from Changchun University of Science and Technology in China.

REFERENCES

1. H. Okazaki *et al*., *Phys. Rev* **82**, pp. 195114 (5 pages) (2010).
2. Y. Yoshida *et al*., *J. Phys. Soc. Jpn* **78**, pp. 034708 (4 pages) (2009).
3. K. Saeki *et al*., *Phys. Rev* **80**, pp. 125406 (5 pages) (2009).
4. Y. Muraoka *et al*., *MRS Proceedings* **1406** (2012).
5. Y. Muraoka *et al*., *Thin Solid Films* **599**, pp. 125-132 (2016).
6. H. Okazaki *et al*., *Appl. Phys. Lett* **106**, pp. 052601 (5 pages) (2015).
7. K. Fujiwara *et al*., *Trans. Mater. Res. Soc. Jpn.* **41**, pp. 139-142 (2016).
8. H. Yoshinaka *et al*., *Carbon.***167**, pp. 504-511 (2020).
9. T. Matsushita *et al*. *Europhys. Lett*. **71**, 597 (2005). *Phys. Status Solidi B* **255**, 1800091 (6 pages) (2018).
10. K. Hayashi, T. Matsushita, *SPring-8 Research Frontiers* **2020**, pp. 12 -15 (2021).

Angle resolved resonant photoemission study of Si 3*p* band

T. Wakita[a], Y. Muraoka[a,b], and T. Yokoya[a,b]

[a]*Research Institute for Interdisciplinary Science, Okayama University*
[b]*Research Laboratory for Surface Science, Okayama University, Okayama 700-8530, Japan*

Keywords: Resonant photoemission, semiconductor, silicon, exciton

Resonant photoemission has been widely used to identify spectral features in valence-band photoemission spectra, for example, as 4*f*- or 3*d*-derived states. Such a resonance is observed when localized and highly correlated states participate to the excitation process. For band insulators with highly dispersive valence bands, some observations of resonant photoemission have also been reported in which a localized core exciton was considered to play an essential role. In 1983, Kobayashi *et al*., for example, reported that photoemission spectra from a Si(111) cleaved surface show two types of resonant enhancement in the vicinity of 2*p*-core excitation threshold, a Fano-type resonance for the 3*p*-like topmost emission band and a stronger intensity enhancement in the deeper binding-energy region around 7.6 eV [1]. For the latter, they proposed that the origin is an Auger-type two-hole decay of the core exciton. A short time later, however, another explanation for these observations has been suggested, that is, both photoemission enhancements can be simulated by a non-resonant Auger signal [2]. There was a similar argument for black phosphorus based on experimental studies [3-5], and in 1986, a theoretical investigation succeeded in reproducing the above-mentioned features in valence band photoemission spectra near P 2*p*-core excitation edge by using the core-exciton picture [6]. They revealed that a core exciton plays an important role both in Fano-type resonance and the enhancement of the Auger electron intensity at the core exciton threshold. In experimental spectra for black phosphorous, however, both contributions are overlapped and the experimental direct verification has been not executed still completely.

In this study, we have performed angle resolved photoemission spectroscopy (ARPES) of Si(111)1x1-H surfaces on the BL5 at HiSOR, in normal emission with various photon energies in the vicinity of Si 2*p* core excitation threshold. A semispherical analyzer with an angular acceptance of ± 0.5° was used. The total energy resolutions were 0.2 – 0.3 eV in the photon energy range from 95 to 105 eV used in our measurements. The Fermi level (E_F) position was determined by photoemission from the metallic (Mo) sample holder. The base pressure was 5×10^{-8} Pa. A Si(111)1x1-H surface was prepared by chemical etching in aqueous NH_4F solution. All measurements were carried out at room temperature.

Figure 1 (a) shows Photon energy dependence of angle resolved photoemission spectra of a Si(111)1x1-H surface in the vicinity of Si 2*p* core excitation threshold (100 – 102 eV) measured with a normal emission configuration and 2nd order synchrotron radiation. The spectra are normalized to the photon intensity. The peak at around 2 eV is the top valence band mainly originated from 3*p* state ("3*p* band"). Si 2*p* signals excited by 4th order lights are also included in the negative range of the binding energy of the spectra. Both signals (the 3*p* band and the 2*p* signal) do not overlap with each other in the photon energy range of 100 – 102 eV. Figure 1 (b) shows a 2D intensity map of the spectra. There are no Auger signals which exhibit a constant kinetic energy structure. In Figure 1 (c), we plot the integrated intensities of the 3*p* band within 1.5 eV of binding energy (in the energy range shown by the red rectangles in (a) and (b)), as red circles. Although they show a clear structure, their variation behavior coincides with neither near edge structure of the Si $L_{2,3}$-edge X-ray absorption spectrum (solid curve) nor the fit result with a Fano line-shape function (dotted curve) in ref. [1]. There are a few possible reasons for these discrepancies. (i) The photon energy dependence of the diffraction efficiency of the monochromator grating can have an effect on the photon energy dependence of the spectral intensity, since we have used the 2nd order light while the photon intensity, which we have used for the normalization of the spectral intensity, includes all orders of light. (ii) The photon energy dependence of the non-resonant photoemission cross section of Si 3*p* can modify the spectral intensity owing to the empty band structure effect beyond the free electron approximation in the final state. For the former

possibility, we will experimentally investigate the photon energy dependence of the intensity of the 2nd order light in the near future. For the latter, we are now working on the theoretical calculation of the photoemission cross section of Si 3*p* state from a Si(111) surface in a normal emission configuration. In addition, we have a plan to investigate the doping dependence of the resonant photoemission from a Si(111)1x1 surface over a wider photon energy range in order to elucidate if the carrier concentration affects the resonance energy.

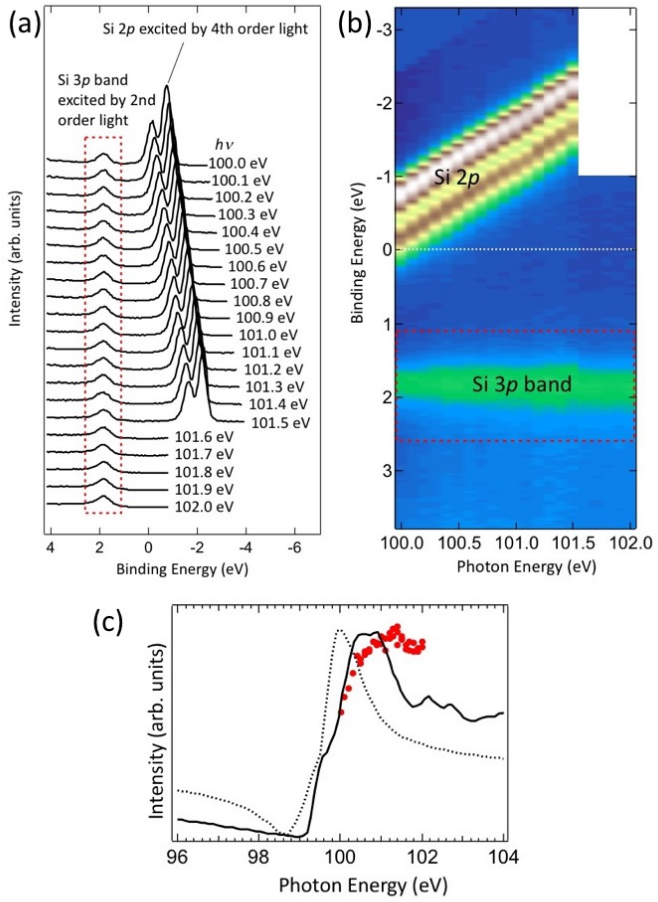

FIGURE 1. (a) Photon energy dependence of angle resolved photoemission spectra of a Si(111)1x1-H surface in the vicinity of Si 2*p* core excitation threshold measured with a normal emission configuration using 2nd order synchrotron radiations. The spectra are normalized to the photon intensity. (b) Intensity map of the spectra in (a). (c) The red circles show the integrated intensities of the observed Si 3*p* band (inside the red dotted squares in (a) and (b)). The black solid curve is a Si $L_{2,3}$-edge x-ray absorption spectrum. The dotted curve shows the fit result with a Fano line-shape function for the photon energy dependence of the intensity of 3*p* band observed in Ref. [1].

REFERENCES

1. K. L. I. Kobayashi *et al*., *Phys. Rev. Lett*. **50**, 1701 (1983).
2. R. A. Riedel *et al*., *Phys. Rev. B* **30**, 6815 (1984).
3. M. Taniguchi *et al*., *Solid State Commun*. **49**, 867 (1984).
4. T. Takahashi *et al*., *Phys. Rev. B* **33**, 1485 (1986).
5. M. Taniguchi *et al*., *Phys. Rev. B* **39**, 11160 (1989).
6. T. Nakano and A. Kotani, *J. Phys. Soc. Jpn.* **55**, 2867 (1986).

Observation of Fast Dirac Nodal-Line Fermions in a Nonsymmorphic Superconductor, $HfP_{1.55}Se_{0.45}$

Y. Nishioka[a], S. Ishizaka[b], K. Kuroda[c], A. Ino[d,e], S. Kumar[e], K. Shimada[e], H. Kito[f], I. Hase[f], S. Ishida[f], K. Oka[f], H. Fujihisa[f], Y. Gotoh[f], Y. Yoshida[f], A. Iyo[f], H. Ogino[f], H. Eisaki[f], K. Kawashima[f,g], Y. Yanagi[f,g], A. Kimura[a,b,c]

[a]*Faculty of Science, Hiroshima University, Higashi-Hiroshima 739-8526*
[b]*Graduate School of Science, Hiroshima University, Higashi-Hiroshima 739-8526*
[c]*Graduate School of Advanced Sciences and Engineering, Hiroshima University, Higashi-Hiroshima 739-8526, Japan*
[d]*Kurume Institute of Technology, 2228-66 Kamitsu, Kurume, Fukuoka 830-0052*
[e]*Hiroshima Synchrotron Radiation Center, Hiroshima University, Higashi-Hiroshima 739-0046, Japan*
[f]*National Institute of Advanced Industrial Science and Technology (AIST), Tsukuba, Ibaraki 305-8568, Japan*
[g]*IMRA JAPAN Co., Ltd., Kariya, Aichi 448-8650, Japan*

Keywords: Dirac nodal-line fermions, nonsymmorphic space group, superconductors, ARPES, Dirac velocity, nodal loops

In recent years, incorporating superconductivity into the Dirac nodal-line semimetal (DNLS) is expected to provide a platform for exotic physical properties. Therefore, such candidates have been extensively explored. Despite extensive exploration of DNLS, only a few superconductors have been found among them to date. For instance, a DNLS, $PbTaSe_2$, exhibits Dirac velocity of 4×10^5 m/s and superconducting critical temperature (T_c) at 3.8 K [1]. Recently, a nodal loop has been observed in $ZrP_{2-x}Se_x$, which crystallizes in a nonsymmorphic space group (P4/nmm) and exhibits the superconductivity below $T_c = 6.2$ K [2]. Notably, it has been reported that $HfP_{2-x}Se_x$ also shows superconductivity below $T_c = 5.5$ K [3]. Replacing Zr (Atomic number, Z=40) with Hf (Z=72) leads to the shrinkage of lattice constants and the increase in spin-orbit coupling strength. Therefore, a substantial impact on the electronic structure is expected. In this study, we determined the electronic structure of $HfP_{1.55}Se_{0.45}$ by using synchrotron-radiation angle-resolved photoemission spectroscopy (ARPES) at BL-1 of Hiroshima Synchrotron Radiation Center, and investigated the Hf substitution effect by comparing $HfP_{1.55}Se_{0.45}$ with $ZrP_{1.24}Se_{0.57}$.

Figure 1(a) shows the Fermi-surface map of $HfP_{1.55}Se_{0.45}$. Two square-shaped Fermi surfaces enclosing M and Γ points, which are denoted by α and β, respectively, are observed. They are separated in wavenumber space by a nearly constant distance of 0.3 π/a, where a is an in-plane lattice constant. Figure 1(b) shows the band structures observed along the Γ-M line of $HfP_{1.55}Se_{0.45}$. Here we have found that two straight dispersions, which form α and β Fermi surfaces, intersect with each other at -0.9 eV and exhibit Dirac velocity of 1.3×10^6 m/s. We have also observed that the crossing point is continuously connected in wavenumber space and forms an in-plane closed nodal loop. These results provide evidence of the Dirac nodal-line fermions in $HfP_{1.55}Se_{0.45}$.

We can deduce the Hf substitution effect from the comparison between the results of $HfP_{1.55}Se_{0.45}$ and $ZrP_{1.24}Se_{0.57}$. The number and shapes of Fermi surfaces are similar between them. However, in the result of $HfP_{1.55}Se_{0.45}$, the energy of the crossing point is closer to the Fermi level and the distance between the α and β Fermi surfaces is narrower than $ZrP_{1.24}Se_{0.57}$. It should be noted that the Dirac velocity, 1.3×10^6 m/s, for $HfP_{1.55}Se_{0.45}$ is even higher than that, 1.2×10^6 m/s, for $ZrP_{1.24}Se_{0.57}$.

Our results indicate that the gapless Dirac nodal loop is robust against the change of lattice parameter and spin-orbit coupling strength by the replacement of Zr with Hf. The decrease in T_c upon replacing Zr with Hf may be related to the substantial difference in the low-energy electronic structure.

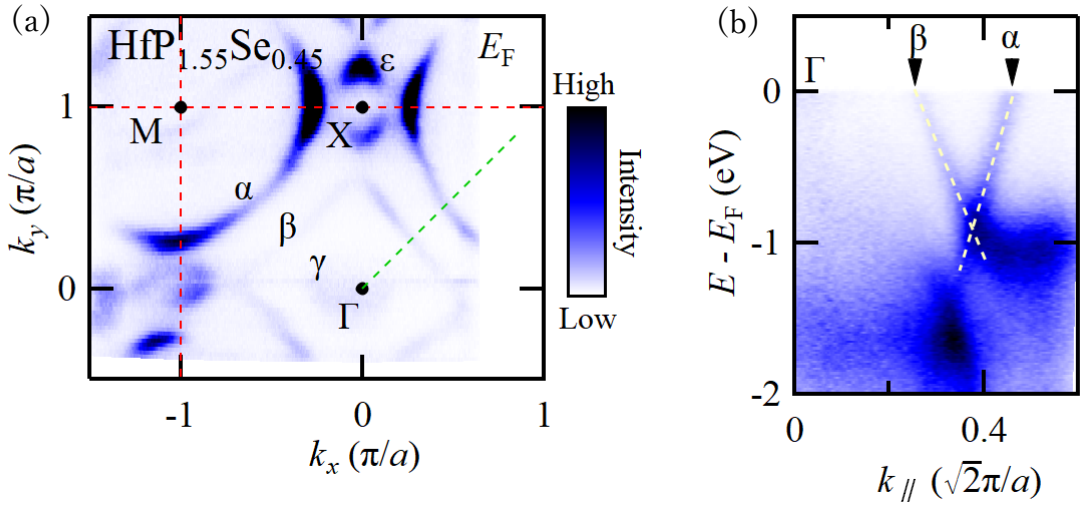

FIGURE 1. ARPES data of $HfP_{1.55}Se_{0.45}$, acquired with $h\nu$ = 50 eV. (a) Fermi-surface map. (b) E-k plot along Γ - M line.

REFERENCES

1. G. Bian *et al*., Nat. Commun. **7**, 10556 (2016).
2. S. Ishizaka *et al*., Phys. Rev. B, in press.
3. H. Kito *et al*., J. Phys. Soc. Jpn. **83**, 074713 (2014).